Injectable Hyaluronic Acid Scaffolds for Cartilage Tissue Engineering

by

Cindy D. Ren

B.S. Chemical Engineering
University of California, Berkeley, 2002

Submitted to the Department of Chemical Engineering in
Partial Fulfillment of the Requirements for the Degree of

Doctor of Philosophy in Chemical Engineering

at the

MASSACHUSETTS INSTITUTE OF TECHNOLOGY

September 2008

Author: _____

Department of Chemical Engineering
June 20, 2008

Certified by: _____

Professor Jackie Y. Ying
Adjunct Professor of Chemical Engineering
Thesis Supervisor

Accepted by: _____

Professor William M. Deen
Professor of Chemical Engineering
Chairman, Departmental Committee for Graduate Studies

ARCHIVES

Injectable Hyaluronic Acid Scaffolds for Cartilage Tissue Engineering

by

Cindy Ren

B.S. Chemical Engineering
University of California, Berkeley, 2002

Submitted to the Department of Chemical Engineering in
Partial Fulfillment of the Requirements for the Degree of
Doctor of Philosophy in Chemical Engineering

Abstract

Every year tens of millions worldwide suffer from cartilage damage, caused by mechanical degradation, trauma or disease. Because of the lack of blood supply and low cell concentration within the tissue, cartilage has very limited regenerative ability. Although current treatments can provide symptomatic relief, the results vary greatly among individuals, and newly formed tissue often does not duplicate the structure, composition or mechanical properties of normal cartilage. Therefore, in recent years, tissue engineering has emerged as an alternative therapy. Tissue engineering enhances the body's natural healing capacity by providing cells, signaling molecules, and an environment in the form of a scaffold that is conducive to tissue growth. This project has focused on the development of a tissue engineering scaffold for cartilage regeneration. Disadvantages to current scaffolds include the fact that they require surgery for implantation, and that they are difficult to mold to the exact shape of the defect site. Hence, the motivation of this thesis is to develop an injectable scaffold that can be administered in a minimally invasive manner, and that allows for scaffold formation *in situ*, naturally shaping the construct into the shape of the defect, and thus promoting integration and stability

To this end, we have developed a thermoresponsive injectable scaffold for cartilage tissue engineering. The scaffold was injected as a liquid at room temperature, and gelled at the target site in response to the change to body temperature, resulting in a biocompatible, bioresorbable substrate for tissue growth. Our approach involved suspending thermoresponsive liposomes, which encapsulated a crosslinking agent, in a polymer solution. At room temperature, the crosslinking agent was separated from the polymer by the lipid membrane, hence the precursor solution remained a liquid and injectable. Upon injection and exposure to body temperature, the lipids experienced a phase transition, which significantly increased the membrane permeability and led to the release of the crosslinking agent and reaction with the polymer, forming a networked scaffold. The scaffold system that we have chosen is a hyaluronic acid-tyramine system (HA-Tyr) that crosslinked in the presence of H_2O_2 and horseradish peroxidase (HRP) to form a hydrogel. Since HA, Tyr, H_2O_2 and peroxidases all occur naturally in the body, scaffold formation could take place with minimal toxicity and in the presence of cells as well as *in situ*. In order to impart temperature sensitivity to this system, HRP was encapsulated within liposomes, and it was shown that HRP was successfully retained at 25°C and released at 37°C. Upon

liposome addition to the HA-Tyr/H_2O_2 solution, the precursor solution remained a liquid for hours at 25°C, yet gelation could be induced within minutes when exposed to 37°C. Furthermore, it was shown that gelation times could be adjusted to meet various clinical needs by modulating HRP encapsulation, liposome concentration and HA-Tyr concentration.

In order to test the potential of the HA-Tyr system for cartilage production, porcine chondrocytes were encapsulated within HA-Tyr/H_2O_2/HRP hydrogels and implanted subcutaneously in mice. Harvested constructs were shown to achieve a GAG content of 1.2 wt% and demonstrated 40% of the collagen content of normal articular cartilage. Matrix production was found to be influenced by the initial cell density, scaffold degradation rate and Type II collagen concentration. The means of HRP delivery, whether by simple addition or through thermoreponsive liposomes, was not shown to have an effect on matrix production. Injected scaffolds were shown to achieve GAG and collagen levels similar to that of implanted scaffolds.

As signaling molecules have been demonstrated to be potent chondrogenic inducers, PLGA-hydroxyapatite nanocomposite microparticles were utilized for the controlled delivery of TGF-β1 and IGF-1. The rate of growth factor release was modulated by the molecular weight of PLGA within the microparticles; increasing molecular weight led to decreasing release rate. The nanocomposite microparticles were encapsulated within HA-Tyr/H_2O_2/HRP/chondrocyte constructs, which were then implanted subcutaneously in mice. Growth factor-induced enhancement of GAG and collagen production was found to be determined by the release rates of TGF-β1 and IGF-1, multifactor release, and the dosage of nanocomposite microparticles. Injection of the microparticles with an HA-Tyr/H_2O_2/HRP liposome/chondrocyte/collagen solution also showed that the microparticles did not interfere with *in situ* scaffold formation, and could induce significant improvements to GAG and collagen production in the injectable system.

Thesis Supervisor:
Jackie Y. Ying
Adjunct Professor of Chemical Engineering

Acknowledgements

I would like to thank my thesis advisor, Professor Jackie Ying, for giving me the opportunity to work with her and for her guidance on this project. I appreciate all of her support, mentorship, and wise words that have helped me through the difficult patches. I would also like to acknowledge my thesis committee, Professors William Deen, Paula Hammond and Myron Spector, whose support and suggestions have been invaluable to me throughout the course of my thesis.

I would like to thank the Nanostructured Materials Research Laboratory for being my family at MIT. I thank Drs. Noreen Zaman, Tseh-Hwan Yong and Pemakorn Pitukmanorom for all of the advice, encouragement, friendship and laughter. I also thank Drs. Yu-Ming Lin, Suniti Moudgil, Todd Zion, Thomas Lancaster, Yee San Su, Xiaohua Huang, Steven Weiss, Jianyi Cui and Hong He, and Ms Linda Mousseau for all of their kind help and camaraderie. I had the pleasure of working with talented students, Ziqing Zhang, Joy Yuan, Connie King, and Sheela Seetharaman. Thank you for all of your hard work and enthusiasm for this project. I learned a great deal from working with you.

I thank everyone at the Institute of Bioengineering and Nanotechnology. In particular, I acknowledge Drs. Motoichi Kurisawa and Joo Eun Chung for their advice and encouragement. I am grateful to Shujun Gao for his tremendous help and surgical expertise in the *in vivo* studies and for his friendship, patience and kindness. I appreciate Dr. Kwong Joo Leck and Fan Lee for their help and useful discussions.

I would like to thank the Department of Comparative Medicine, particularly Kathy Cormier, for the help with histology and for use of the microtome. I thank the Sabatini Lab for use of the Coulter counter.

I would like to thank Levi for all of his love and support. Last but not least, I thank my beloved parents for their unwavering support, encouragement, faith and love throughout this thesis. I thank my father for doing everything to help make my dreams come true. I am grateful to my mother for teaching me courage, discipline and compassion, and for helping me to gain perspective during the difficult moments.

This research was funded by the Singapore-MIT Alliance and the Institute of Bioengineering and Nanotechnology (Biomedical Research Council, Agency for Science, Technology and Research, Singapore).

Table of Contents

List of Figures

List of Table

Chapter 1 – Background and Motivation

1.1 Cartilage Regeneration

Every year tens of millions worldwide suffer from cartilage damage, and over 1 million surgical procedures in the United States alone involve cartilage reconstruction [1,2]. The main function of cartilage is to serve as a shock absorber and lubricant in the joints, but mechanical degradation, trauma, or diseases, such as arthritis, can lead to the irreversible loss of cartilage's structure and function [3]. This, in turn, results in a great deal of pain, swelling, limited mobility, and eventually joint deformation. The problem is that, unlike bone and skin, cartilage has very limited regenerative ability, largely due to the lack of blood supply and low cell concentration within the tissue [4, 5, 6]. Current treatments include lavage, subchondral bone penetration, transplantation, or implantation of prosthetics [7]. The disadvantages of these therapies arise from infliction of additional injury, donor site morbidity, limited donor supply, and prosthetic durability [4, 8, 9]. In addition, although these treatments can provide symptomatic relief, any newly formed tissue has a limited life span because it does not duplicate the structure, composition and mechanical properties of natural articular cartilage [3].

1.2 Cartilage Tissue Engineering

In recent years, tissue engineering has emerged as an alternative therapy. Tissue engineering involves the construction of a biological device that either elicits tissue regeneration or replaces damaged tissue. This is generally accomplished by three components: (1) patient or donor cells, (2) regulators that guide the regenerative activity of the cells, and (3) a scaffold that acts as a delivery vehicle for the cells and regulators, as well as a substrate for tissue growth [8]. By introducing a cell-seeded matrix supplemented with signaling molecules that promote tissue synthesis, the low cell concentration and avascular nature of cartilage can be addressed. This method may enhance the healing capacity within the defect site without the need to augment injury, use prosthetics and, perhaps with the advent of stem cell technology, sacrifice healthy cartilage.

Several studies have already shown the feasibility of tissue engineering in cartilage restoration. Perhaps the most established tissue engineering solution today is the injection of autologous cells into a cartilaginous defect, which is subsequently covered by a periosteal flap.

The advantage of this solution lies in the *in vitro* expansion of a relatively small quantity of cells, isolated from non-load-bearing cartilage, which are re-implanted to induce regeneration by increasing the local cell concentration in the defect site. Results, in particular long-term findings, have been controversial, however, and in a recent study in canines, cartilage had begun to degrade 12–18 months post-implantation [6, 8, 10]. One possible reason is the leakage of chondrocytes out of the sutured flap, particularly upon application of mechanical loads [5]. Another possibility is the uneven tissue growth due to the imbalanced distribution of cells post-implantation, with chondrocytes accumulating at an edge dictated by gravity. It is proposed that these issues can be addressed by the incorporation of a scaffold. Cells seeded on a matrix may be less likely to escape the defect site, and the spatial distribution of cells can be more easily controlled. Lee *et al.* have demonstrated that chondrocyte-seeded Type II collagen sponges implanted in cartilage defects resulted in greater reparative tissue than untreated defects or cells implanted alone [11].

1.3 Injectable Scaffolds

Significant research has been devoted to the development of suitable scaffolds as the matrix plays a key role in tissue engineering. The scaffold must act as a temporary extracellular matrix (ECM), support and guide cell growth, and provide mechanical support [12]. In order to meet these requirements, the scaffold needs to possess the following properties: (1) be non-toxic and non-inflammatory, (2) promote cell stability and tissue production, (3) possess interconnecting pores that allow cell migration and tissue growth, (4) be bioresorbable, degrading either during or after healing, (5) be mechanically robust, and (6) be capable of being fabricated to fit the shape of various defect sites [13, 14]. The scaffold materials most commonly used for cartilage are either natural polymers, such as hyaluronic acid (HA), collagen, alginate, agarose and fibrin, or synthetic polymers, such as poly(glycolic acid), poly(lactic acid) and poly(ethylene glycol) (PEG) [3, 6, 8, 11, 12, 15, 16, 17, 18, 19]. Chondrocytes grown on such scaffolds *in vitro* and *in vivo* have synthesized tissue resembling articular cartilage histologically and mechanically [20, 21].

Currently, several limitations remain in the development of an appropriate scaffold. First, implantation of the scaffold generally requires invasive surgery, which inherently involves risks, such as infection and failure to heal [22]. Secondly, it is difficult to mold a material to perfectly

fit a defect site [14]. A poorly fitted scaffold can result in failure of the newly formed tissue to integrate with the host tissue, which may subsequently lead to dead space and implant instability. Dead space can cause fluid accumulation and chronic inflammation, while implant instability can cause micromotion, producing forces at the construct interface [23]. Both result in the degradation and limited lifetime of the reparative tissue.

In order to address these issues, injectable scaffolds have been investigated as a possible approach to tissue engineering. This method is based on the injection of a liquid that cures in the defect site in response to a stimulus. The liquid is generally composed of a soluble monomer or polymer that forms a hydrogel by crosslinking, polymerization or phase transition. Gelation can be induced by various stimuli, including a change in temperature or pH and application of high-energy light [18, 24, 25, 26, 27]. This approach would not only eliminate the need for surgery and potentially reduce patient recovery time, but also enable the scaffold to take the shape of the defect as scaffold formation occurs *in situ* [28]. Integration of the scaffold with the existing tissue would be improved, due to the intimate contact of the polymer with the surrounding tissue during scaffold formation, and the mechanical interlocking that occurs as a result of surface microroughness [18].

Previous research has shown the feasibility of this approach. Elisseeff *et al.* have demonstrated the potential of *in situ* scaffold formation by transdermal photopolymerization for cartilage repair [18, 19]. Although the newly formed tissue has been shown to histologically resemble cartilage, photopolymerization is limited by the penetration depth of high-energy light. Ultraviolet (UV) light, for example, has been shown to have a penetration depth of only 2 mm in human skin, restricting the defect sites that can be treated by transdermal photopolymerization [18]. Furthermore, high-energy light is known to cause cell and tissue damage [29, 30].

1.4 Research Objectives

To avoid the use of radiation, the objective of our research is to design a scaffold such that solidification can be induced by an environmental stimulus that is constant throughout the body, namely temperature. Since the curing process is initiated simply by exposing the scaffold to a physiological condition, the scaffold could potentially be induced to gel anywhere in the body. The ideal characteristics of the scaffold include:

1. Stability as a liquid at room temperature – to allow sufficient working time for clinicians.

2. Rapid gelation at body temperature – to prevent diffusion out of the defect and minimize waiting time.
3. Tunable gelation kinetics – to allow clinicians to decide upon the working and setting times appropriate for various applications and situations.
4. Effective promotion of cartilage production.

Other desirable properties of the scaffold include porosity, biodegradability, bioactivity and ease of manufacture.

To achieve the research objectives, the following approach was taken:

1. Synthesis of thermoresponsive microcapsules that encapsulate a crosslinking agent (Chapter 2).
2. Combination of microcapsules with polymer solution to form a precursor solution that is injectable as a liquid at room temperature (25°C), and cures to form a scaffold at the target site in response to the change to body temperature (37°C) (Chapter 2).
3. Encapsulation of cells and evaluation of efficacy of the scaffold for cartilage production in vivo (Chapter 3).
4. Incorporation of growth factor carriers for the controlled release of TGF-β1 and IGF-1 to enhance cartilage synthesis by cells (Chapter 4).

1.5 Thermoresponsive Liposomes for Thermally Triggered Injectable Scaffolds

Our approach for creating a thermally triggered injectable scaffold involves the dispersion of thermoresponsive liposomes (which encapsulate a crosslinking agent) within a polymer solution. At room temperature, the crosslinking agent and polymer are segregated from each other, and the precursor solution remains a liquid. At body temperature, however, the crosslinking agent is released, causing the polymer to form a three-dimensional network and the precursor solution to cure. Encapsulating the crosslinking agent potentially enables the injection of scaffolds that would otherwise require implantation, eliminates the need for co-injections (which can lead to inhomogeneous constructs), and prolongs the working time of pre-mixed systems significantly.

Liposomes are composed of amphiphilic molecules that self-assemble into a spherical bilayer around an aqueous core. They were chosen to carry the crosslinking agent because they are biocompatible, versatile encapsulating agents that have been studied extensively for the

delivery of various therapeutic agents [31, 32, 33, 34]. Furthermore, many phospholipids are known to experience a gel-to-liquid phase transition at a given temperature, where the alkyl chains experience a trans-to-gauche conformational change [35, 36]. During this process, the membranes of liposomes, composed of such lipids, become more disordered, significantly enhancing membrane permeability and allowing the encapsulated molecules to be released from the liposomes. In order to achieve the thermally triggered scaffold system described above, the crosslinking agent was encapsulated within liposomes with a phase transition temperature near 37°C. The mechanism of gelation is depicted in Figure 1.1.

Systematic modulation of gelation kinetics may be possible by changing variables that affect the crosslinking reaction rate, such as the polymer concentration, the loading of crosslinking agent within the liposomes, and the liposome concentration.

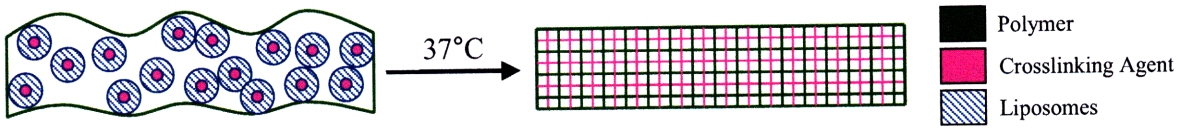

Figure 1.1. The precursor solution is a liquid at room temperature. Exposure to body temperature results in the release of the crosslinking agent, which subsequently leads to polymer crosslinking and scaffold formation.

Several phospholipids experience phase transition temperatures in the range of body temperature, and can be blended to achieve an overall phase transition near 37°C. Possible lipid candidates include dimyristoylphosphatidlycholine (T_m = 23°C), dipalmitoylphosphatidlycholine (T_m = 41°C), dimyristoylphosphatidylglycerol (T_m = 23°C), dipalmitoylphosphatidylglycerol (T_m = 41°C), dimyristoylphosphatidylserine (T_m = 35°C), dilauroyl phosphatidic acid (T_m = 31°C), dimyristoyl phosphatidic acid (T_m = 50°C), dilauroylphosphatidylethanolamine (T_m = 29°C), and dimyristoylphosphatidylethanolamine (T_m = 50°C) [37].

This platform can be applied to impart temperature sensitivity to a broad scope of polymer crosslinking agent or monomer catalyst systems. Candidates for the polymeric/monomeric component and their respective crosslinking agents/catalysts include collagen and lysyl oxidase, elastin and lysyl oxidase, alginate and Ca^{2+}, polyethylene oxide-dimethacrylate and 1-hydroxycyclohexyl phenyl ketone, fibrin and thrombin, fibrinogen and α-transglutaminase, and biotinylated polymers and avidin [18, 19, 27, 38, 39, 40, 41, 42].

HA is an attractive scaffold candidate as it is one of the main components of the cartilage ECM, and would therefore mimic the natural tissue environment [41]. Moreover, it is a highly hydrophilic polysaccharide that contributes to the high Young's modulus and load-bearing abilities of cartilage, and has been shown to be important in cartilage homeostasis [23, 43, 44]. Recently, a HA-tyramine (HA-Tyr) system was developed by Kurisawa *et al.*, in which tyramine groups were conjugated onto a HA backbone [45]. In the presence of hydrogen peroxide (H_2O_2) and horseradish peroxidase (HRP), the tyramine groups react with each other to form crosslinks between and within the HA polymer, which subsequently forms a hydrogel network (Figure 1.2). Whereas other crosslinking methods often employ relatively toxic reactions such as carbodiimide coupling and esterification, tyramine, H_2O_2 and peroxidases all naturally occur in the body, achieving network formation without sacrificing the biocompatibility of HA [46, 47, 48, 49]. This enables curing to occur in the presence of cells and tissue, making this system a promising candidate as an injectable scaffold. Furthermore, temperature sensitivity can be achieved by pairing the HA-Tyr polymer with thermoresponsive liposomes, in which the crosslinking agent, HRP, can be encapsulated.

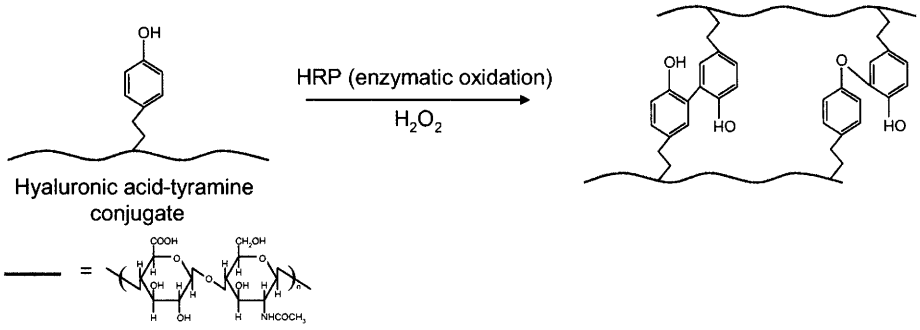

Figure 1.2. Crosslinking reaction of HA-Tyr in the presence of HRP and H_2O_2.

1.6 References

[1] Langer, R., Vacanti, J. P., *Science* **260**, 920–926 (1993).

[2] Elisseeff, J., Lee, A., Kleinman, H. K., *et al.*, *Ann NY Acad Sci* **961**, 118–122 (2002).

[3] Buckwalter, J. A., Mankin, H. J., *J Bone Joint Surg* **79-A**, 612–632 (1997).

[4] Raghunath, J., Rollo, J., Sales, K. M., *et al.*, *Biotechnol Appl Biochem* **46**, 73–84 (2007).

[5] Tuli, R., Li, W. J., Tuan, R. S., *Arthritis Res Ther* **5**, 235–238 (2003).

[6] O'Driscoll, S. W., *J Bone Joint Surg* **80-A**, 1795–1812 (1998).

[7] Cancedda, R., Dozin, B., Giannoni, P., *et al.*, *Matrix Biol* **22**, 81–91 (2003).

[8] Nesic, D., Whiteside, R., Brittberg, M., *et al.*, *Adv Drug Deliv Rev* **58**, 300–322 (2006).

[9] Buckwalter, J. A., Mankin, H. J., *J Bone Joint Surg* **79-A**, 600–611 (1997).

[10] Temenoff, J. S., Mikos, A. G., *Biomaterials* **21**, 431–440 (2000).

[11] Lee, C. R., Grodzinsky, A. J., Hsu, H.-P., *et al.*, *J Orthop Res* **21**, 272–281 (2003).

[12] Drury, J. L., Mooney, D. J., *Biomaterials* **24**, 4337–4351 (2003).

[13] Curtis, A., Riehle, M., *Phys Med Biol* **26**, R47–R65 (2001).

[14] Griffith, L. G., *Ann NY Acad Sci* **961**, 83–95 (2002).

[15] Lavik, E., Langer, R., *App Microbiol Biotechnol* **65**, 1–8 (2004).

[16] Vunjak-Novakovic, G., Obradovic, B., Martin, I., *et al.*, *Biotechnol Prog* **14**, 193–202 (1998).

[17] Mauck, R. L., Seyhan, S. L., Ateshian, G. A., *et al.*, *Ann Biomed Eng* **30**, 1046–1056 (2002).

[18] Elisseeff, J., Anseth, K., Sims, D., *et al.*, *Proc Natl Acad Sci USA* **96**, 3104–3107 (1999).

[19] Elisseeff, J., Anseth, K., Sims, D., *et al.*, *Plast Reconstr Surg* **104**, 1014–1022 (1999).

[20] Freed, L. E., Vunjak-Novakovic, G., Langer, R., *J Cell Biochem* **51**, 257–264 (1993).

[21] Ma, P. X., Langer, R., *J Biomed Mater Res* **44**, 217–221 (1999).

[22] Hou, Q., De Bank, P. A., Shakesheff, K. M., *J Mater Chem* **14**, 1915–1923 (2004).

[23] Temenoff, J. S., Mikos, A. G., *Biomaterials* **21**, 431–440 (2000).

[24] Gutowska, A., Jeong, B., Jasionowski, M., *Anat Rec* **263**, 342–349 (2001).

[25] Jeong, B., Gutowska, A., *Trends Biotechnol* **20**, 305–311 (2002).

[26] Balakrishnan, B., Jayakrishnan, A., *Biomaterials* **26**, 3941–3951 (2005).

[27] Ritter Jones, M., Messersmith, P. B., *Oral Maxillofac Surg Clin North Am* **13**, 29–38 (2002).

[28] Hubbell, J. A., *Curr Opin Solid State Mater Sci* **3**, 246–251 (1998).

[29] Bailey, A. J., *Mech Ageing Dev* **122**, 735–755 (2001).

[30] Scoltock, A. B., Cidlowski, J. A., *Exp Cell Res* **297**, 212–223 (2004).

[31] Chrai, S. S., Murari, R., Ahmad, I., *Biopharm* **14**, 10–14 (2001).

[32] Gregoriadis, G., *Trends Biotechnol* **13**, 527–537 (1995).

[33] Sharma, A., Sharma, U. S., *Int J Pharm* **154**, 123–140 (1997).

[34] Lasic, D. D., *Handbook of Biological Physics* (Elsevier Science, Amsterdam, 1995).

[35] Taylor, K. M. G., Craig, D. Q. M., in *Liposomes: A Practical Approach*, edited by V. Torchilin and V. Weissig (Oxford University Press, New York, 2003), p. 92–95.

[36] Bergstrand, N., Ph.D. Thesis: *Liposomes for Drug Delivery: From Physico-chemical Studies to Applications* (Uppsala University, Uppsala, 2003).

[37] Silvius, J. R., in *Lipid-Protein Interactions*, edited by P. C. Jost and O. H. Griffith (John Wiley & Sons, New York, 1982), Vol. 2, p. 239–281.

[38] Elbjeirami, W. M., Yonter, E. O., Starcher, B. C., *et al.*, *J Biomed Mater Res* **66A**, 513–521 (2003).

[39] Paige, K. T., Cima, L. G., Yaremchuk, M. J., *et al.*, *Plast Reconstr Surg* **97**, 168–178 (1996).

[40] Elisseeff, J., McIntosh, W., Anseth, K., *et al.*, *J Biomed Mater Res* **51**, 164–171 (2000).

[41] Raghunath, J., Rollo, J., Sales, K. M., *et al.*, *Biotechnol Appl Biochem* **46**, 73–84 (2007).

[42] Salem, A. K., Rose, F. R. A. J., Oreffo, R. O. C., *et al.*, *Adv Mater* **15**, 210–213 (2003).

[43] Chow, G., Nietfeld, J. J., Knudson, C. B., *et al.*, *Arthritis Rheum* **41**, 1411–1419 (1998).

[44] Goessler, U. R., Hormann, K., Riedel, F., *Int J Mol Med* **13**, 505–513 (2004).

[45] Kurisawa, M., Chung, J. E., Gao, S., *et al.*, *Chem Commun* **34**, 4312–4314 (2005).

[46] Allison, D. D., Grande-Allen, K. J., *Tissue Eng* **12**, 2131–2140 (2006).

[47] Grigolo, B., Roseti, L., Fiorini, M., *et al.*, *Biomaterials* **22**, 2417–2424 (2001).

[48] Wurzinger, S., Bratu, M., Wonisch, W., *et al.*, *Life Sci* **78**, 1754–1759 (2006).

[49] Zhang, W. P., Ming, O. Y., Thomas, S. A., *Neuropharmacology* **47**, 438–449 (2004).

Chapter 2 – Liposomal Encapsulation of Horseradish Peroxidase for Thermoresponsive Hyaluronic Acid-Tyramine Scaffold

2.1 Introduction

2.1.1 Thermoresponsive Materials

Several methods have been investigated for the stimuli-responsive release of proteins from particles or microcapsules. In many of these cases, polymers are grafted into the pores of a polymer shell and serve as a gate. In the resting state, the capsule encloses the protein because the grafted polymer covers the pores and limits permeability. Upon exposure to an external stimulus, such as ionic strength, light, oxidoreduction, or pH, the polymers would experience a phase change or shift in hydrophobicity, shrink and release the contents of the particle [1, 2, 3, 4, 5]. Okahato *et al.* and Lee *et al.*, for example, grafted poly(methacrylate) (PMA) and poly(acrylic acid) into the pores of a nylon membrane to synthesize capsules whose membrane permeabilities were controlled by pH [1, 2]. Ito *et al.* grafted poly[3-carbamoyl-1-(p-vinylbenzyl)pyridium chloride] onto a porous membrane, and showed that release could be induced by the switch from an oxidizing solution (H_2O_2) to a reducing solution ($Na_2S_2O_4$) [3]. Similar methods that utilize polymers that respond to ionic strength and UV light have also been explored [4, 5].

The disadvantage of these systems lies in the fact that the materials, such as PMA, are generally non-biodegradable, which would likely result in the material's remaining in the body for extended periods and increase the possibility of a foreign body response [6]. In addition, the grafting processes could involve complex and expensive synthesis procedures, such as glow discharge or plasma grafting. Furthermore, many of these stimuli could affect the viability of the cells and potentially result in local cell necrosis. Use of pH-responsive delivery, for example, requires the injection of material under conditions either more basic or acidic than physiological pH, which has the potential to cause local tissue necrosis. Exposure to strong oxidizing/reducing agents, UV light or osmotic stresses is also widely known to cause cell death [7, 8, 9].

Thermoresponsiveness has been chosen for this study because temperature change is a milder stimulus and because there is a convenient and substantial gap between room temperature (25°C) and body temperature (37°C). Several studies have explored the synthesis of thermoresponsive microcapsules for the release of proteins, with poly(N-isopropylacrylamide)

(NIPAAM) perhaps being the most common system employed. NIPAAM demonstrates a lower critical solution temperature (LCST) just below body temperature, where the hydrophobicity of the material increases and the polymer precipitates out of solution to form a hydrogel [10]. Similar to that described above, several studies have shown the ability to graft NIPAAM into the porous membrane of capsules [2, 11, 12, 13]. At room temperature, NIPAAM covers the pores and blocks the passage of the contents out of the capsule. At body temperature, the volume of NIPAAM dramatically decreases, opening the pores and allowing for passage. The disadvantage of these systems lies again in the inability of NIPAAM to degrade in the body.

In this study, we have chosen hyaluronic acid-tyramine (HA-Tyr) as our hydrogel system because hyaluronic acid (HA) is biocompatible, biodegradable and non-immunogenic. The HA-Tyr system, developed by Kurisawa *et al.*, consists of the HA polymer, onto which tyramine groups are conjugated [23]. The tyramine groups react with each other in the presence of H_2O_2 and horseradish peroxidase (HRP) to form a hydrogel network that can be used as a tissue engineering scaffold. Since each reactant occurs naturally in the body, the scaffold formation takes place with minimal toxicity.

In order to impart temperature sensitivity to the HA-Tyr system, we have encapsulated the crosslinking agent, HRP, into thermoresponsive microcapsules. By segregating HRP from HA-Tyr/H_2O_2 at room temperature, the mixture would remain as a liquid and injectable through a syringe. Upon injection into defect site and exposure to body temperature, the microcapsules would release HRP, resulting in the subsequent reaction between HRP and HA-Tyr/H_2O_2 and the formation of a hydrogel scaffold.

Specifically, we have encapsulated HRP within thermoresponsive liposomes. Liposomes have been chosen in this study because they are biocompatible and biodegradable materials that have been widely studied for drug and gene delivery [14]. They have been shown to be stable in the body and versatile encapsulating agents, with the ability to successfully hold and deliver ions (e.g. Ca^{2+}), cancer therapeutics (e.g. doxorubicin), as well as antifungal compounds (e.g. amphotecerin) [14, 15, 16]. Furthermore, temperature sensitivity can be achieved by the appropriate choice of phospholipid. Many phospholipids undergo a phase transition at the main lamellar chain-melting phase transition temperature, T_m, above which the alkyl chains undergo a trans-gauche transition (Figure 2.1) [17]. In the gauche state, the lipids in the bilayer become disordered, and permeability of the membrane significantly increases, permitting its contents to

be released into the environment. Dipalmitoyl-phosphatidylcholine (DPPC) (T_m = 41°C) and dimyristoylphosphatidylcholine (DMPC) (T_m = 23°C) were combined together to form liposomes with an overall T_m just below the body temperature, 37°C.

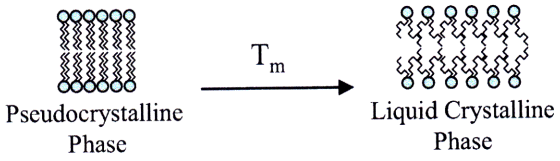

Figure 2.1. Trans-gauche transition of phospholipids: (•) phospholipids head and (〰) alkyl tail.

2.1.2 Conventional Methods for Liposome Preparation

Several methods for encapsulating proteins and enzymes within liposomes have been explored [18, 19]. Most approaches begin with the deposition of a lipid film on a surface, which is then hydrated with an enzymatic solution. The mixture is heated above T_m and vortexed such that the lipid film lifts off the surface to form liposomes around the enzyme solution. This process can be followed by a variety of steps, such as sonication, extrusion, repeated freeze-thawing, or ethanol addition (to induce interdigitation), to control size distribution and enhance entrapment efficiency.

Various methods that employ organic solvents have also been studied [20, 21]. Reverse-phase evaporation, for example, involves dissolving the lipid in a water-miscible organic solvent with a low boiling point. Upon addition to an aqueous enzyme solution, a reverse emulsion is formed with the aid of vortexing and/or sonication. The solvent is then removed under reduced pressure to form a dispersion of vesicles with aqueous cores that contain the enzyme. The ethanol injection method is similar, except that an ethanol/methanol solution containing the lipid is injected into the aqueous enzyme solutions to form vesicles, in which with enzyme are entrapped.

2.1.3 Dehydration-Rehydration Vesicle Method

The dehydration-rehydration vesicle (DRV) method was chosen for the encapsulation of HRP primarily with the aim of preventing enzyme denaturation. Developed by Gregoriadis *et al.* [22], this technique involves mixing blank pre-formed liposomes with the enzyme of interest at room temperature (Figure 2.2). This mixture is then freeze-dried and rehydrated. During the

freezing and lyophilization steps, the liposome vesicles are destabilized, causing many to deflate and merge with neighbors to form lipid sheets between which HRP is sandwiched. Upon rehydration, the lipids would re-form liposomes, many of which have fused with their neighbors around the HRP, effectively encapsulating HRP within the new vesicles. This method avoids exposure of HRP to high temperatures, organic solvents and repeated freeze-thaw cycles that are employed in other liposome encapsulation procedures, and that are known to denature proteins and reduce enzymatic activity.

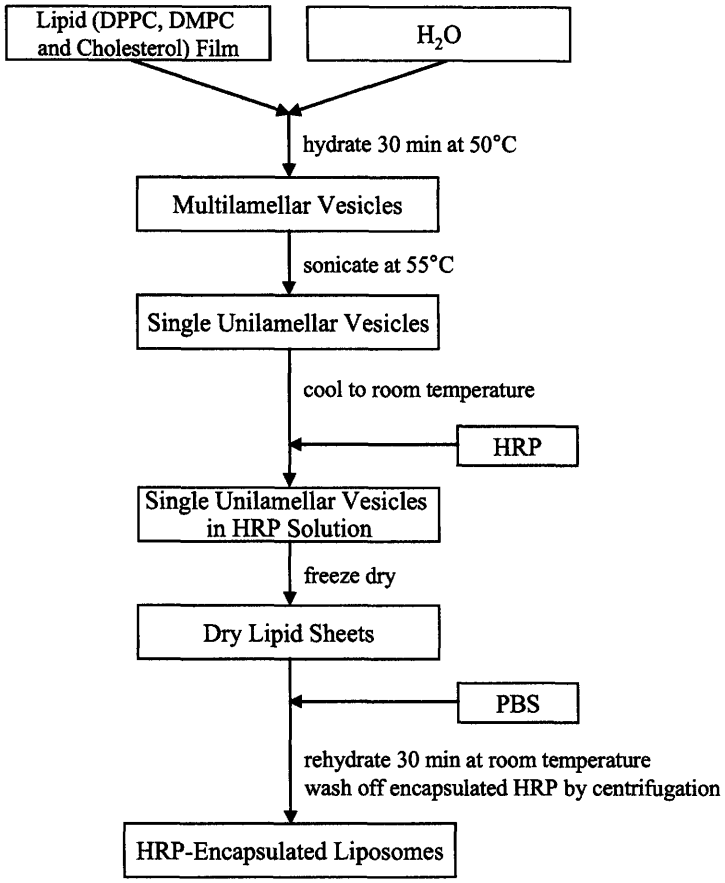

Figure 2.2. Schematic of the DRV method for preparing HRP liposomes.

2.2 Experimental

2.2.1 Conjugation of Tyramine to Hyaluronic Acid Backbone

HA-Tyr conjugation was performed as described by Kurisawa *et al.* [23]. Briefly, Tyr was covalently attached to the HA (90–150 kDa) backbone by a reaction with N-(3-dimethylaminopropyl)-N'-ethylcarbodiimide (EDC) and N-hydroxysuccinimide (NHS).

Unreacted Tyr and the by-products of the reaction were removed by dialysis. Tyr substitution was verified by nuclear magnetic resonance (NMR) spectroscopy, and ranged from 8% to 9%. HA and EDC were purchased from Lifecore and Alfa Aesar, respectively. Tyr and NHS were purchased from Sigma-Aldrich.

2.2.2 Synthesis of Liposomes

Liposomes were synthesized with varying concentrations of DPPC, DMPC and cholesterol. HRP was encapsulated by the DRV method [22]. The lipid-cholesterol mixture was dissolved in chloroform, which was then evaporated to form a film in a round-bottom flask. The film was incubated with deionized water at 50°C for 30 min with intermittent vortexing. The solution was sonicated with a probe-tip sonicator at 55°C for 30 min or until optically transparent. After the solution had cooled to room temperature, an equal volume of enzyme solution was added. The mixture was then frozen and freeze-dried. The liposomes were rehydrated with phosphate buffer solution (PBS), and incubated at room temperature for 30 min. Unencapsulated HRP was then rinsed off by repeated centrifugation (2500g, 1 min). The lipids, cholesterol and PBS were purchased from Avanti Polar Lipids, Alfa Aesar and VWR, respectively. HRP and all other chemicals were purchased from Sigma-Aldrich.

2.2.3 Measurement of HRP Liposome Release

HRP release was measured by adding PBS to a given volume of liposomes. The mixture was then incubated for a set amount of time at either room temperature or 37°C. The liposomes were then centrifuged (20000g, 10 min) into a pellet, and the HRP concentration in the supernatant was measured calorimetrically with the Amplex Red dye (Invitrogen) at 560 nm. HRP liposome release was measured in terms of units of enzymatic activity derived from each mL of liposomes (corresponding to ~ 300 mg of phospholipids).

2.2.4 DSC of Liposomes

Liposomes (~ 5 mg) prepared as described in Section 2.2.2 were added to aluminum hermetic pans. Differential Scanning Calorimetry (DSC) was conducted on a TA Instrument Q100 at a ramp rate of 10°C/min.

2.2.5 Measurement of Liposome Size

Liposomes were suspended in PBS, and their sizes were characterized with a Coulter counter (Beckman Coulter Z2) for 2–6 μm, 6–10 μm and 9–30 μm. The liposome size was calculated as the number average diameter.

2.2.6 Measurement of Gelation Kinetics

Hydrogels were formed by adding HRP liposomes to HA-Tyr/H_2O_2 (5 wt%, 5 μL per 25 mg of HA-Tyr) solutions. The gelation of the hydrogel networks was studied by oscillatory rheometry on a TA Instrument AR 2000. HA-Tyr/H_2O_2/HRP liposome solutions were pipetted onto a Peltier plate (set at 20°C or 37°C) upon which a 60-mm, 2° cone was lowered. Measurements were obtained at a controlled strain of 1% and at a frequency of 1.0 Hz. The point at which the storage modulus (G') and the loss modulus (G") intersected was considered the gel point. G' values of hydrogel were taken after 12 h, by which time G' had reached a plateau.

HRP deactivation was measured by incubating HRP in various solutions for 1 h at room temperature. HRP activity was then measured calorimetrically with the Amplex Red dye. HRP deactivation was calculated as:

$$\text{Deactivation} = 1 - (\text{Activity}_x)/(\text{Activity}_{H_2O})$$

where Activity_{H_2O} was assumed to be the enzymatic activity of HRP in H_2O (which corresponded to the least deactivation or the maximum activity), and Activity_x was the enzymatic activity in solution x.

2.2.7 In Situ Gelation Study

Sterile HRP liposomes, aseptically prepared as described in Section 2.2.2., were combined with sterile-filtered HA-Tyr (25 mg/1.5 mL of PBS)/H_2O_2 (5 wt%, 5 μL per 25 mg of HA-Tyr) solution. The mixture was then injected subcutaneously into the dorsum of a BALB/c mouse. The mouse was sacrificed after ~ 2 h, and the gel that had formed was harvested and analyzed.

2.3 Results and Discussion

2.3.1 Modulation of HRP Encapsulation within Liposomes

Following the DRV method, HRP liposomes composed of DPPC and DMPC were prepared such that HRP remained encapsulated within the liposome at 25°C, and was released rapidly at 37°C (see Figure **2.3.**2.3).

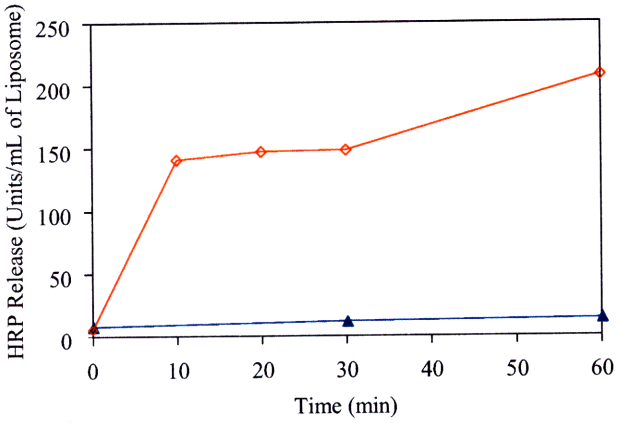

Figure 2.3. Thermally triggered HRP release from liposomes at (▲) 25°C and (◊) 37°C. Liposomes were synthesized with 60 mg/mL of lipid (DPPC:DMPC weight ratio = 2.3), 2 mg/mL of HRP, 30-min sonication, -20°C freezing, and rehydration volume ratio = 0.1.

In order to synthesize liposomes that could be thermally triggered at body temperature, DPPC and DMPC were chosen. By blending the two at the appropriate ratio, an overall phase transition temperature just below 37°C could be achieved. As shown in Figure 2.4, an increase in DPPC:DMPC weight ratio increases the phase transition temperature since $T_{mDPPC} > T_{mDMPC}$. An increase in the DPPC:DMPC weight ratio decreased the permeability of HRP at 37°C (Figure 2.5). The overall T_m should be a few degrees below 37°C to allow for effective release at 37°C. Otherwise, there would not be sufficient energy to disorder the alkyl chains significantly for complete HRP release at 37°C.

Cholesterol was added to modify bilayer fluidity and decrease enzyme leakage at room temperature [19]. The addition of cholesterol, however, was found to do little for room-temperature stability and actually decreased HRP encapsulation and liposome size (Figure **2.6.** 2.6). Similar results were shown by Moribe *et al.*; the encapsulation efficiency of nystatin was decreased with the incorporation of cholesterol in liposomes that were synthesized by repeated freeze-thaw cycles [24]. Cholesterol is known to rigidify and stabilize liposome membranes, but the increased stability also hinders the fusion of liposomes during the freezing and dehydration process [25, 26]. Cholesterol is also shown to prevent the fusion of liposomes by decreasing the zeta potential, and thereby increasing repulsion between the vesicles [25]. However, this process

of liposome fusion was critical in the DRV process for the HRP encapsulation. The lower extent of fusion was also corroborated by the size of the resulting liposomes. Prior to freeze drying, single unilamellar vesicles (SUV's) have a size of 20–50 nm [19, 27]. After rehydration, the liposomes became much larger due to fusion of neighboring liposomes. The resulting size could thus be seen as a measure of the degree of fusion. The smaller liposome size with the incorporation of cholesterol confirmed the reduced degree of fusion, which resulted in a lower HRP encapsulation efficiency.

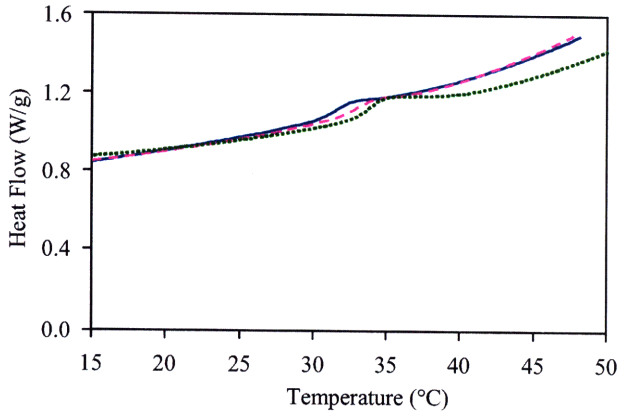

Figure 2.4. DSC curves of HRP liposomes synthesized with 60 mg/mL of lipid (DPPC/DMPC weight ratio = (–) 2.3, (--) 3.0 and (···) 4.0), 2 mg/mL of HRP, 30-min sonication, -20°C freezing, and rehydration volume ratio = 0.1.

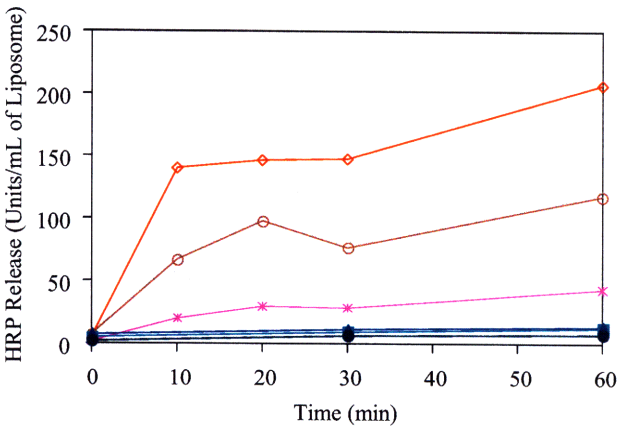

Figure 2.5. Thermally triggered HRP release from liposomes at (▲,■,●) 25°C and (◊,○,*) 37°C. Liposomes were synthesized with 60 mg/mL of lipid (DPPC/DMPC weight ratio = (▲,◊) 2.3, (■,○) 3.0 and (●,*) 4.0), 2 mg/mL of HRP, 30-min sonication, -20°C freezing, and rehydration volume ratio = 0.1.

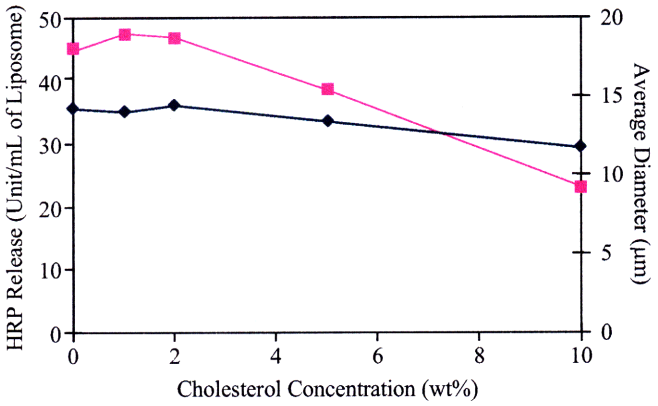

Figure 2.6. Effect of the cholesterol concentration on (■) the total HRP release from liposomes after 1 h at 37°C, and (♦) the liposome size. Liposomes were synthesized with 20 mg/mL of lipid (DPPC:DMPC weight ratio = 2.3), 2 mg/mL of HRP, 30-min sonication, -20°C freezing, and rehydration volume ratio = 0.1.

Figure 2.7 shows that as lipid concentration increased, HRP entrapment increased. This was due to the increase in contact between the HRP and lipid vesicles. An increase in lipid concentration increased the probability of contact between HRP molecules and lipid sheets, thereby increasing the total encapsulation during vesicle fusion.

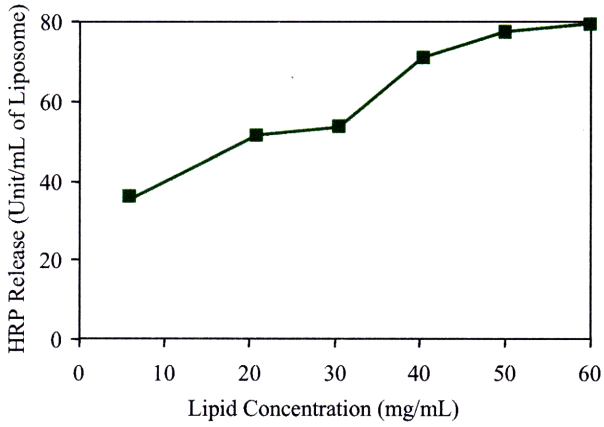

Figure 2.7. Effect of the lipid concentration on the total HRP release after 1 h at 37°C. Liposomes were synthesized with various lipid concentrations (DPPC:DMPC weight ratio = 2.3), 2 mg/mL of HRP, 30-min sonication, -20°C freezing, and rehydration volume ratio = 0.1.

Freezing and dehydration stresses can lead to significant denaturation of proteins during liposome synthesis due to ice-induced unfolding and water removal from the protein's hydration shell [28, 29]. Therefore, as shown in Table 2.1, the means by which the enzyme/liposome solutions were frozen, which determined the rate of cooling, was important in controlling the

enzymatic activity recovered. The slower the freezing rate, the less the enzyme would be damaged during synthesis. In addition, the freezing process was a key factor in liposome fusion and HRP encapsulation. When frozen under liquid nitrogen, the freezing process might occur too quickly and inhibit liposome fusion, subsequently lowering HRP encapsulation. This was evidenced by a smaller liposome size.

Table 2.1. Effect of the freezing method on the total HRP release after 1 h at 37°C and the liposome size. Liposomes were synthesized with 60 mg/mL of lipid (DPPC:DMPC weight ratio = 2.3), 2 mg/mL of HRP, 30-min sonication, and rehydration volume ratio = 0.1.

Freezing Method	HRP Release (Unit/mL of Liposome)	Liposome Size (μm)
Liquid Nitrogen	89.6	11.5
-20°C Freezer	108.0	15.3

Sonicating the liposomes prior to freezing was found to increase the enzyme encapsulation (Figure 2.8). The sonication step converted the multi-lamellar vesicles (MLV's) with an onion-like structure into small SUV's. Sonication broke up the liposome agglomeration and dispersed the vesicles homogeneously within the solution, increasing the interaction between the lipid and HRP prior to freeze drying, and thereby improving HRP encapsulation.

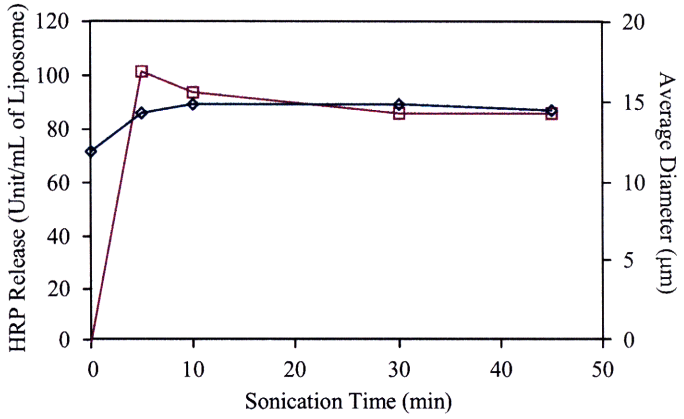

Figure 2.8. Effect of the sonication time on (□) the total HRP release after 1 h at 37°C and (◊) the liposome size. Liposomes were synthesized with 60 mg/mL of lipid (DPPC:DMPC weight ratio = 2.3), 2 mg/mL of HRP, -20°C freezing, and rehydration volume ratio = 0.1.

It was also found that varying the rehydration volume ratio (volume of PBS added during rehydration/volume of initial liposome solution) greatly affected the final HRP encapsulation (Figure 2.9). During the rehydration process, the lipids blanketed the surrounding solution to

form liposomes. A rehydration volume ratio of zero, i.e. no incubation time, was not favorable, as this would not give the liposomes time to re-form prior to washing by centrifugation. However, increasing the volume of solution used for rehydration would dilute the HRP concentration within each liposome. The optimal rehydration volume ratio was found to be 0.1.

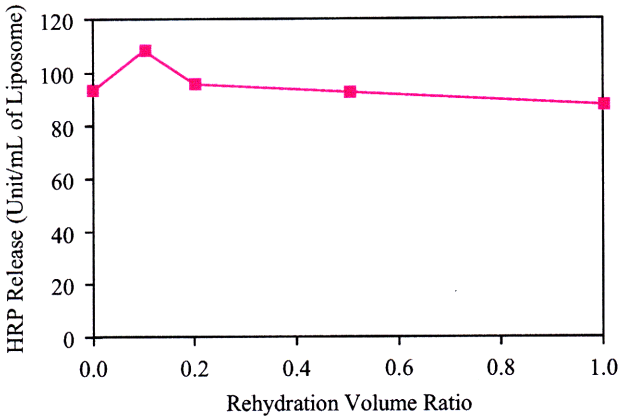

Figure 2.9. Effect of the rehydration volume ratio on the total HRP release after 1 h at 37°C. Liposomes were synthesized with 60 mg/mL of lipid (DPPC:DMPC weight ratio = 2.3), 2 mg/mL of HRP, 30-min sonication, and -20°C freezing.

The HRP release at 37°C could also be tuned by the initial HRP concentration of the solution added to the blank liposomes prior to freezing. Figure **2.10.**2.10 shows that as the HRP concentration in the precursor solution increased, the HRP encapsulated increased. However, above a HRP concentration of 2 mg/mL in the precursor solution, the protein (which also has surfactant properties) would destabilize the liposomes and cause leakage in the membrane, leading to lower HRP encapsulation. Previous research has also shown that the presence of proteins can perturb the lipid bilayer, resulting in leakage of the liposomes' contents [30, 31].

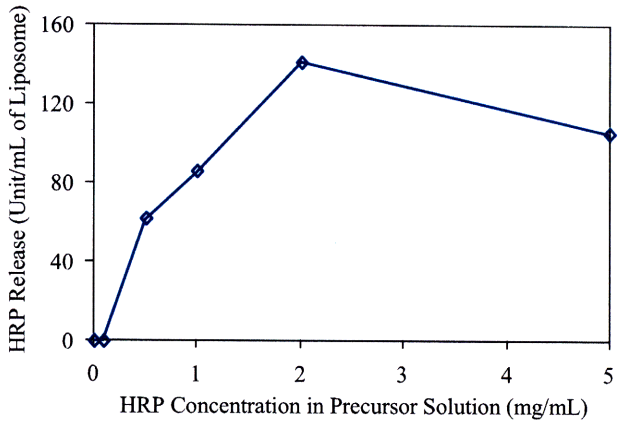

Figure 2.10. Effect of HRP concentration in the precursor solution on the total HRP release after 1 h at 37°C. Liposomes were synthesized with 60 mg/mL of lipid (DPPC:DMPC weight ratio = 2.3), 30-min sonication, -20°C freezing, and rehydration volume ratio = 0.1.

2.3.2 Modulation of Gelation Time

When HRP-containing liposomes were suspended in the HA-Tyr/H_2O_2 solution and heated to 37°C, the elastic modulus, G', began to increase within 3 min, indicating the onset of gelation (Figure 2.11). The gel point was reached in ~ 7 min at 37°C. On the other hand, the solution remained as a liquid for over several hours at 20°C, and the magnitude of G' remained small and constant over time. This behavior and time frame reflected the HRP release observed in Figure **2.3.**2.3.

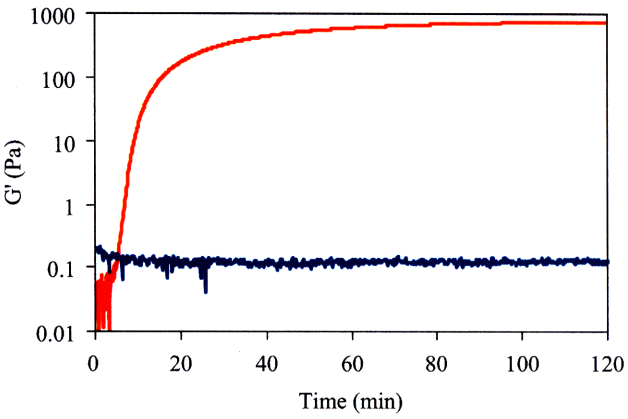

Figure 2.11. G' of HA-Tyr/H_2O_2/HRP liposome solution at (—) 20°C and (—) 37°C. The solution contained 1.7 wt% of HA-Tyr and 20 μL/mL of liposomes. Liposomes were synthesized with 60 mg/mL of lipid (DPPC:DMPC weight ratio = 2.3), 2 mg/mL of HRP, 30-min sonication, -20°C freezing, and rehydration volume ratio = 0.1, and were washed with 0.1 M of $CaCl_2$.

For various clinical needs, gelation times (at both 20°C and 37°C) could be modulated by parameters such as the liposome loading, the HRP concentration in the liposomes, and the HA-Tyr concentration. As the liposome loading increased, gelation time was reduced at both 20°C and 37°C (Figure 2.12). Likewise, as the HRP loading within the liposomes increased, gelation time was also decreased (Figure 2.13). In both cases, the HRP added was increased, thereby reducing the gelation time. In a similar manner, the gel point could be further tuned by adjusting the parameters described in Section 2.3.1 to control the total HRP released from the liposomes. The gelation time could also be adjusted by the concentration of HA-Tyr to vary the Tyr or crosslinking groups in the solution. Figure 2.14 shows that the gelation time decreased as HA-Tyr concentration increased.

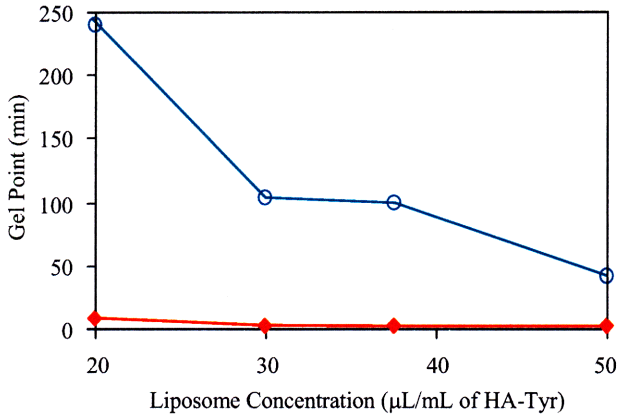

Figure 2.12. Effect of the liposome concentration on the gelation time at (○) 20°C and (♦) 37°C. The solution contained 1.7 wt% of HA-Tyr. Liposomes were synthesized with 60 mg/mL of lipid (DPPC:DMPC weight ratio = 2.3), 2 mg/mL of HRP, 30-min sonication, -20°C freezing, and rehydration volume ratio = 0.1, and were washed with 0.1 M of $CaCl_2$.

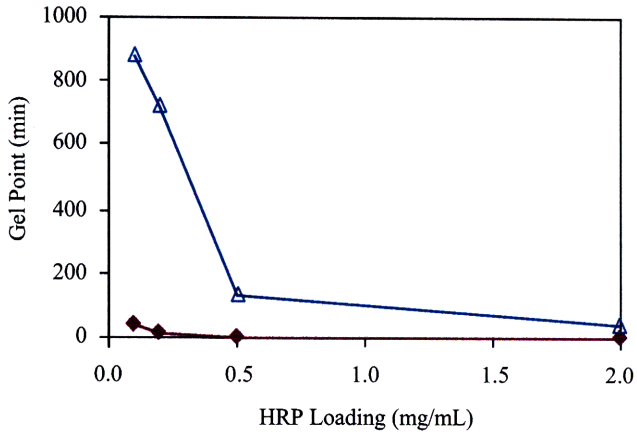

Figure 2.13. Effect of the HRP loading within liposomes on the gelation time at (Δ) 20°C and (♦) 37°C. The solution contained 1.7 wt% of HA-Tyr and 50 μL/mL of liposomes. Liposomes were synthesized with 60 mg/mL of lipid (DPPC:DMPC weight ratio = 2.3), 30-min sonication, -20°C freezing, and rehydration volume ratio = 0.1, and were washed with 0.1 M of $CaCl_2$.

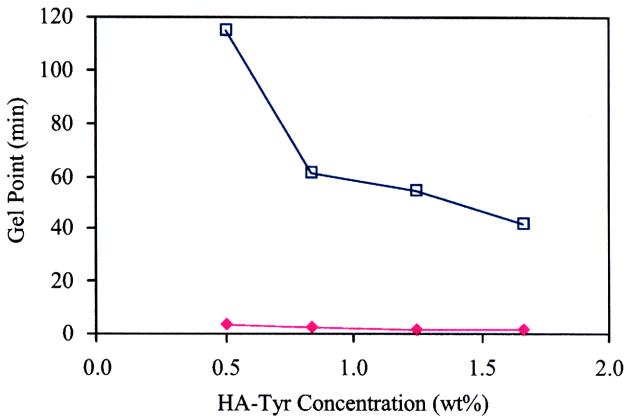

Figure 2.14. Effect of the HA-Tyr concentration on the gelation time at (□) 20°C and (♦) 37°C. The solution contained 50 μL/mL of liposomes. Liposomes were synthesized with 60 mg/mL of lipid (DPPC:DMPC weight ratio = 2.3), 2 mg/mL of HRP, 30-min sonication, -20°C freezing, and rehydration volume ratio = 0.1, and were washed with 0.1 M of $CaCl_2$.

In order to maximize the gelation time at room temperature without compromising the gelation time at 37°C, it was important to select an appropriate solution for rinsing off the liposomes after rehydration. HRP, a natural protein that resides on the cell membrane [32], tends to adhere to liposome membranes [33], and insufficient deactivation of the unencapsulated HRP on the outer liposome membrane would cause prematured gelation at room temperature. Figure **2.15.** 2.15 shows that this deactivation was dependent on the composition of the wash solution used. PBS and H_2O solutions did little to deactivate HRP, resulting in rapid gelation at room

temperature. NaCl gave rise to a small amount of deactivation, but the increase in ionic strength might have helped to control the osmotic stresses and prevent HRP leakage, thereby prolonging the gelation time at 20°C. The divalent cations, in particular Ca^{2+}, led to significant HRP deactivation, resulting in slow gelation at room temperature without a significant increase of gelation time at 37°C. Previous studies have shown that high Ca^{2+} concentration reduces peroxidase activity, and can destabilize and change the native conformation of peroxidases [34, 35]. Gelation time at 37°C was not significantly changed by the wash solutions because the HRP within the liposomes was not affected by the exterior cations, since small, charged ions have low permeability through the lipid membranes [36].

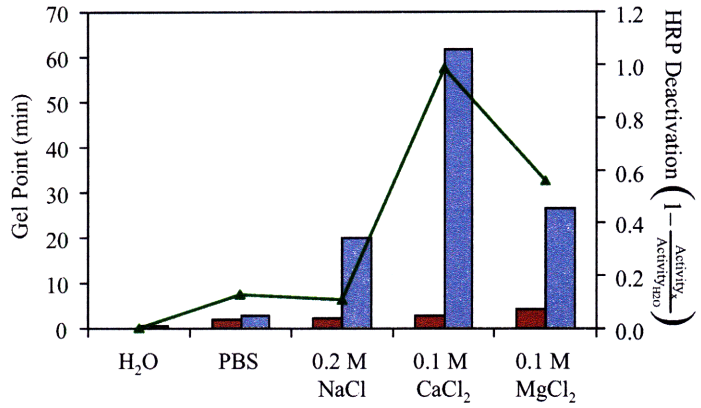

Figure 2.15. Effect of the liposome wash solution on the gel point of HA-Tyr/H_2O_2/HRP liposome mixture at (■) 20°C and (■) 37°C, and (▲) the HRP deactivation in the respective solutions. The solution contained 1.7 wt% of HA-Tyr and 50 μL/mL of liposomes. Liposomes were synthesized with 60 mg/mL of lipid (DPPC:DMPC weight ratio = 2.3), 2 mg/mL of HRP, 30-min sonication, -20°C freezing, and rehydration volume ratio = 0.1.

While $CaCl_2$ was found to best deactivate surface HRP, the gel point was found to be very sensitive to the $CaCl_2$ concentration of the wash solution. Figure 2.16 shows that the gel point at 20°C was maximized at a $CaCl_2$ concentration of ~ 0.1 M. Higher salt concentration would likely result in a hyperosmotic environment, with a flux of water carrying HRP out of the liposomes. The size of liposomes, incubated at various concentrations of $CaCl_2$, is shown in Figure 2.17. The liposome size decreased at $CaCl_2$ concentrations above 0.1 M, indicating liposome shrinkage due to HRP flow out of liposome's aqueous core. This release of HRP then caused premature gelation at room temperature.

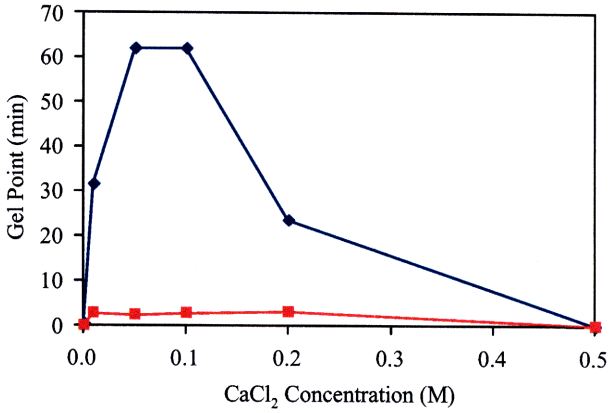

Figure 2.16. Effect of the $CaCl_2$ concentration on the gelation time at (♦) 20°C and (■) 37°C. The solution contained 1.7 wt% of HA-Tyr and 50 μL/mL of liposomes. Liposomes were synthesized with 60 mg/mL of lipid (DPPC:DMPC weight ratio = 2.3), 2 mg/mL of HRP, 30-min sonication, -20°C freezing, and rehydration volume ratio = 0.1.

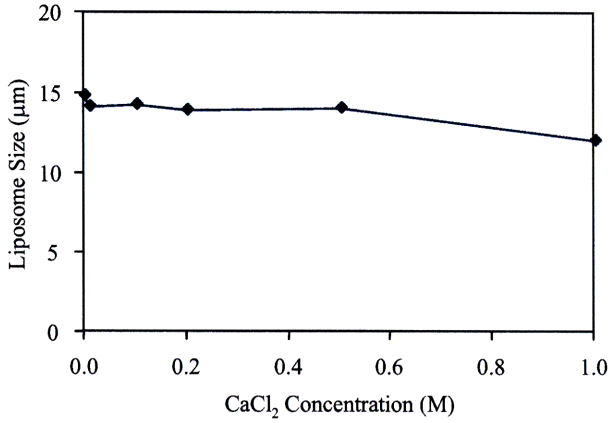

Figure 2.17. Effect of the $CaCl_2$ concentration on the liposome size. Liposomes were synthesized with 60 mg/mL of lipid (DPPC:DMPC weight ratio = 2.3), 2 mg/mL of HRP, 30-min sonication, -20°C freezing, and rehydration volume ratio = 0.1.

The benefit of the HRP liposome system is illustrated in Figure 2.18. As discussed in the Introduction, the working time and mechanical strength of polymer-crosslinker systems are generally modulated by adjusting the crosslinker concentration. For the HA-Tyr system, the working time was gauged by the gel point, while the mechanical strength was characterized by the storage modulus, G'. G' and gel point of the HA-Tyr/H_2O_2/HRP solution were obtained at various HRP concentrations, and an inverse relationship was found for G' and gel point (Figure 2.18). Thus, there was a trade-off between the working time and mechanical strength for the system derived with HA-Tyr/H_2O_2/HRP solution. However, by utilizing thermally triggered

liposomes to encapsulate HRP, the working time could be prolonged without greatly sacrificing the mechanical strength. Figure 2.18 also illustrates an inverse relationship between G' and gel point for the HA-Tyr/H_2O_2/HRP liposomes. However, the gel point for the HA-Tyr/H_2O_2/HRP liposomes was on the order of hours, which was considered well above the required working time (typically on the order of minutes) for injectable materials [37, 38]. To further illustrate, in order to obtain a stiff scaffold with G' of 3000 Pa, clinicians would have less than 30 sec to prepare and inject a HA-Tyr/H_2O_2/HRP solution. In contrast, the use of HA-Tyr/H_2O_2/HRP liposomes would allow for a working time of > 1 h, while maintaining a curing time in the defect site of 2 min.

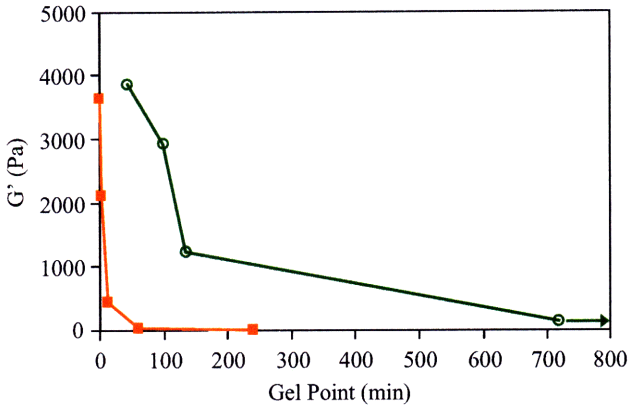

Figure 2.18. Storage modulus vs. the gelation time at 20°C for (■) HA-Tyr/H_2O_2/HRP solution and (○) HA-Tyr/H_2O_2/HRP liposomes. HA-Tyr concentration was 1.7 wt% in PBS. Liposomes were synthesized with 60 mg/mL of lipid (DPPC:DMPC weight ratio = 2.3), 30-min sonication, -20°C freezing, and rehydration volume ratio = 0.1. The HRP concentration in the precursor solution was varied from 0.1 to 2 mg/mL. Liposomes were added at a concentration of 50 μL/mL of HA-Tyr solution. Note: the arrow refers to a gel point longer than 720 min.

2.3.3 Injectability Study In Vivo

In vivo studies were conducted by injecting HA-Tyr/H_2O_2/HRP liposomes subcutaneously in a mouse model. The solution remained a liquid at room temperature, and was injected without difficulty through a syringe. Based on palpitation, the solution cured within 7 min of exposure to body temperature, and an intact gel was harvested upon sacrifice of the mouse (Figure 2.19). This study illustrated that there was no interfering reaction *in vivo* that inhibited the enzyme release or crosslinking reaction.

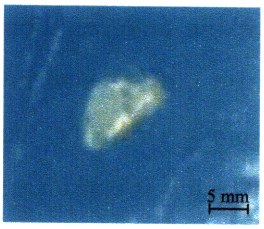

Figure 2.19. Intact gel harvested 2 h after injection. The solution contained 1.7 wt% of HA-Tyr and 20 μL/mL of liposomes. Liposomes were synthesized with 60 mg/mL of lipid (DPPC:DMPC weight ratio = 2.3), 2 mg/mL of HRP, 30-min sonication, and rehydration volume ratio = 0.1.

2.4 Summary

A thermally triggered injectable HA scaffold was created by encapsulating a crosslinking agent, HRP, in thermoresponsive liposomes, which were then suspended in an HA-Tyr solution. At room temperature, HRP was enclosed within the liposomes and prevented from reacting with the polymer. This allowed the system to remain as a liquid and be injected through a syringe. Upon introduction into the defect site and exposure to body temperature, the permeability of the lipid membrane was significantly enhanced, releasing the HRP for reaction with HA-Tyr to form a hydrogel scaffold.

The uniqueness of the system lies in the development of an injectable tissue engineering scaffold through the encapsulation of a crosslinking agent, in particular a protein, within liposomes that have traditionally been employed for drug and gene delivery. Since liposomes are versatile carriers, this platform can potentially be extended to impart temperature sensitivity and injectability to a variety of crosslinking agent-polymer systems, such as α-transglutaminase-collagen, or active catalyst-monomer systems, such as thrombin-fibrin.

The premise that HRP would be released and result in gelation was supported by release studies and gelation kinetic studies. It was shown that the liposomes successfully encapsulated HRP at 25°C. HRP was rapidly released into the environment at 37°C. When the liposomes were suspended in a HA-Tyr solution, rheometry showed that the liposome/polymer solution remained a liquid at room temperature for extended periods, while curing and forming a hydrogel network rapidly at body temperature.

It was critical to optimize the encapsulation of HRP within the liposomes, while retaining the enzymatic activity. The dehydration-rehydration vesicle synthesis was selected so as to avoid exposure of the enzyme to high temperatures and organic solvents that could potentially damage

the peroxidase activity. Parameters influencing liposome fusion during freezing and lyophilization were found to be very important as enhanced liposome fusion would promote HRP encapsulation. Increased lipid concentration and sonication time were shown to increase HRP encapsulation, while increased cholesterol concentration and freezing rate decreased HRP encapsulation. The optimal HRP concentration of the precursor solution added to the blank liposomes was 2 mg/mL. As the amount of HRP added increased, encapsulation increased, but excess HRP would result in liposome destabilization/leakage and reduced HRP encapsulation. The optimal rehydration volume ratio was 0.1, which balanced the need to incubate the re-formed liposomes prior to washing and the excessive dilution of HRP during re-formation.

The gelation times at 20°C and 37°C were controlled by varying parameters, such as the concentration of HRP loaded within the liposomes, the concentration of HRP-loaded liposomes, and the HA-Tyr concentration. By increasing the first two parameters, the concentration of HRP added was effectively increased, decreasing the gelation time. By increasing the HA-Tyr concentration, the crosslinking group was increased, reducing the gelation time.

The most important parameter in managing the gelation time at room temperature was found to be the solution used to wash the liposomes. Since proteins tended to adhere to liposome surface, deactivation of HRP on the exterior of liposomes was crucial in preventing prematured gelation at room temperature. Divalent cations, particularly Ca^{2+}, were shown to be effective in deactivating HRP on the surface. However, excess Ca^{2+} concentration would cause osmotic stresses, resulting in HRP leakage and rapid gelation at room temperature. The optimal Ca^{2+} concentration was found to be ~ 0.1 M.

With an understanding of the optimization of HRP encapsulation and modulation of gelation times, we could design injectable scaffolds with specific gelation kinetics and mechanical properties. For example, to attain a scaffold with a working time of > 2 h and a G' of > 1000 Pa, liposomes were synthesized with a high HRP content (e.g. 0% cholesterol, 60 mg/mL of lipid, 2 mg/mL of HRP), 30-min sonication, -20°C freezing, and 0.1 rehydration volume ratio, and added at a concentration of 30 μL/mL to the HA-Tyr solution. Both working time and G' could be easily tuned by adjusting the HRP loaded within the liposomes, the liposomes added to the solution, and the HA-Tyr concentration. The next chapter describes the application of the HA-Tyr system to cartilage regeneration *in vivo*, and the various factors that affect the rate and quality of tissue synthesis.

2.5 References

[1] Okahata, Y., Noguchi, H., Seki, T., *Macromolecules* **20**, 15–21 (1987).

[2] Lee, Y. M., Ihm, S. Y., Shim, J. K., *et al.*, *Polymer* **36**, 81–85 (1995).

[3] Ito, Y., Nishi, S., Park, Y. S., *et al.*, *Macromolecules* **30**, 5856–5859 (1997).

[4] Okahata, Y., *Acc Chem Res* **19**, 57–63 (1986).

[5] Kono, K., Nishihara, Y., Takagishi, T., *J Appl Polym Sci* **56**, 707–713 (1995).

[6] Griffith, L. G., *Ann NY Acad Sci* **961**, 83–95 (2002).

[7] Diker-Cohen, T., Koren, R., Liberman, U. A., *et al.*, *Ann NY Acad Sci* **1010**, 350–353 (2003).

[8] Scoltock, A. B., Cidlowski, J. A., *Exp Cell Res* **297**, 212–223 (2004).

[9] Michea, L., Ferguson, D. R., Peters, E. M., *et al.*, *Am J Physiol Renal Physiol* **278**, F209–218 (2000).

[10] Hubbell, J. A., *Curr Opin Solid State Mater Sci* **3**, 246–251 (1998).

[11] Okahata, Y., Noguchi, H., Seki, T., *Macromolecules* **19**, 493–494 (1986).

[12] Peng, T., Cheng, Y.-L., *J Appl Polym Sci* **70**, 2133–2142 (1998).

[13] Chu, L.-Y., Park, S.-H., Yamaguchi, T., *et al.*, *Langmuir* **18**, 1856–1864 (2002).

[14] Lasic, D. D., *Handbook of Biological Physics* (Elsevier Science, Amsterdam, 1995).

[15] Messersmith, P. B., Starke, S., *Chem Mater* **10**, 117–124 (1998).

[16] Westhaus, E., Messersmith, P. B., *Biomaterials* **22**, 453–462 (2001).

[17] Taylor, K. M. G., Craig, D. Q. M., in *Liposomes: A Practical Approach*, edited by V. Torchilin and V. Weissig (Oxford University Press, New York, 2003), p. 92–95.

[18] Walde, P., Ichikawa, S., *Biomol Eng* **18**, 143–177 (2001).

[19] Szoka, F., Papahadjopoulos, D., *Annu Rev Biophys Bioeng* **9**, 467–508 (1980).

[20] Szoka, F., Papahadjopoulos, D., *Proc Natl Acad Sci USA* **75**, 4194–4198 (1978).

[21] Batzri, S., Korn, E. D., *Biochim Biophys Acta* **298**, 1015–1019 (1973).

[22] Kirby, C., Gregoriadis, G., *Biotechnology* **2**, 979–984 (1984).

[23] Kurisawa, M., Chung, J. E., Gao, S., *et al.*, *Chem Commun* **34**, 4312–4314 (2005).

[24] Moribe, K., Maruyama, K., Iwatsuru, M., *Int J Pharm* **188**, 193–202 (1999).

[25] Liu, D.-Z., Chen, W.-Y., Tasi, L.-M., *et al.*, *Colloids Surf A Physicochem Eng Asp* **172**, 57–67 (2000).

[26] Liang, X., Mao, G., Ng, K. Y. S., *J Colloid Interface Sci* **278**, 53–62 (2004).

[27] Pagano, R. E., Weinstein, J. N., *Annu Rev Biophys Bioeng* **7**, 435–468 (1978).

[28] Jiang, S., Nail, S. L., *Eur J Pharm Biopharm* **45**, 249–257 (1998).

[29] Carpenter, J. F., Prestrelski, S. J., Arakawa, T., *Arch Biochem Biophys* **303**, 456–464 (1993).

[30] Gennis, R. B., Jonas, A., *Annu Rev Biophys Bioeng* **6**, 195–238 (1977).

[31] Kimelberg, H. K., Papahadjopoulos, D., *J Biol Chem* **246**, 1142–1148 (1971).

[32] Liu, E. H., Lamport, D. T. A., *Plant Physiol* **54**, 870–876 (1974).

[33] Dimitrova, M. N., Matsumura, H., *Colloids Surf B Biointerfaces* **8**, 287–294 (1997).

[34] Orlova, M. A., Chubar, T. A., Fechina, V. A., *et al.*, *Russ Chem Bull* **47**, 505–509 (1998).

[35] Omidiji, O., Okpuzor, J., Otubu, O., *J Sci Food Agric* **82**, 1881–1885 (2002).

[36] Nelson, D. L., Cox, M. M., *Lehninger Principles of Biochemistry* (Worth Publishers, New York, 2000).

[37] Sarvestani, A. S., He, X. Z., Jabbari, E., *Biomacromolecules* **8**, 406–415 (2007).

[38] Wagh, A. S., Primus, C., US 7,083,672 (2006).

Chapter 3 – Cartilage Synthesis in Hyaluronic Acid-Tyramine Constructs

3.1 Introduction

3.1.1 Cartilage

Articular cartilage is a tissue that serves as a shock absorber and lubricant in the joint environment. It is characterized by its low-friction surface and ability to withstand compression, which act together to provide stable movement. These properties are attributed to the unique composition of the tissue. The extracellular matrix (ECM) mainly consists of water (~ 85% of the total weight), collagen (67–86% of the dry weight), and proteoglycans (15–25% of the dry weight) [1, 2]. The collagen fibrils, 95% of which are Type II collagen, form a mesh-like network, through which the proteoglycans are interspersed. The negatively charged glycosaminoglycans (GAGs), including hyaluronic acid (HA), chondroitin sulfate, dermatan sulfate, keratan sulfate, and heparan sulfate, are highly hydrophilic and tend to repel each other while simultaneously complexing with the positively charged collagen fibers. The high water content and strong network lead to the high compressibility and flexibility unique to cartilage [3].

3.1.2 Cartilage Tissue Engineering Scaffolds

When damaged, cartilage has limited reparative ability largely due to the fact that it has a low cell concentration and very little vasculature [4]. It lacks the number of cells to synthesize a sufficient amount of new tissue, and the blood to deliver cells and signaling molecules that promote healing to the defect site. In recent years, tissue engineering has been proposed as a means to introduce these cells and signaling molecules into the defect site in order to enhance the tissue's natural regenerative ability.

As discussed in the Introduction, the scaffold is one of the most important aspects of tissue engineering and must possess several key features: (1) be non-toxic and non-inflammatory, (2) promote cell stability and matrix synthesis, (3) possess interconnecting pores that allow cell migration and tissue growth, (4) be bioresorbable, degrading either during or after healing, (5) be mechanically robust, and (6) be capable of being fabricated to fit the shape of defect sites [5, 6].

Various synthetic and natural scaffold materials have been studied to meet these criteria for cartilage regeneration. Synthetic materials are often chosen because the chemical composition can be tailored for specific chemical and mechanical properties, and because they

can be mass produced. Poly(lactic acid), poly (glycolic acid) and their copolymers have been widely studied as they are biodegradable and FDA approved for use in therapeutic devices [7, 8]. Chondrocytes seeded on these scaffolds have demonstrated cell attachment and proteoglycan synthesis [9, 10]. The disadvantages of these scaffolds lie in their brittleness. Implantation of these materials also require surgery, and the acidic by-products of degradation have been reported to cause local cell necrosis [3, 11, 12]. Alternatively, poly(ethylene glycol) (PEG) derivatives have been investigated as they are relatively inert, and can be modified to be injectable. These scaffolds have been shown to enable cell stability, and facilitate the production of a cartilaginous matrix when implanted *in vivo* [5, 10]. However, as PEG is not naturally biodegradable, the scaffold would never be completely replaced by regenerated tissue.

Natural polymers, on the other hand, have been studied due to their favorable cytocompatibility and bioactivity [9]. Perhaps the most widely used for cartilage regeneration has been collagen, of which cartilage is largely composed. Collagen, in particular Type II collagen, has shown the ability to maintain the chondrocyte phenotype and promote matrix production [5, 13, 14, 15]. The concern with the use of collagen lies in the possibility of an immune response and transfer of pathogens as collagen is generally derived from xenogenic sources [3, 6]. Alginate and agarose are derivatives of algae and kelp, respectively, and are also commonly chosen materials, as they have demonstrated good biocompatibility. Both are linear polysaccharides that have been shown to support the chondrocyte phenotype, and to demonstrate the production of cartilage-specific markers [5]. The limitation of these materials is that both are non-biodegradable in mammals because they are derived from plant sources, and would remain in the defect site indefinitely.

Like collagen, HA is one of the main components of cartilage and was chosen in this study because it is biocompatible, biodegradable and non-immunogenic. Furthermore, its presence has been shown to be important in cartilage function, as the blockage of the CD44 receptor for HA in chondrocytes has been found to induce degradation of the cartilage matrix [16, 17]. However, HA cannot be used as a scaffold in its native form because it is a liquid in solution that cannot form a three-dimensional (3D) structure without modification. Various methods have been explored to achieve HA crosslinking, such as those involving carbodiimides, divinyl sulfones, polyvalent hydrazides, and esterification [18, 19, 20]. However, these reactions require relatively toxic reagents, limiting the ability of scaffold formation in the presence of cells or *in*

situ. In order to enable HA crosslinking to occur under mild conditions, Kurisawa *et al.* developed the HA-tyramine (HA-Tyr) system, in which tyramine groups are conjugated onto the HA backbone [21]. In the presence of H_2O_2 and horseradish peroxidase (HRP), the tyramine groups would react with each other to form a hydrogel scaffold. Because Tyr, peroxidases and H_2O_2 are all natural components of the human body, crosslinking and scaffold formation occur with minimal toxicity. Furthermore, the resulting hydrogel, of which over 98% is water, forms a highly porous network and, as described in Chapter 2, can be made to be injectable, enabling the scaffold to fill the shape of the defect through a minimally invasive procedure.

In this study, chondrocytes were encapsulated within HA-Tyr hydrogels to investigate the potential of the HA-Tyr system as a scaffold for cartilage tissue engineering. As shown in Figure 3.1, cartilage cells, harvested from porcine joints, were suspended in an HA-Tyr/H_2O_2 solution, to which HRP was added to form a hydrogel around the cells. The cell-seeded constructs were then implanted subcutaneously into a mouse model, and harvested at 2, 4 and 8 weeks. As GAG and collagen represent the major dry components of natural cartilage [22], the constructs were evaluated biochemically for GAG content and by histomorphometry for collagen content.

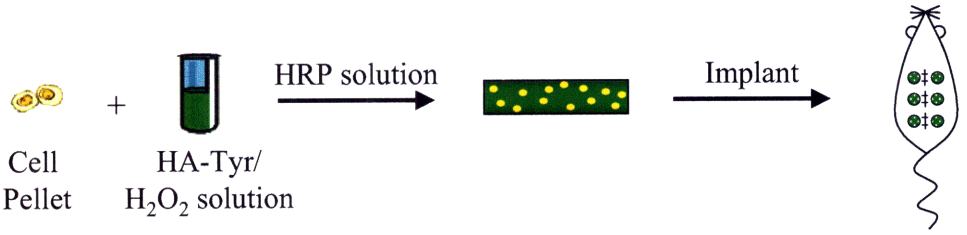

Figure 3.1. Cells were suspended within the HA-Tyr/H_2O_2 solution to form hydrogel disks upon HRP addition. The hydrogel disks were then implanted subcutaneously into a mouse model.

3.2 Experimental

3.2.1 Chondrocyte Isolation

Chondrocytes were isolated from the articular cartilage of the femur, patella and tibia of porcine legs (5–6 months old) that were obtained from the local abattoir. The tissue was cut into small pieces (1 mm^3) and digested in a 0.2 wt% Type 2 collagenase solution (in F-12 medium supplemented with 0.1 M of non-essential amino acids, 0.5 μg/mL of fungizone, 1 wt% of penicillin-streptomycin, and 0.4 mM of L-proline) at 37°C for 12 h. The cell solution was then filtered through a 100-μm strainer and centrifuged (8000g, 10 min) twice with PBS. The

collagenase was purchased from Worthington Biochemical. The F-12 medium, non-essential amino acids and fungizone were purchased from Invitrogen. The penicillin-streptomycin and L-proline were purchased from Sigma-Aldrich.

3.2.2 Toxicity Study

Chondrocytes were seeded in a 96-well plate at 1000 cells/well (n = 5), and maintained at 37°C and 5% of CO_2 in F-12 medium supplemented with 10% of fetal bovine serum (FBS), 0.1 M of non-essential amino acids, 0.5 μg/mL of fungizone, 1 wt% of penicillin-streptomycin, and 0.4 mM of L-proline, which will herein be referred to as "complete medium". HA-Tyr hydrogels (400 μL) prepared with various HA-Tyr, HRP or HRP liposome, and H_2O_2 concentrations were aseptically synthesized, and incubated with 5 mL of complete F-12 medium. HA-Tyr was synthesized as described by Kurisawa *et al.* with 132 kDa HA and 7–8% substitution of tyramine [21]. Liposomes were synthesized as described in Chapter 2 with 60 mg/mL of lipid (DPPC:DMPC weight ratio = 2.3), 2 mg/mL of HRP, 30-min sonication, -20°C freezing, and rehydration volume ratio = 0.1, and were washed with 0.1 M of $CaCl_2$. At each time point, medium was removed from the respective hydrogel tubes, and used to replenish the medium for the chondrocytes. Cell viability was measured with the MTT assay for mitochondrial activity. The MTT assay kit was purchased from ATCC.

3.2.3 Subcutaneous Implantation of HA-Tyr Constructs

Chondrocytes were suspended in a sterile-filtered HA-Tyr (dissolved in complete medium) and H_2O_2 (5 wt%, 5 μL per 25 mg of HA-Tyr) solution. 50 μL of the HA-Tyr/H_2O_2/chondrocyte solution were combined with 5 μL of HRP (0.125 mg/mL), and placed in a mold to create a cylindrical gel with a diameter of 8 mm and a thickness of ~ 1 mm. The gels (n = 6) were then implanted subcutaneously in the dorsum of SCID mice, which were sacrificed at weeks 2, 4 and 8. Chondrocytes used for implantation were encapsulated immediately post-harvest, and each experiment, i.e. each graph shown, was conducted with one set of chondrocytes harvested from an individual pig.

3.2.4 Histology

Harvested constructs were fixed in formalin for at least 24 h. The constructs (n = 2) were then paraffin-embedded and stained with Safranin O and Masson's Trichrome. Masson's Trichrome was purchased from Richard-Allan Scientific. Safranin O and Fast Green were purchased from Alfa Aesar.

Histomorphometry was performed on sections stained with Masson's Trichrome to quantify collagen content. Digital images were acquired at the same brightness and exposure time on an Olympus DP71 camera mounted on an Olympus BX51 microscope. Images were then split into red, green and blue (RGB) planes on Image J software, and the data were loaded onto Matlab. To measure the blue intensity of the sections, a method similar to that developed by Martin *et al.* was employed [23]. For each pixel, the blue fraction, B_F, was defined as $B_F = B/(R+G+B)$. B_F was then normalized to $B_{F,N}$, where $B_{F,N}$ was set to 0 if $B_F < 0.38$ and if $R/G < 0.98$. This eliminated pixels that were either not stained blue or were stained purple (the nuclei). All other pixels were proportionally scaled from 0 to 1, i.e. $B_{F,N} = \frac{1}{1-0.38}B_F - \frac{0.38}{1-0.38}$. The blue content for each pixel was then calculated as $B_C = B_F * B_{F,N}$, and the blue content of the image ($\overline{B_C}$) was calculated as the average of all pixels in the image. Results were reported as a percentage of the blue content of natural porcine articular cartilage stained at the same time, so as to account for variations in staining procedure and reagents. Three sections of each sample were stained, and four to five images were taken of each section. Images shown represent the average.

Immunohistochemistry was performed by deparaffinizing and rehydrating tissue sections. The sections were then enzymatically treated with hyaluronidase (2%) for 30 min and trypsin (4%) for 30 min at room temperature. Non-specific binding was then blocked by incubating sections with horse serum (5%) for 1 h at room temperature. The primary antibody (monoclonal mouse anti-Type II collagen) was then added at a concentration of 10 μg/mL overnight. After incubating with the secondary antibody (goat anti-mouse IgG-FITC) at 20 μg/mL for 1 h at room temperature and then 4',6-diamidino-2-phenylindole (DAPI) for 10 min, the slides were mounted. Porcine articular cartilage was used as a positive control, and porcine fibrocartilage, which mainly consisted of Type I collagen, was used as a negative control. Hyaluronidase and trypsin were purchased from Sigma-Aldrich. Horse serum, the secondary antibody and DAPI were obtained from Invitrogen. The primary antibody was purchased from Chondrex.

3.2.5 GAG Quantification

Harvested constructs (n = 4) were sonicated with a probe-tip sonicator for 40–60 sec, and then digested in papain (0.125 mg/mL in 100 mM of phosphate buffered saline (PBS) solution, 10 mM of ethylenediaminetetraacetic acid (EDTA) and 10 mM of cysteine) at 60°C for 15 h. Digested constructs were filtered through a 0.45-μm syringe filter, and the GAG concentration was calorimetrically determined by the Blyscan dimethylmethylene blue assay. Papain was purchased from Worthington, PBS was purchased from EMD Biosciences, EDTA and cysteine were purchased from Sigma, and the Blyscan reagents were purchased from Biocolor.

3.2.6 Statistics

Graphs of GAG and blue content were depicted as mean ± standard deviation. Two-factor analysis of variance (ANOVA) was conducted to determine whether significance existed at $p < 0.05$. Tukey post hoc analysis was also performed to determine whether there was significance at $p < 0.05$ between experimental groups. Calculations were conducted on Matlab.

3.2.7 Degradation Study

Hydrogels were synthesized by mixing 1 mL of HA-Tyr and collagen at various concentrations, with H_2O_2 (5 wt%, 5 μL per 25 mg of HA-Tyr) and 100 μL of HRP (0.125 mg/mL). The mixture was quickly pipetted between two glass plates, which were separated by a 0.75-mm spacer, and allowed to set for 1 h. Hydrogel disks (1 cm-diameter) were cut out with a punch, and placed in complete medium to swell overnight. The hydrogels were then placed in a hyaluronidase solution (125 Units/mL in complete medium), and the wet weight was measured over time. Bovine testicular hyaluronidase was purchased from Sigma.

3.2.8 Incorporation of Collagen

Type II collagen (5 μg/mL in 0.1 M of acetic acid) was incorporated into the hydrogels by mixing the collagen solution with an HA-Tyr solution (0.5 wt% in PBS), and incubating the mixture overnight at room temperature. H_2O_2 (5 wt%, 5 μL per 25 mg of HA-Tyr) and HRP (0.125 mg/mL) were then added. The resulting hydrogel's stiffness, measured by the storage modulus, G', was evaluated by oscillatory rheometry at 37°C on a ThermoHaake Rheoscope 1

with a 25-mm, 1° titanium cone at 1% strain at a frequency of 1.0 Hz. Bovine Type II collagen was purchased from AbD Serotec.

Chondrocytes were encapsulated as described in Section 3.2.3. The constructs were composed of HA-Tyr (0.5 wt%), sterile-filtered Type II collagen, H_2O_2 (5 wt%, 5 μL per 25 mg of HA-Tyr), HRP (0.125 mg/mL), and 50×10^6 cells/mL. HA-Tyr/collagen/H_2O_2/HRP/ chondrocyte constructs were implanted subcutaneously in mice.

3.2.9 Comparison with Other Scaffolds

Chondrocytes were suspended in steam-sterilized low melting point agarose (2 wt%). Agarose was heated until it became a liquid, and was allowed to cool to ~ 37°C, upon which cells were added to achieve a concentration of 50×10^6 cells/mL. The solution was pipetted into cylindrical molds (50 μL, 8 mm in diameter, ~ 1 mm in thickness), and solidification occurred as the mixture further cooled to room temperature. Agarose was purchased from Invitrogen.

Alginate/chondrocyte constructs were created by combining steam-sterilized alginate (1.5 wt%) with a cell suspension to arrive at a final cellularity of 50×10^6 cells/mL. The mixture was then added drop-wise (50 μL) to a sterile-filtered $CaCl_2$ solution (0.1 M) to form hydrogel beads. Alginate was purchased from Sigma.

Chondrocytes in solution were injected through a 21-gauge needle into the mid-line of pre-cut Helistat® sponges (50 μL, 3 mm × 6 mm × 5 mm sponges) to achieve a final cell concentration of ~ 50×10^6 cells/mL. Helistat® sponges were purchased from Integra LifeSciences.

All constructs were implanted subcutaneously in SCID mice as described in Section 3.2.3.

3.2.10 Incorporation of Liposomes

Liposomes were aseptically synthesized as described in Section 3.2.2. The HRP release at 37°C was measured to be 90 Units/mL of liposome. HRP-encapsulated liposomes were combined at 30 μL/mL with a solution of HA-Tyr (0.5 wt%), Type II collagen (0.05 wt%), H_2O_2 (5 wt%, 3 μL/mL) and chondrocytes (50×10^6 cells/mL). The mixture was added drop-wise (50 μL) onto a temperature-controlled plate (Leica HI 1220) set at 37°C to form hydrogel disk constructs. HRP activity was assessed by the Amplex Red Assay for peroxidase activity.

In order to compare with the above, 50 μL of a solution of HA-Tyr (0.5 wt%), Type II collagen (0.05 wt%), H_2O_2 (5 wt%, 3 μL/mL) and chondrocytes (50×10^6 cells/mL) were

combined with 5 μL of HRP (30 Units/mL). As an additional comparison, constructs were synthesized by combining 50 μL of a solution of HA-Tyr (0.5 wt%), Type II collagen (0.05 wt%), H_2O_2 (5 wt%, 3 μL/mL), chondrocytes (50×10^6 cells/mL), and a blank liposome (30 μL/mL) solution with 5 μL of HRP (30 Units/mL). Blank liposomes were synthesized in the same manner as the HRP-encapsulated liposomes, except that water instead of HRP solution was added prior to freeze drying.

3.2.11 Injection Studies

Liposomes, as described in Section 3.2.10, were combined at 30 μL/mL (90 Units/mL of liposome) with a solution of HA-Tyr (0.5 wt%), Type II collagen (0.05 wt%), H_2O_2 (5 wt%, 4 μL/mL) and chondrocytes (50×10^6 cells/mL). The precursor solution (100 μL, n = 6) was then injected subcutaneously in SCID mice.

3.3 Results and Discussion

3.3.1 Toxicity Studies

In order to evaluate the safety of the HA-Tyr system for application to cartilage regeneration, the materials were first tested for cytotoxicity *in vitro*. Hydrogels were incubated in complete medium, which was subsequently used to culture chondrocytes seeded on a plate. The cell number at each time point was measured, and compared to that of cells cultured in medium without HA-Tyr hydrogels. Figures 3.2–3.4 show that within the hydrogel concentration ranges examined, the presence of HA-Tyr, H_2O_2 and HRP within the hydrogels had little effect on cell viability and growth over 7 days, and were therefore non-cytotoxic. Figure 3.5 shows the effect of hydrogels that were formed by the thermally triggered release of HRP from HRP-encapsulated liposomes. It was found that the use of HRP liposomes as well as the further addition of blank liposomes did not affect cell viability, demonstrating that neither the means of HRP delivery nor the presence of DPPC and DMPC in the form of liposomes resulted in toxicity.

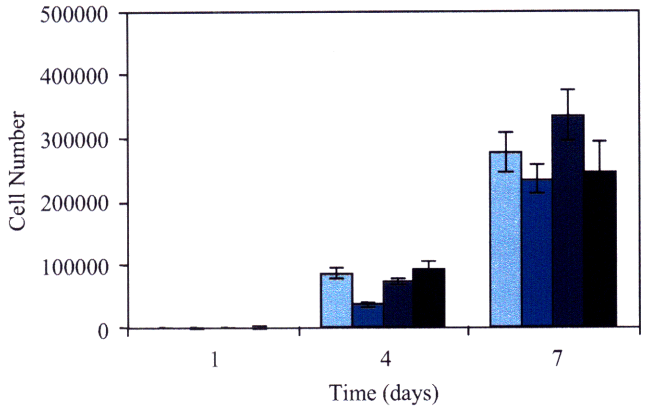

Fig 3.2. Cell viability of culture (■) with untreated medium, and with medium conditioned with hydrogels composed of 0.5 μM of H_2O_2, 10 μg/mL of HRP, and (■) 1.3 wt%, (■) 2.5 wt% and (■) 3.3 wt% of HA-Tyr.

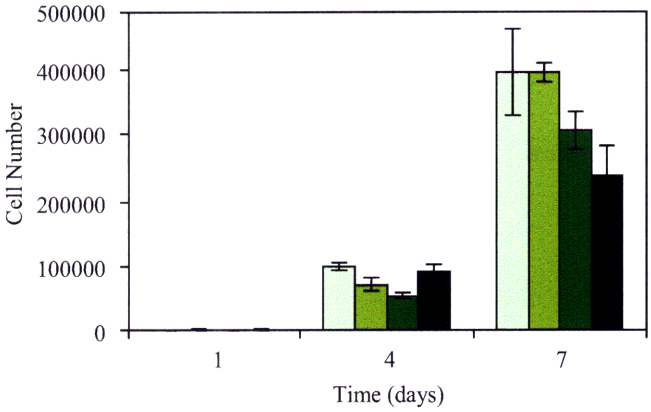

Fig 3.3. Cell viability of culture (■) with untreated medium, and with medium conditioned with hydrogels composed of 1.7 wt% of HA-Tyr, 10 μg/mL of HRP, and (■) 0.5 μM, (■) 4 μM and (■) 10 μM of H_2O_2.

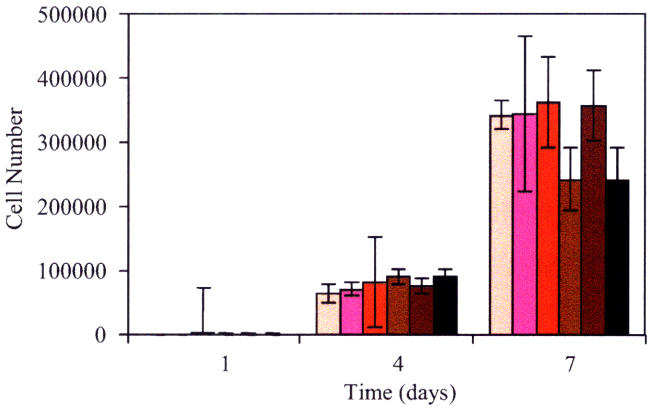

Fig 3.4. Cell viability of culture (■) with untreated medium, and with medium conditioned with hydrogels composed of 1.7 wt% of HA-Tyr, 0.5 μM of H_2O_2, and (■) 10 μg/mL, (■) 23 μg/mL, (■) 45 μg/mL, (■) 90 μg/mL and (■) 180 μg/mL of HRP.

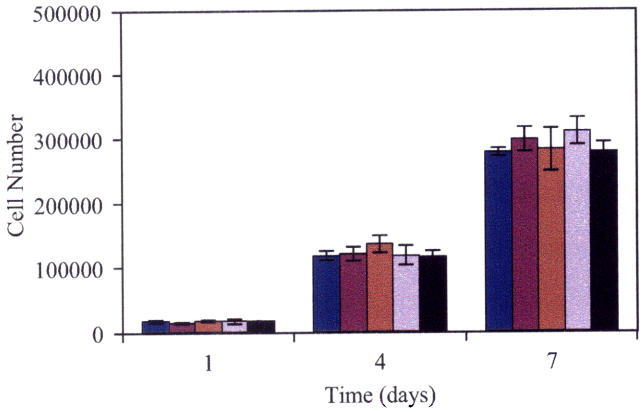

Figure 3.5. Cell viability of culture (■) with untreated medium, and with medium conditioned with hydrogels composed of 1.7 wt% of HA-Tyr, 0.5 μM of H_2O_2, and (■) 30 μL/mL of HRP liposomes, (■) 30 μL/mL of HRP liposomes + 10 μL/mL of blank liposomes, (■) 30 μL/mL of HRP liposomes + 20 μL/mL of blank liposomes and (■) 30 μL/mL of HRP liposomes + 30 μL/mL of blank liposomes.

3.3.2 Implantation of Cell-Seeded Scaffolds

Chondrocytes isolated from porcine joints were encapsulated within HA-Tyr hydrogel scaffolds, and implanted subcutaneously in SCID mice. As illustrated in Figure 3.6, natural chondrocytes have an ovoid to round shape with small, acentric nuclei. They are responsible for secreting the ECM, and are immobilized in isogenous groups of 2–4 cells, which arise from the mitosis of a single cell. Chondrocytes encapsulated in the HA-Tyr scaffolds displayed similar morphologies as well as isogenous groups, demonstrating that this system promoted chondrocyte stability and proliferation.

The cartilage matrix is mainly composed of GAG and collagen, and appears amorphous and smooth with an invisible network of collagen fibers [24]. Because of the high concentrations of acidic sulfhydryl and carboxyl groups, the matrix is basophilic, particularly in the territorial matrices immediately around the cells, which stain more richly in basic dyes such as Safranin O [25, 26, 27, 28]. Figure 3.6 shows that significant GAG and collagen were produced within HA-Tyr/H_2O_2/HRP/chondrocyte constructs over 8 weeks, and that, of the collagen, the majority appeared to be composed of Type II collagen, one of the defining characteristics of articular cartilage. Furthermore, the dense matrix synthesized resembled that of natural cartilage, with a ground glass appearance and more intense staining for Safranin O immediately adjacent to the cells. The GAG content of natural porcine articular cartilage was measured to be ~ 3% of the wet

weight, while that produced in the HA-Tyr/chondrocyte constructs was found to be ~ 1.2 wt% after 8 weeks; the collagen content, based on histomorphometry, reached ~ 40% that of natural cartilage over 8 weeks. Observing constructs over longer periods would likely show further GAG and collagen production, approaching the natural composition. This difference might have also been due to the fact that the HA-Tyr constructs were implanted ectopically. Constructs implanted in the joint would be exposed to the joint fluid and mechanical forces important to cartilage development, and therefore produce matrix components further resembling natural cartilage.

As a point of comparison, HA-Tyr scaffolds that did not contain any cells were also implanted *in vivo*, and they showed no sign of cells or matrix deposition, as verified by GAG quantification and histology (Figure 3.6). Therefore, the GAG and collagen produced were attributed to the presence of chondrocytes within the scaffolds.

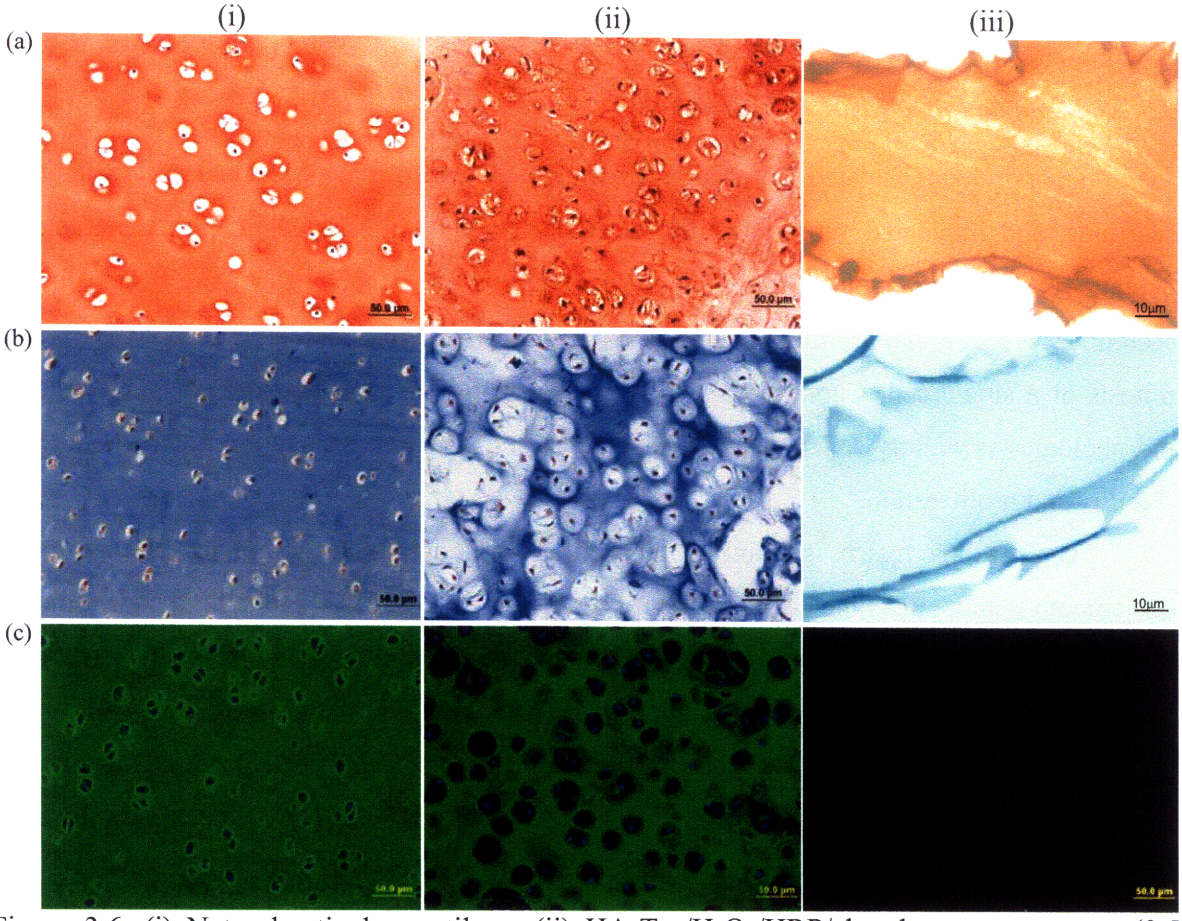

Figure 3.6. (i) Natural articular cartilage, (ii) HA-Tyr/H_2O_2/HRP/chondrocyte constructs (0.5 wt% HA-Tyr, 50×10^6 cells/mL), and (iii) HA-Tyr/H_2O_2/HRP constructs (0.5 wt% HA-Tyr) at Week 8 stained by (a) Safranin O for GAG and (b) Masson's Trichrome for collagen, and (c) immunostained for Type II collagen.

3.3.3 *Effect of Crosslink Density and Degradation Rate*

For tissue engineering scaffolds, the degradation rate is an important consideration. Based on the idea of isomorphous replacement, the scaffold degradation rate should match the tissue synthesis rate [5, 29, 30]. Therefore, in optimizing the HA-Tyr system for cartilage production, various degradation rates were examined. HA mainly degraded via cleavage of the glycosidic bonds by hyaluronidase, which was produced by chondrocytes as a means of tissue remodeling [31, 32]. In order to vary the degradation rate, the hydrogels were crosslinked to different degrees by adjusting the HA-Tyr concentration. As the HA-Tyr concentration increased, the number of tyramine groups and crosslink points was effectively increased, and the degradation rate of the scaffold decreased (see Figure 3.7).

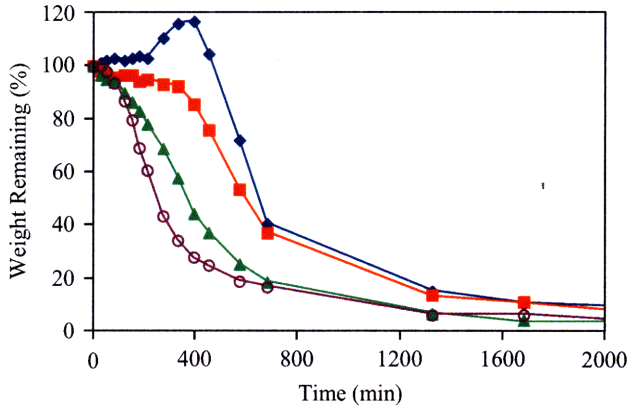

Figure 3.7. Degradation of HA-Tyr/H_2O_2/HRP hydrogel with (○) 0.5 wt%, (▲) 0.8 wt%, (■) 1.3 wt% and (♦) 1.7 wt% of HA-Tyr in hyaluronidase solution.

The effect of the degradation rate *in vivo* was then studied by implanting subcutaneously HA-Tyr/H_2O_2/HRP/chondrocyte scaffolds at various HA-Tyr concentrations. In order to control the response of the cells to the presence of HA, 64 kDa HA was added to maintain a constant HA concentration, creating a semi-interpenetrating network. Low molecular weight HA was chosen to enable rapid diffusion of HA out of the scaffold pores, facilitating rapid degradation at low HA-Tyr concentrations. Figure 3.8 shows that as HA-Tyr concentration decreased and degradation rate increased, GAG production within the constructs increased. At lower HA-Tyr concentrations, histological sections in Figures 3.9 also showed larger areas of collagen secreted by cells and greater collagen content, measured by the overall blue content. The trend could be explained as follows: (1) rapid degradation created more space for the cells to synthesize matrix

components, (2) lower crosslink densities enhanced diffusion of nutrients and oxygen, (3) lower crosslink densities, and therefore softer materials, allowed chondrocytes within the scaffold to contract, resulting in dynamic pore reduction (DPR) during which the intercellular space decreased and the effective cell density increased, promoting chondrogenesis [33], and (4) rapid degradation produced higher concentrations of low molecular weight HA, which have been known to induce cytokine activity and stimulate ECM turnover [18].

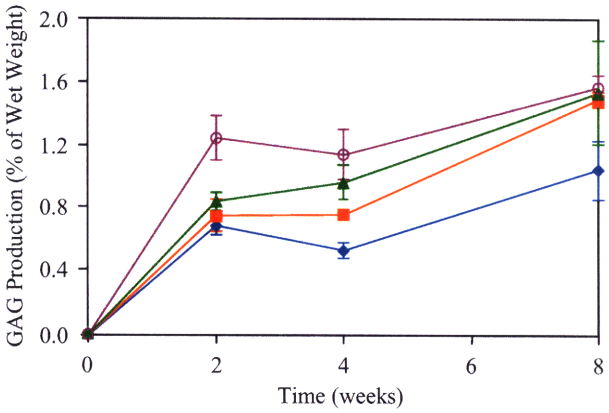

Figure 3.8. GAG production within HA-Tyr/H_2O_2/HRP/chondrocyte constructs with (○) 0.5 wt%, (▲) 0.8 wt%, (■) 1.3 wt% and (♦) 1.67 wt% of HA-Tyr, and 50×10^6 cells/mL.

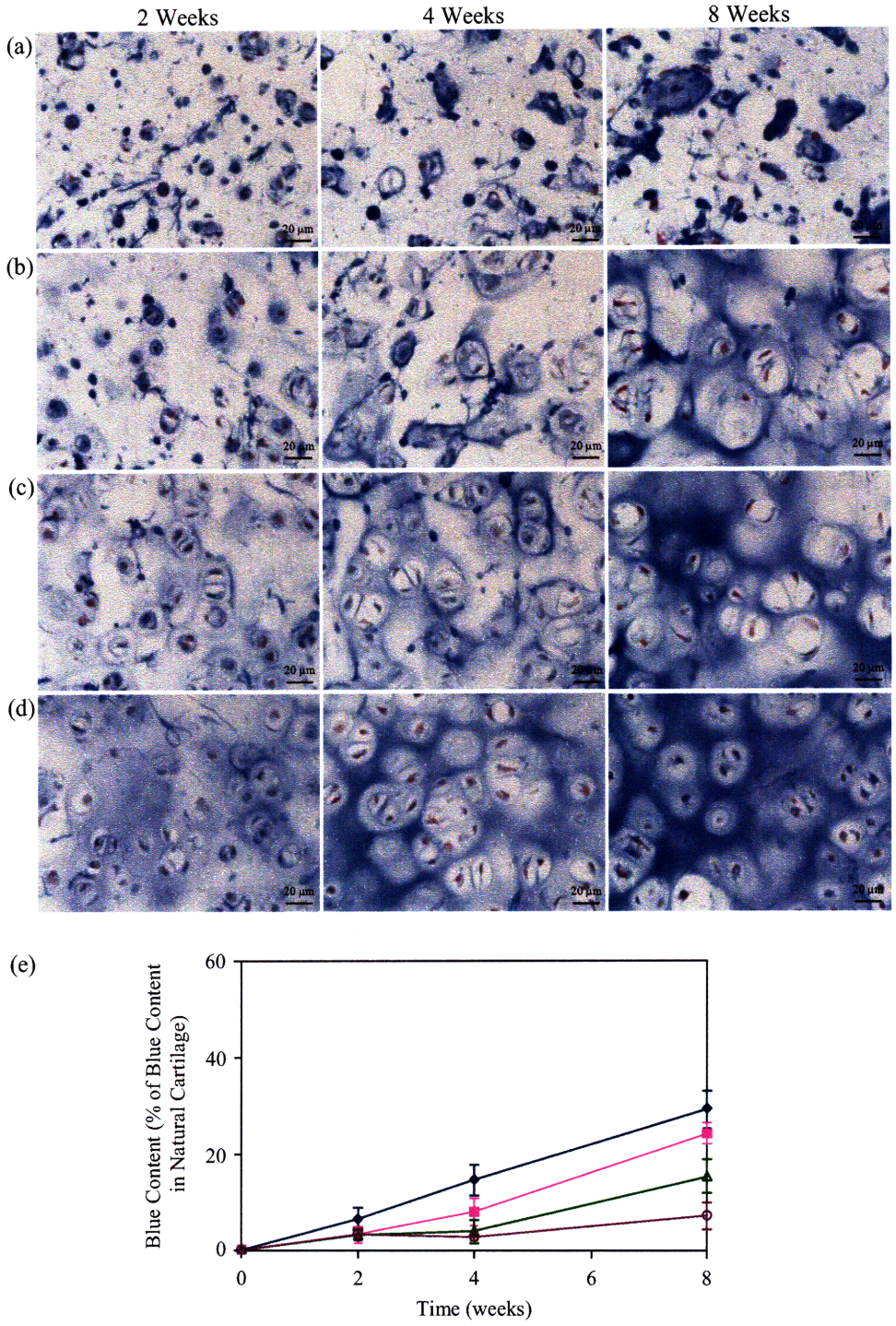

Figure 3.9. (a–d) Masson's Trichrome staining for collagen and (e) quantification of blue content within HA-Tyr/H_2O_2/HRP/chondrocyte constructs with (a, ♦) 0.5 wt%, (b, ■) 0.8 wt%, (c, Δ) 1.3 wt% and (d, ○) 1.7 wt% of HA-Tyr, and 50×10^6 cells/mL.

3.3.4 Effect of Collagen Incorporation

Though rapid degradation was shown to be favorable for cartilage generation, the scaffold should also not be too soft, as cartilage is a structural tissue and must be able to withstand the physiological stresses within the joint. Therefore, it was proposed that Type II collagen, which is rapidly resorbed *in vivo*, be incorporated into the scaffold to increase its mechanical strength without decreasing degradation rate. The anionic HA can form a polyionic complex with cationic collagen, and in natural cartilage, this interaction provides mechanical strength to the tissue [34]. Figure 3.10 shows that incorporating small amounts of collagen into the HA-Tyr hydrogels increased the scaffold mechanical stiffness, measured by G'. The maximum G' was achieved with 0.05 wt% of collagen, whose value was more than double of that without collagen. Further addition of collagen, however, resulted in phase separation and eventual precipitation of the complex, and therefore lower mechanical strength.

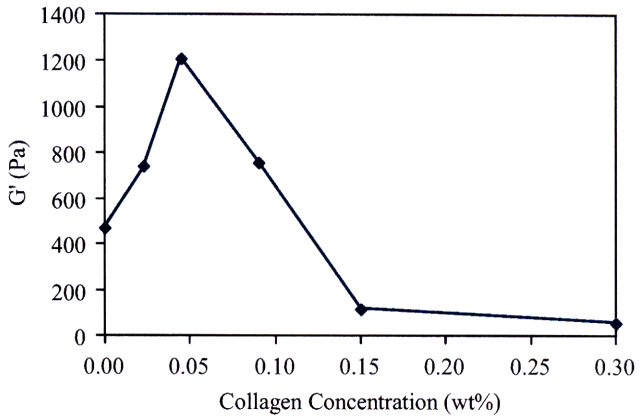

Figure 3.10. Effect of collagen incorporation on the G' of HA-Tyr/collagen/H_2O_2/HRP hydrogels with 0.5 wt% of HA-Tyr.

Despite increasing the mechanical strength, Figure 3.11 shows that 0.05 wt% and 0.10 wt% of collagen did not significantly affect the degradation rate of the hydrogels in hyaluronidase solution. This suggested that low concentrations of collagen did not inhibit the diffusion of hyaluronidase into the hydrogel or block the hyaluronidase binding sites on the HA chain.

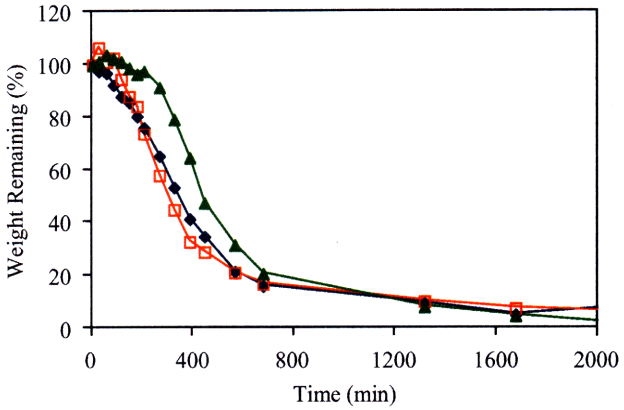

Figure 3.11. Degradation of HA-Tyr/H_2O_2/HRP hydrogels with 0.5 wt% of HA-Tyr and (♦) 0 wt%, (□) 0.05 wt% and (▲) 0.10 wt% of Type II collagen in hyaluronidase.

HA-Tyr/collagen/H_2O_2/HRP/chondrocyte constructs were implanted *in vivo* to study the effect of collagen on cartilage regeneration. Type II collagen is one of the major components of cartilage, and chondrocytes are known to have a cell surface protein, Annexin V, that binds Type II collagen and anchors the cell onto the ECM [35]. Type II collagen has also been shown to stabilize the chondrocyte morphology, as well as improve GAG and protein production within cartilage scaffolds [14, 15]. Figure 3.12 shows that a collagen concentration of 0.05 wt% within the hydrogels enhanced GAG production over that without collagen at Weeks 2 and 4, but that the two experimental groups had become almost similar by Week 8. Figure 3.13, on the other hand, shows a more delayed effect, where statistically greater collagen production within the 0.05 wt% constructs was not observed until Weeks 4 and 8. Type II collagen was insoluble in water and was dissolved in dilute acetic acid, and collagen concentrations of $\geq$ 0.10 wt% resulted in an overall acetic acid concentrations of $\geq$ 20 mM within the hydrogel. Figures 3.12–3.13 suggest that these concentrations of acetic acid inhibited both GAG and collagen production. The histological sections clearly showed that the majority of cells within constructs with 0.24 wt% of collagen had died. The cells appeared almost as shadows, and did not take up the hematoxylin dye, which would normally stain for nuclei.

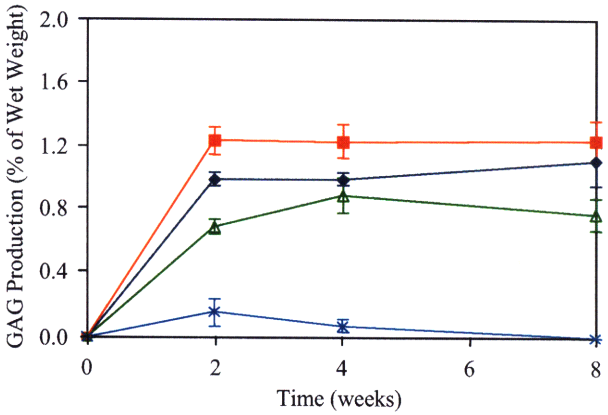

Figure 3.12. GAG production within HA-Tyr/collagen/H_2O_2/HRP/chondrocyte constructs with 0.5 wt% of HA-Tyr, 50×10^6 cells/mL, and (♦) 0 wt%, (■) 0.05 wt%, (Δ) 0.10 wt% and (×) 0.24 wt% of Type II collagen.

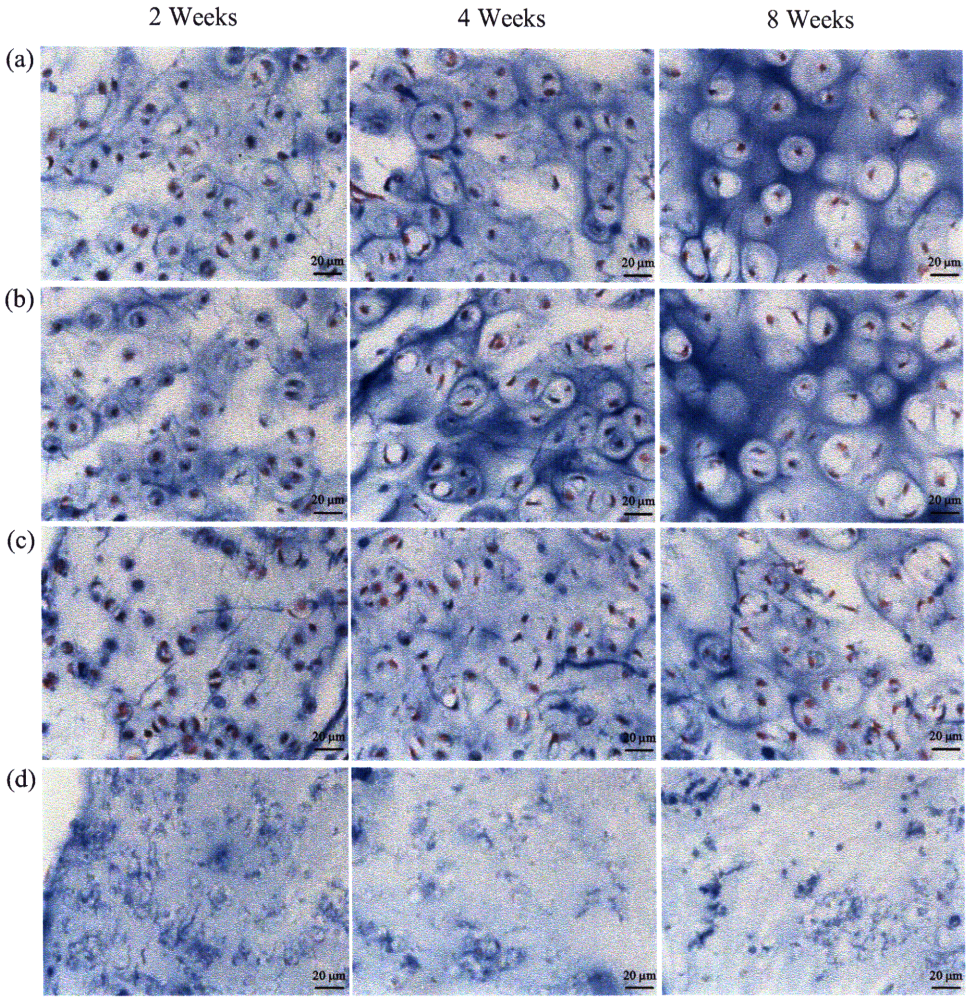

(e)

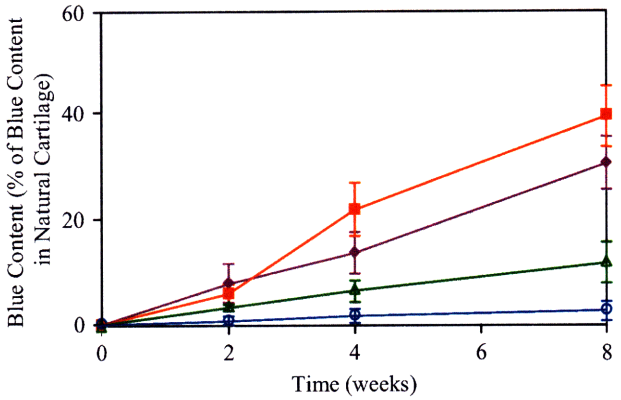

Figure 3.13. (a–d) Masson's Trichrome staining for collagen and (e) quantification of blue content within HA-Tyr/collagen/H_2O_2/HRP/chondrocyte constructs with 0.5 wt% of HA-Tyr, 50×10^6 cells/mL, and (a, ♦) 0 wt%, (b, ■) 0.05 wt%, (c, Δ) 0.10 wt% and (d, ○) 0.24 wt% of Type II collagen.

3.3.5 Effect of Cell Concentration

The seeding density of chondrocytes within the scaffold was also found to be important in determining the rate of tissue synthesis. The natural chondrocyte concentration in human cartilage is estimated to be $11–27\times10^6$ cells/mL [36]. Therefore, in staying near this range, cellularities of 20×10^6, 50×10^6 and 100×10^6 cells/mL were tested in the HA-Tyr scaffolds. Figures 3.14–3.15 show that as the cell concentration increased, GAG and collagen production within the scaffold increased. Higher cellularities were expected to improve construct composition because the more cells were incorporated, the more means for tissue synthesis. High cell concentrations have also been shown to promote cell-cell and cell-matrix interactions, which would be important in maintaining cell phenotype and increasing GAG and collagen production [37, 38]. Though a high cell concentration would be beneficial in promoting early healing, the levels of GAG and collagen content for the 100×10^6 cells/mL constructs approached that of the 50×10^6 cells/mL constructs by Week 8. This might be due to the increased density of the construct as matrix components were deposited. The increased density might have prevented sufficient diffusion of nutrients and oxygen to support cell concentrations as high as 100×10^6 cells/mL, and therefore impacted the rates of biosynthesis.

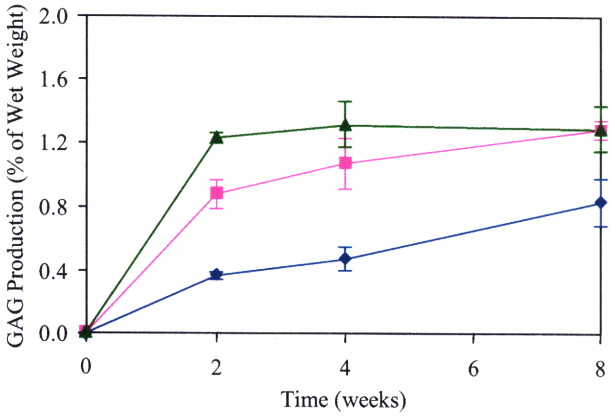

Figure 3.14. GAG production within HA-Tyr/collagen/H_2O_2/HRP/chondrocyte constructs with 0.5 wt% of HA-Tyr, 0.05 wt% of Type II collagen, and (♦) 20×10^6 cells/mL, (■) 50×10^6 cells/mL and (▲) 100×10^6 cells/mL.

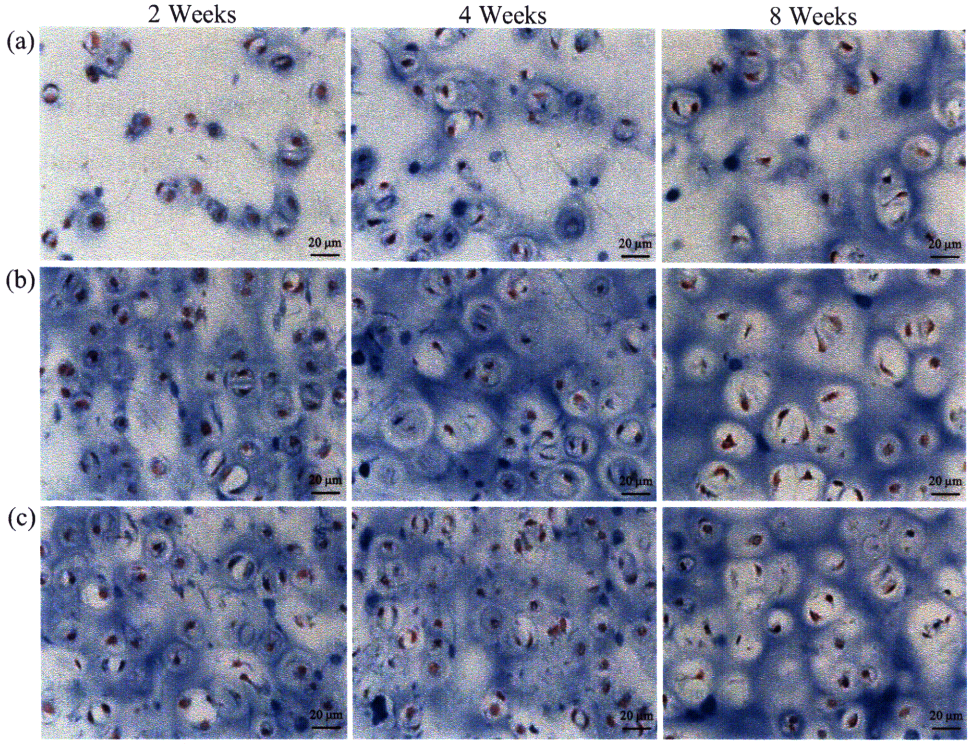

(d)

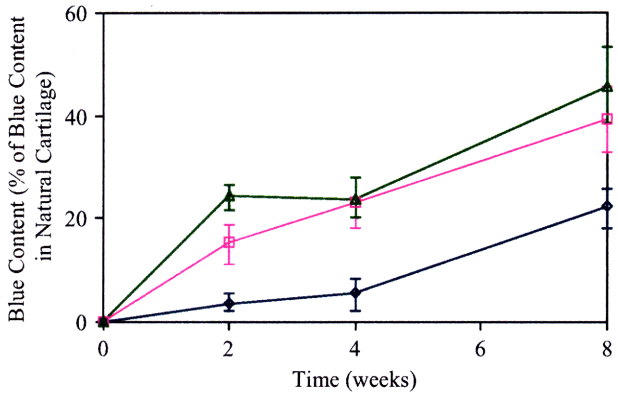

Figure 3.15. (a–c) Masson's Trichrome staining for collagen and (d) quantification of blue content within HA-Tyr/collagen/H_2O_2/HRP/chondrocyte constructs with 0.5 wt% of HA-Tyr, 0.05 wt% of Type II collagen, and (a, ◊) 20×10^6 cells/mL, (b, □) 50×10^6 cells/mL and (c, Δ) 100×10^6 cells/mL.

3.3.6 Effect of Material on Cartilage Regeneration

To compare the HA-Tyr system to other scaffold materials, chondrocytes were seeded in various commonly used natural biomaterials for cartilage tissue engineering. An HA-Tyr concentration of 0.5 wt% and Type II collagen concentration of 0.05 wt% was chosen because it showed the best GAG and collagen production. Agarose and alginate were selected based on previous studies showing positive results for cartilage phenotype and matrix production [39]. Helistat® sponges are commercially available Type I collagen scaffolds, and were chosen because they are clinically used and have been investigated for implantation in joint defects [40]. Figure 3.16 shows that GAG production within agarose, alginate and HA-Tyr were comparable throughout the 8 weeks; for most time points, the differences were not statistically significant ($p < 0.05$). In contrast, Figure 3.17 illustrates that collagen levels were greater in HA-Tyr scaffolds than in alginate and agarose. Similarity in GAG production was not unexpected since all three materials are linear polysaccharides with similar chemical structures. Collagen production, on the other hand, might be more sensitive to the specific polymer composition of the scaffold, and HA-Tyr, being native to cartilage, might have been more conducive to collagen synthesis.

In contrast, GAG production within the Helistat® sponge was lower than that of the other scaffolds and decreased over time. This was likely due to the fact that this scaffold was made up of Type I collagen, as opposed to Type II collagen of which articular cartilage is mainly composed. As previously shown, the chondrocytic phenotype tended to be less stable in Type I

than in Type II collagen sponges [13], and this could have led to decreased production of GAG. In addition, the histological sections in Figure 3.17, although staining heavily for collagen, show the production of a visibly fibrous matrix that did not have the finely, granular makeup of natural articular cartilage. It was improbable that these fibers were due to the sponge itself, as the Helistat® sponge has been known to degrade subcutaneously in rats within 8 weeks. Since the GAG content and structure of articular cartilage have been known to be critical to its mechanical properties and load-bearing function, these results suggested that the Helistat® sponge might not be optimal for articular cartilage production.

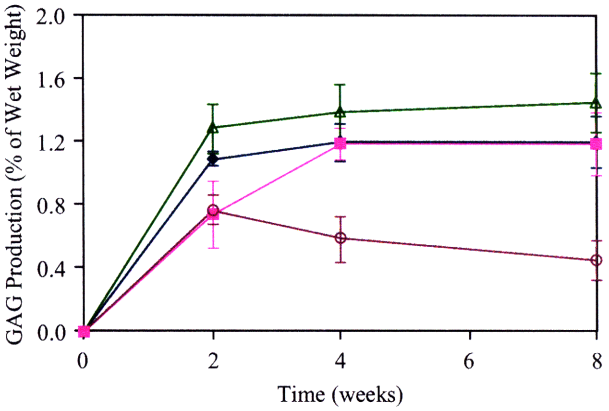

Figure 3.16. GAG production within constructs of (♦) HA-Tyr/collagen/H_2O_2/HRP, (■) agarose, (Δ) alginate and (○) Type I collagen, seeded with 50×10^6 cells/mL.

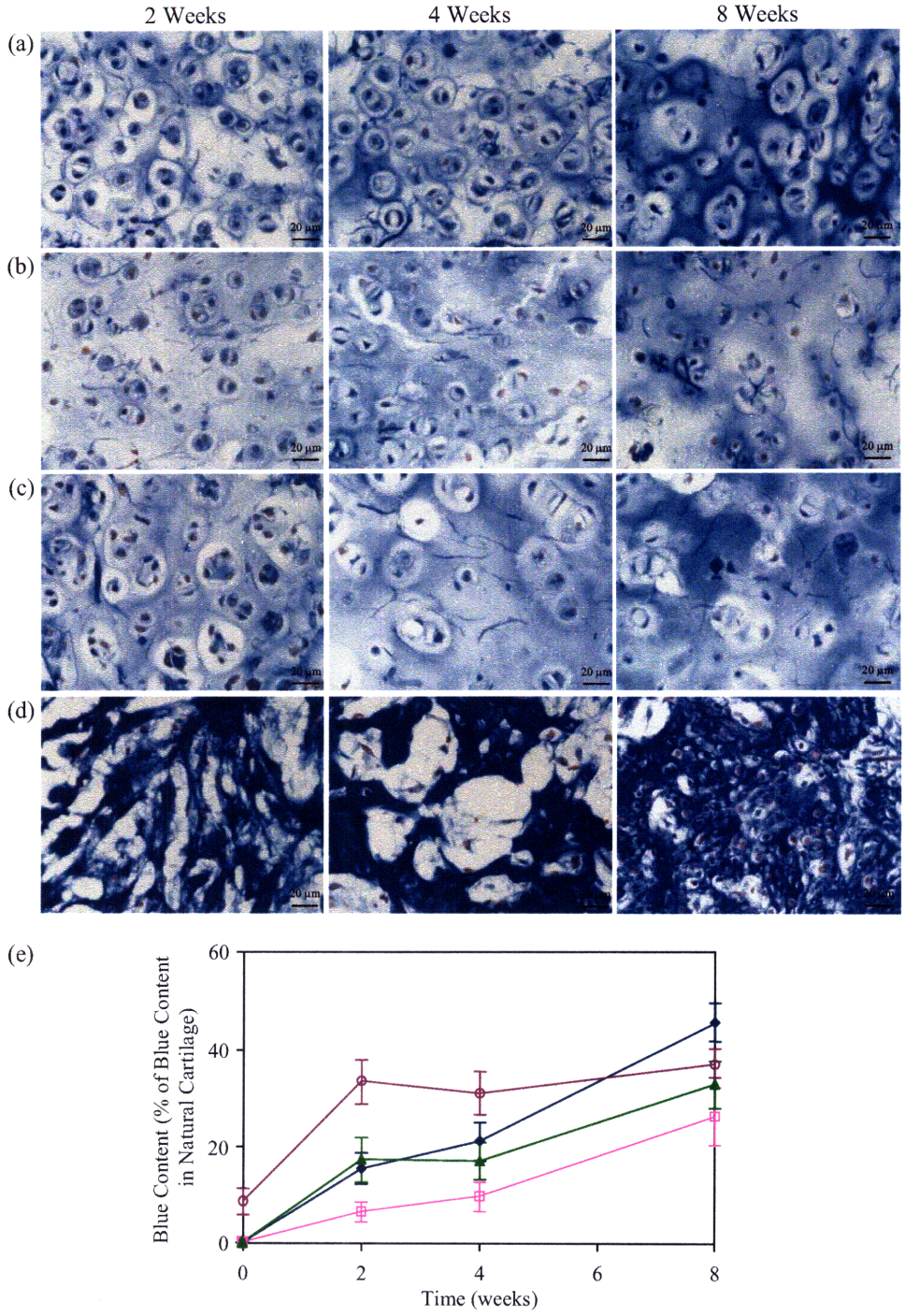

Figure 3.17. (a–d) Masson's Trichrome staining for collagen and (e) quantification of blue content within constructs of (a, ♦) HA-Tyr/collagen/H_2O_2/HRP, (b, □) agarose, (c, ▲) alginate and (d, ○) collagen, seeded with 50×10^6 cells/mL.

3.3.7 Effect of Liposome Incorporation

HRP-loaded liposomes were synthesized as described in Chapter 2 [41] and added to an HA-Tyr/collagen/H_2O_2/chondrocyte solution. Scaffold formation was then induced by heating the mixture to 37°C, as a result of which HRP was released to initiate crosslinking. HA-Tyr/collagen/H_2O_2/HRP liposome/chondrocyte constructs were compared *in vivo* to HA-Tyr/ collagen/H_2O_2/HRP/chondrocyte and HA-Tyr/collagen/H_2O_2/HRP/blank liposome/chondrocyte constructs, keeping the total amounts of HRP constant. Figure 3.18 shows that the GAG production in the presence of HRP-loaded liposomes or blank liposomes was comparable to that of constructs without liposomes. The histological sections in Figures 3.19 also confirmed that collagen content was equivalent in all three constructs. This illustrated that the liposomes or by-products of lipid degradation did not result in cytotoxicity, and that the manner in which HRP was delivered did not affect the matrix production.

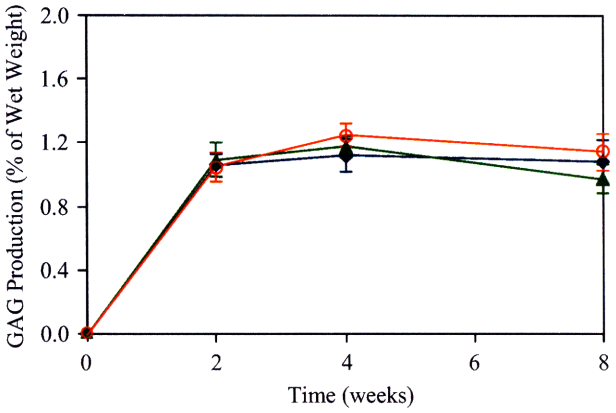

Figure 3.18. GAG production within HA-Tyr/collagen/H_2O_2/chondrocyte constructs with 0.5 wt% of HA-Tyr, 0.05 wt% of Type II collagen, 50×10^6 cells/mL, and (♦) HRP liposomes, (▲) blank liposomes + HRP and (○) HRP.

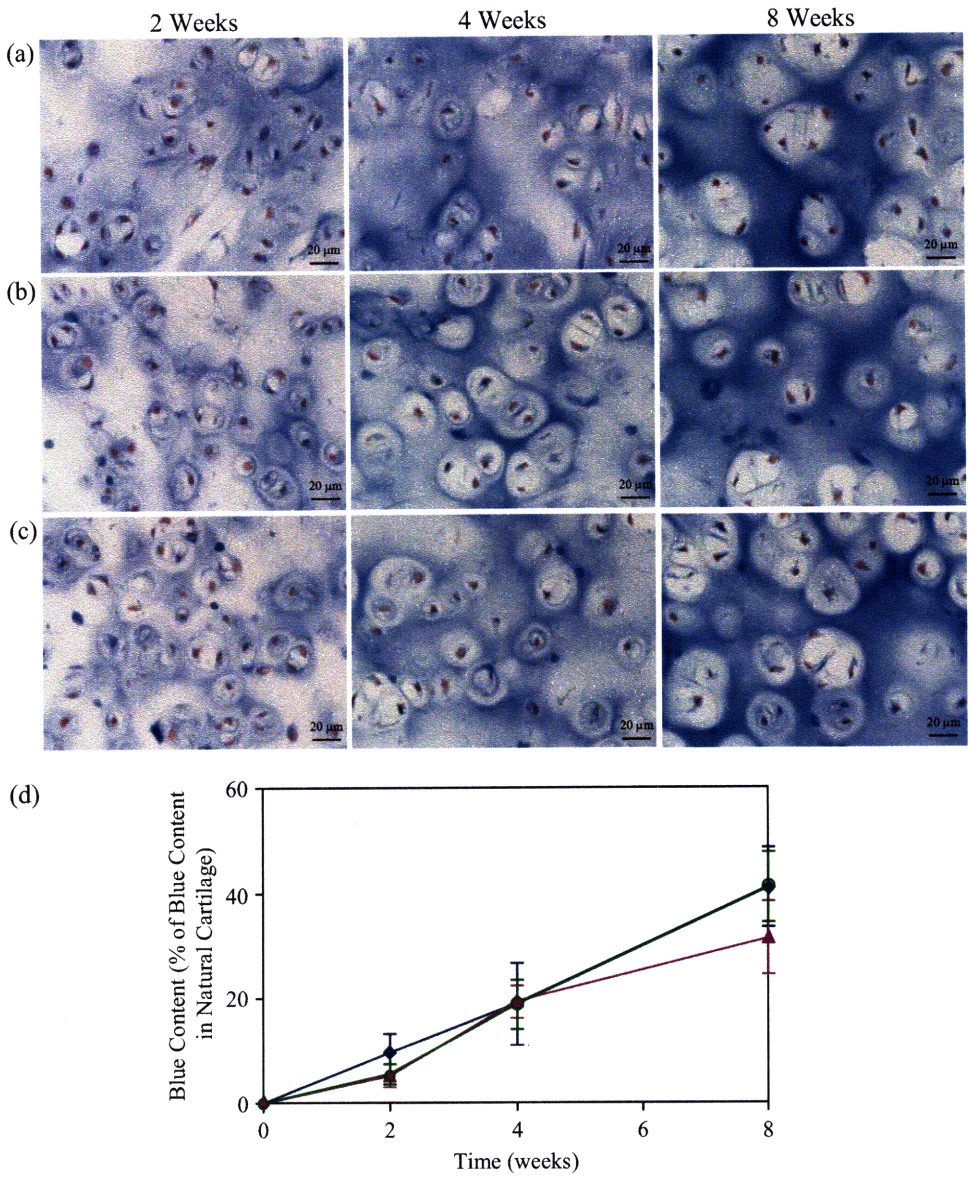

Figure 3.19. (a–c) Masson's Trichrome staining for collagen and (d) quantification of blue content within HA-Tyr/collagen/H_2O_2/chondrocyte constructs with 0.5 wt% of HA-Tyr, 0.05 wt% of Type II collagen, 50×10^6 cells/mL, and (a, ♦) HRP liposomes, (b, ○) blank liposomes + HRP and (c, ▲) HRP.

3.3.8 Injection Studies

In order to test the effect of injecting the scaffold, an HA-Tyr/collagen/H_2O_2/HRP liposome/chondrocyte precursor solution was injected subcutaneously in a mouse model. Figures 3.20–3.21 show that by Week 8, GAG production within the constructs was ~ 1.2% of the wet weight, and that the collagen content measured by histomorphometry was ~ 35% that of natural

articular cartilage. These results were comparable to those shown in Section 3.3.7, where constructs of the same composition were implanted rather than injected.

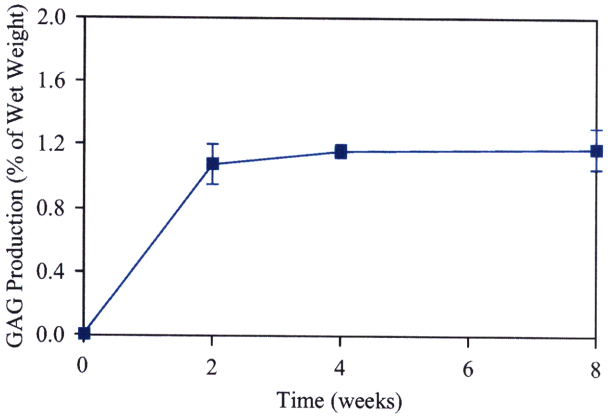

Figure 3.20. GAG production within HA-Tyr/collagen/H_2O_2/HRP liposome/chondrocyte constructs with 0.5 wt% of HA-Tyr, 0.05 wt% of Type II collagen, and 50×10^6 cells/mL.

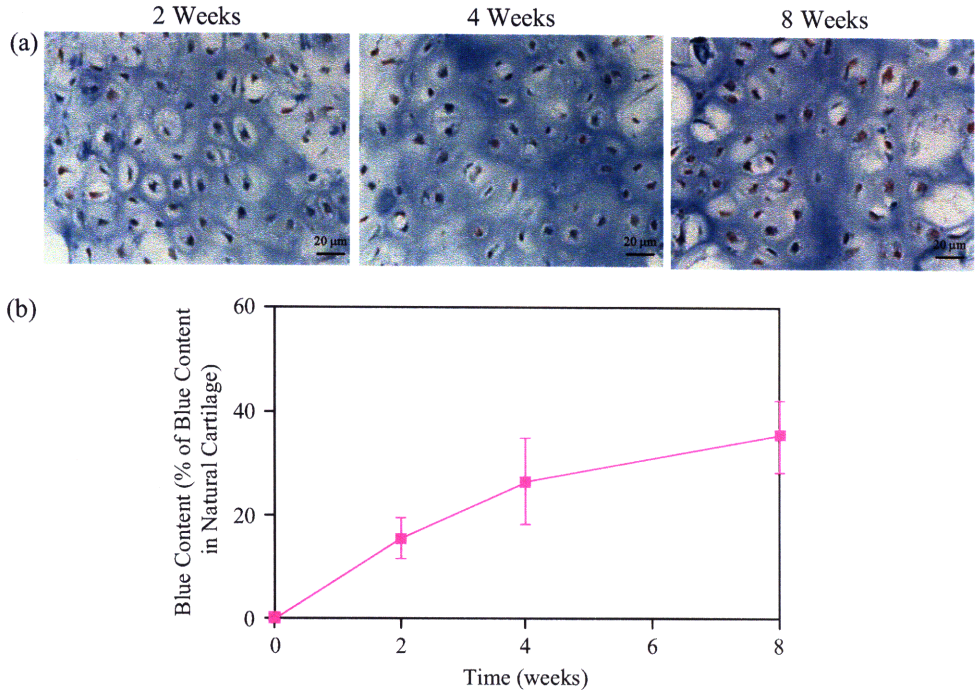

Figure 3.21. (a) Masson's Trichrome staining for collagen and (b) quantification of blue content within HA-Tyr/collagen/H_2O_2/HRP liposome/chondrocyte constructs with 0.5 wt% of HA-Tyr, 0.05 wt% of Type II collagen, and 50×10^6 cells/mL.

3.4 Summary

The potential of the HA-Tyr system as a cartilage tissue engineering scaffold was demonstrated in this study. Chondrocytes were isolated from porcine joints, and encapsulated within HA-Tyr hydrogels, which were then implanted or injected subcutaneously in SCID mice. Cartilaginous tissue was produced, as confirmed by measuring the GAG content within the constructs and staining for chondrocyte morphology, GAG and collagen. After 8 weeks, the GAG content was found to reach ~ 1.2 wt%, while histological sections of harvested constructs illustrated that the cells could maintain their characteristic rounded morphology and produce ~ 40% of the collagen content in articular cartilage. Immunohistochemistry further confirmed that this collagen was mainly composed of Type II collagen, which was characteristic of articular cartilage. As discussed in Chapter 1, one disadvantage of current therapies is that reparative tissue produced is often composed of Type I collagen, characteristic of fibrocartilage, which has inferior mechanical properties and therefore durability [3, 42, 43]. The high content of Type II collagen in our HA-Tyr constructs showed the potential of this system in producing articular cartilage, which could better restore joint function and relieve pain.

Several parameters were shown to be important to increasing the tissue generated. An increase in degradation rate, for example, was found to improve tissue production. In order to modulate degradation rate, the HA-Tyr concentration was varied, while maintaining the total HA concentration. As the HA-Tyr concentration decreased, the crosslink density decreased, the degradation rate increased and more GAG and collagen were produced. This was evidenced in both histological sections and quantitative GAG measurements. The benefit of rapid degradation could be associated with (i) more room for cells to secrete matrix components, (ii) improved diffusion of nutrients and oxygen through the scaffold, (iii) dynamic pore reduction, and (iv) positive signaling to cells from degradation by-products.

However, a construct that was less crosslinked would be softer and more likely to be damaged *in vivo*. Therefore, the incorporation of collagen was studied to strengthen the scaffold, while maintaining rapid degradation. Since negatively charged HA and positively charged collagen could form a polyion complex, the presence of collagen increased the mechanical strength of the construct, as evidenced by the increase in G'. At a collagen concentration of 0.5 wt%, G' more than doubled, while the degradation rate in hyaluronidase did not change substantially. At collagen concentrations exceeding 0.5 wt%, however, phase separation became visible and G' began to drop. Implanted HA-Tyr/collagen/H_2O_2/HRP/chondrocyte constructs

showed a parallel trend, where a collagen concentration of 0.05 wt% provided more rapid GAG production and induced greater collagen content, likely due to the positive signaling from the Type II collagen. Higher collagen concentrations, however, resulted in poor matrix production and even cell death, due to the excess acetic acid in which the collagen was dissolved.

An increase in cell concentration also enhanced cell-cell and cell-matrix interaction, and improved matrix production, particularly at short times. By Week 8, however, as the construct became denser, diffusion of nutrients and oxygen through the construct might not have been sufficient to support a cell concentration as high as 100×10^6 cells/mL, and the GAG and collagen contents approached that of the 50×10^6 cells/mL constructs, indicating a decrease in biosynthesis rate.

HA-Tyr was compared to several other natural polymers that have been commonly utilized for cartilage regeneration. It was shown that GAG production within HA-Tyr constructs was comparable to that of agarose and alginate, while collagen production was higher in HA-Tyr than in alginate and agarose. The Type I collagen Helistat® sponge, on the other hand showed lower GAG production than HA-Tyr, agarose and alginate, and led to a visibly fibrous matrix, unlike that of articular cartilage.

Constructs were also created by adding thermoresponsive HRP-encapsulated liposomes to an HA-Tyr/collagen/H_2O_2/chondrocyte solution, and heating the mixture to 37°C. By comparison with constructs created with blank liposomes+HRP and with only HRP, it was shown that the liposomes were not toxic and that the temperature-induced release of HRP from liposomes did not affect the matrix production.

An HA-Tyr/collagen/H_2O_2/HRP liposome/chondrocyte precursor solution was also injected subcutaneously in a mouse model, and it was shown that GAG and collagen production were comparable to that in constructs that were implanted. This suggested that *in situ* scaffold formation, with the additional benefit of minimally invasive administration, could be as effective in matrix production as the implantation of a pre-formed construct.

This chapter demonstrates that the HA-Tyr system, including the incorporation of thermosensitivity through liposomes, has great potential as a scaffold for cartilage repair. The next chapter describes the incorporation of growth factors to further improve cartilage matrix synthesis.

3.5 References

[1] Riesle, J., Hollander, A. P., Langer, R., *et al.*, *J Cell Biochem* **71**, 313–327 (1998).

[2] Hu, J. C. Y., Athanasiou, K. A., in *Handbook of Histology Methods for Bone and Cartilage*, edited by Y. H. An and K. L. Martin (Humana Press, Totowa, 2003), p. 73–95.

[3] Temenoff, J. S., Mikos, A. G., *Biomaterials* **21**, 431–440 (2000).

[4] Lee, C. R., Breinan, H. A., Nehrer, S., *et al.*, *Tissue Eng* **6**, 555–565 (2000).

[5] Raghunath, J., Rollo, J., Sales, K. M., *et al.*, *Biotechnol Appl Biochem* **46**, 73–84 (2007).

[6] Cancedda, R., Dozin, B., Giannoni, P., *et al.*, *Matrix Biol* **22**, 81–91 (2003).

[7] Ouyang, H. W., Goh, J. C. H., Mo, X. M., *et al.*, *Ann NY Acad Sci* **961**, 126–129 (2002).

[8] Taluja, A., Youn, Y. S., Bae, Y. H., *J Mater Chem* **17**, 4002–4014 (2007).

[9] Sharma, B., Elisseeff, J. H., *Ann Biomed Eng* **32**, 148–159 (2004).

[10] Tuli, R., Li, W. J., Tuan, R. S., *Arthritis Res Ther* **5**, 235–238 (2003).

[11] Poshusta, A. K., Burdick, J. A., Mortisen, D. J., *et al.*, *J Biomed Mater Res A* **64A**, 62–69 (2003).

[12] Lavik, E., Langer, R., *App Microbiol Biotechnol* **65**, 1–8 (2004).

[13] Bottaro, D. P., Liebmann-Vinson, A., Heidaran, M. A., *Ann NY Acad Sci* **961**, 143–153 (2002).

[14] Nehrer, S., Breinan, H. A., Ramappa, A., *et al.*, *J Biomed Mater Res* **38**, 95–104 (1997).

[15] Veilleux, N. H., Yannas, I. V., Spector, M., *Tissue Eng* **10**, 119–127 (2004).

[16] Chow, G., Nietfeld, J. J., Knudson, C. B., *et al.*, *Arthritis Rheum* **41**, 1411–1419 (1998).

[17] Goessler, U. R., Hormann, K., Riedel, F., *Int J Mol Med* **13**, 505–513 (2004).

[18] Allison, D. D., Grande-Allen, K. J., *Tissue Eng* **12**, 2131–2140 (2006).

[19] Radice, M., Pastorello, A., Pavesio, A., *et al.*, US 7,157,080 B2 (2007).

[20] Redman, S. N., Oldfield, S. F., Archer, C. W., *Eur Cell Mater* **9**, 23–32 (2005).

[21] Kurisawa, M., Chung, J. E., Gao, S., *et al.*, *Chem Commun* **34**, 4312–4314 (2005).

[22] Buckwalter, J. A., Mankin, H. J., *J Bone Joint Surg* **79-A**, 600–611 (1997).

[23] Martin, I., Obradovic, B., Freed, L. E., *et al.*, *Ann Biomed Eng* **27**, 656–662 (1999).

[24] Nerlich, A. G., in *Handbook of Histology Methods for Bone and Cartilage*, edited by Y. H. An and K. L. Martin (Humana Press, Totowa, 2003), p. 295–314.

[25] Young, B., Lowe, J. S., Stevens, A., *et al.*, *Wheater's Functional Histology* (Churchill Livingstone, Sydney, 2006).

[26] Gartner, L. P., Hiatt, J. L., *Color Atlas of Histology* (Lippincott Williams & Wilkins, Baltimore, 2005).

[27] Nehrer, S., Spector, M., in *Handbook of Histology Methods for Bone and Cartilage*, edited by Y. H. An and K. L. Martin (Humana Press, Totowa, 2003), p. 411–422.

[28] Junqueira, L. C., Carneiro, J., (Lange Medical Books McGraw-Hill, New York, 2003), p. 135–140.

[29] Drury, J. L., Mooney, D. J., *Biomaterials* **24**, 4337–4351 (2003).

[30] Gordon, T. D., Schloesser, L., Humphries, D. E., *et al.*, *Tissue Eng* **10**, 1287–1295 (2004).

[31] Zhong, S. P., Campoccia, D., Doherty, P. J., *et al.*, *Biomaterials* **15**, 359–365 (1994).

[32] Flannery, C. R., Little, C. B., Hughes, C. E., *et al.*, *Biochem Biophys Res Commun* **251**, 824–829 (1998).

[33] Vickers, S. M., Squitieri, L. S., Spector, M., *Tissue Eng* **12**, 1345–1355 (2006).

[34] Taguchi, T., Ikoma, T., Tanaka, J., *J Biomed Mater Res* **61**, 330–336 (2002).

[35] Kurtis, M. S., Tu, B. P., Gaya, O. A., *et al.*, *J Orthop Res* **19**, 1122–1130 (2001).

[36] Sah, R. L., Wong, B. L., Bae, W. C., *et al.*, *Trans Orthop Res Soc* **27**, 363 (2002).

[37] Vunjak-Novakovic, G., Obradovic, B., Martin, I., *et al.*, *Biotechnol Prog* **14**, 193–202 (1998).

[38] Mauck, R. L., Seyhan, S. L., Ateshian, G. A., *et al.*, *Ann Biomed Eng* **30**, 1046–1056 (2002).

[39] Paige, K. T., Cima, L. G., Yaremchuk, M. J., *et al.*, *Plast Reconstr Surg* **97**, 168–178 (1996).

[40] Sellers, R. S., Zhang, R., Glasson, S. S., *et al.*, *J Bone Joint Surg* **82-A**, 151–160 (2000).

[41] Ren, C. D., Kurisawa, M., Chung, J. E., *et al.*, to be submitted to Biomaterials.

[42] Buckwalter, J. A., Mankin, H. J., *J Bone Joint Surg* **79-A**, 612–632 (1997).

[43] Chung, C., Burdick, J. A., *Adv Drug Deliv Rev* **60**, 243–263 (2008).

Chapter 4 – Incorporation of PLGA-HAP Composite Particles for the Controlled Release of TGF-β1 and IGF-1

4.1 Introduction

In the last chapter [1], it was demonstrated that the hyaluronic acid-tyramine (HA-Tyr) scaffold has great potential for cartilage tissue engineering. Since biochemical signals are potent modulators of cellular activity, stimulating proliferation, migration, adhesion, differentiation and gene expression [2, 3], the goal of this chapter is to incorporate the controlled release of growth factors so as to further enhance cartilage production.

4.1.1 Chondrogenic Effects of TGF-β1 and IGF-1

Growth factors are integral in the development and maintenance of cartilage [4]. Insulin-like growth factor (IGF-1), a protein hormone, is synthesized locally by chondrocytes and stored in the extracellular matrix (ECM) of articular cartilage [5]. It is known to stimulate cell division, and is considered to be the main anabolic factor in cartilage [3, 6, 7]. Moreover, it has been shown to inhibit chondrocyte apoptosis induced by stresses, such as ECM degradation or compression [8]. In engineered constructs, the addition of IGF-1 can significantly increase biosynthesis level [9]. Medium supplemented with IGF-1, for example, increased GAG production up to fivefold *in vitro* in chondrocyte-seeded poly(glycolic acid) (PGA) scaffolds [10]. *In vivo*, IGF-1-loaded gelatin microparticles coencapsulated with chondrocytes in an oligo(poly(ethylene glycol) fumarate) scaffold were shown to improve neo-surface repair in full thickness defects in rabbit joints [11].

Transforming growth factor type-β1 (TGF-β1) is also known to be a potent chondrogenic inducer, and is present in high concentrations in articular cartilage [6, 12]. It regulates the proliferation and expression of the differentiated phenotype of chondrocytes [3], and has been shown to induce the cartilaginous phenotype in rat mesenchymal stem cells [13]. Several studies have shown the ability of TGF-β1 to induce increased tissue synthesis *in vitro* and *in vivo* [5, 6, 10, 14, 15]. For example, TGF-β1 added to culture medium *in vitro* increased collagen production by chondrocytes in PGA scaffolds [10], and increased cell proliferation and matrix production in fibrin matrices [6]. *In vivo*, it has been reported that successive injections of TGF-β1 stimulated proteoglycan synthesis in cartilage-depleted murine joints [15].

4.1.2 Controlled Release

In natural tissue development and healing, molecular signals and cellular responses unfold in time [18], where cells differentiate and produce tissue in response to the sequence and concentrations of cytokines. Therefore, in the delivery of growth factors within tissue engineered constructs, the gradient as well as absolute concentration at each time point are important considerations for achieving the correct cell phenotype and for effective matrix synthesis. Moreover, because tissue development often takes place over the course of several weeks, growth factors should be delivered over a prolonged period. It has been shown that the direct injection of growth factors into defect sites is generally ineffective, as proteins either rapidly diffuse out of the site or are digested by enzymes [16]. Similarly, the direct encapsulation of IGF-1 and TGF-β1 with chondrocytes in PEG-based hydrogels showed no improvement in ECM production over the control *in vitro* [5].

In order to address these issues, various methods of delivery have been studied, including the incorporation into polymer scaffolds and encapsulation within polymer particles [2, 11, 17]. In these systems, the duration, magnitude and rate of release can be determined by parameters, such as growth factor loading, and carrier degradation rate, porosity and particle size [18]. Furthermore, since growth factors often have short half-lives, the carrier can serve as a barrier to protect them from the environment, thereby prolonging bioactivity [4].

4.1.3 PLGA-HAP Nanocomposite Microparticles

Double emulsion processing is a common technique for the synthesis of polymeric microparticles. Particles are synthesized by adding an aqueous solution containing the therapeutic agent, e.g. growth factors, to an organic phase and agitating to form a water-in-oil (W/O) emulsion, which is then added to water and again agitated to create a water-in-oil-in-water (W/O/W) emulsion. Particles are subsequently formed around the growth factor as the organic phase is removed either by evaporation or extraction [19]. However, since surface proteins are loosely associated with the polymer, these particles tend to exhibit a high initial burst, limiting the period over which the growth factor is released at therapeutic levels. Furthermore, although parameters, such as polymer molecular weight, surfactant type, and

addition of hydrophilic or hydrophobic agents, have been studied to control release kinetics, results have shown that the effects of these parameters can be unpredictable [20, 21, 22, 23].

In order to address these issues, Yong *et al.* of our group have developed a solid-in-oil-in-water (S/O/W) processing technique to synthesize apatite-polymer nanocomposite microparticles (Figure 4.1) [24]. In this system, proteins are pre-adsorbed onto hydroxyapatite (HAP), the mineral component of bone, which has been shown to have a high affinity for proteins [25, 26]. The protein-apatite complex is then suspended in an organic poly(lactic-co-glycolic acid) (PLGA) solution to form a solid-in-oil suspension, which is added to an aqueous solution and homogenized to create a S/O/W emulsion. By evaporating off the organic phase, microparticles composed of apatite-protein complexes dispersed within PLGA are formed. As PLGA degrades via hydrolysis, the acidic by-products would cause the dissolution of the apatite substrate and release of the protein. This method has shown versatility in protein delivery, as well as control over initial burst and growth factor release rate. This system was therefore applied for the controlled release of IGF-1 and TGF-β1 in this study so as to enhance cartilage production.

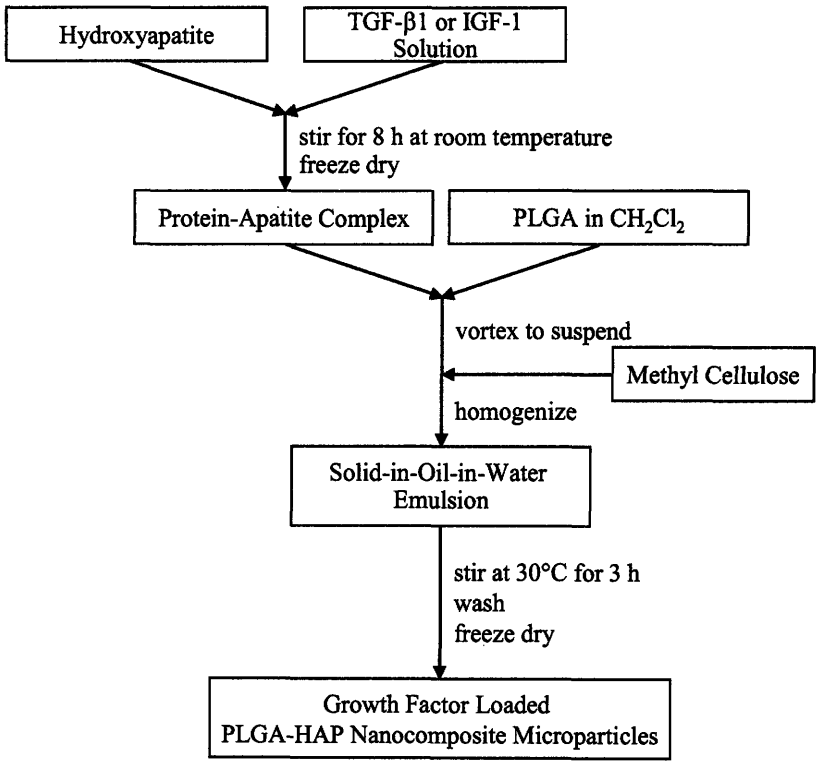

Figure 4.1. Schematic of the S/O/W method for preparing PLGA-HAP nanocomposite microparticles loaded with growth factor.

4.2 Experimental

4.2.1 Synthesis of Hydroxyapatite

Nanocrystalline HAP was synthesized by the method developed by Ahn *et al* [27]. Briefly, equal volumes of calcium nitrate (8.3 mM in water) and ammonium phosphate (5 mM in water) were combined and aged for 2 days at room temperature. The precipitate was washed with solutions of decreasing pH and two ethanol washes. The gel was then dried under ambient conditions overnight, and further dried at 120°C for 24 h. The dried cake was then ground with a heated mortar and pestle, and calcined at 500°C for 2 h (ramp rate = 4°C/min). The resulting powder was sieved through a 45-μm mesh for uniformity. Calcium nitrate and ammonium phosphate were purchased from Sigma.

Powder X-ray diffraction (XRD) patterns were obtained with a Siemens D5000 θ-θ diffractometer (45 kV, 40 mA, Cu Kα). The major peaks at 25.88°, 31.77°, 32.20°, 32.90° and 39.82°, corresponding to (002), (211), (112), (300) and (310) diffractions, were used to verify the pure apatitic phase. The grain size was calculated to be 21 nm from the width of the <002> peak.

4.2.2 Protein Adsorption

To adsorb the protein of interest onto HAP's surface, the protein solution was added to UV-sterilized HAP powder, and the suspension was stirred at room temperature for 8 h. Typical adsorption was performed with 50 mg of HAP in 5 mL of cell culture grade water, and either 120 μL of TGF-β1 (10 μg/mL in 1 mg/mL of bovine serum albumin (BSA) in 4 mM hydrochloric acid (HCl)) or 800 μL of IGF-1 (100 μg/mL in 1 mg/mL of BSA in phosphate buffered saline (PBS)). Water was then removed by freeze drying.

Unadsorbed protein was removed by centrifuging the protein-apatite complex (20,000g, 10 min) prior to freeze drying; the supernatant was then removed and tested by ELISA to measure protein concentration. TGF-β1, IGF-1, TGF-β1 ELISA kits, and IGF-1 ELISA kits were purchased from R&D Systems. HCl, BSA and PBS were purchased from Sigma-Aldrich.

4.2.3 Synthesis of Nanocomposite Microparticles

Microparticles were aseptically synthesized as described by Yong *et al* [24]. In brief, protein-apatite complex (20 mg) was suspended in a sterile-filtered PLGA dichloromethane

(DCM) solution (250 mg in 1.5 mL). This mixture was then added to 50 mL of steam-sterilized 0.1 wt% methyl cellulose. The emulsion was homogenized (8000 rpm, 2 min) and then stirred at 30°C for 3 h to evaporate DCM. Methyl cellulose was washed off with 3 centrifugations (500 rpm, 1 min) with sterile water. Water was removed by freeze drying. PLGA was purchased from Lakeshore Biomaterials, methyl cellulose was purchased from Alfa Aesar, and DCM was purchased from Sigma.

4.2.4 Release Studies

Release studies were conducted in complete F-12 medium (supplemented with 10% of fetal bovine serum (FBS), 0.1 M of non-essential amino acids, 0.5 μg/mL of fungizone, 1 wt% of penicillin-streptomycin, and 0.4 mM of L-proline) at 37°C, at a particle concentration of 10 mg/mL. At each time point, the solution was centrifuged (2500g, 1 min), and the supernatant was removed. TGF-β1 and IGF-1 concentrations in the supernatant were then tested by ELISA. Release studies were performed in duplicates. The F-12 medium, non-essential amino acids and fungizone were purchased from Invitrogen, and penicillin-streptomycin and L-proline were obtained from Sigma-Aldrich.

For total protein release studies, IGF-1 and TGF-β1 microparticles were synthesized such that the total protein loading was equal in both types of microparticles. Microparticles were synthesized as described in Section 4.2.3, except with apatite-protein complexes, where adsorption was carried out with 50 mg of apatite and 80 μg of each protein. Total protein release studies were performed as described above, except in an N,N-bis(2-hydroxyethyl)-2-aminoethanesulfonic acid (BES) buffer (pH = 7.4). The supernatant was tested for the total protein concentration by the Coomassie assay. Release studies were conducted in duplicates. The Coomassie dye was purchased from Pierce Biochemicals, and BES was purchased from Sigma-Aldrich.

4.2.5 Turbidity Measurements

The effect of pH on IGF-1 and TGF-β1 precipitation was measured by incubating IGF-1 (250 μg/mL) and TGF-β1 (100 μg/mL) in HCl/NaOH solutions of varying pH for 24 h at 37°C. The absorbance of each solution was then measured at 450 nm.

4.2.6 Particle Size

Environmental scanning electron microscopy (ESEM) images of the microparticles were taken with an FEI/Philips XL30 FEG. The size of the microparticles was calculated as the number average diameter of at least 100 particles.

4.2.7 Chondrocyte Isolation

Chondrocytes were isolated from the articular cartilage of the femur, patella and tibia of pig legs (5–6 months old) that were obtained from the local abattoir. The tissue was cut into small pieces (1 mm^3), and digested in a 0.2 wt% Type 2 collagenase solution (in F-12 medium supplemented with 0.1 M of non-essential amino acids, 0.5 μg/mL of fungizone, 1 wt% of penicillin-streptomycin, and 0.4 mM of L-proline) at 37°C for 12 h. The cell solution was then filtered through a 100-μm strainer and centrifuged (8000g, 10 min) twice with PBS. The collagenase was purchased from Worthington Biochemical.

4.2.8 Subcutaneous Implantation of Particle Constructs In Vivo

HA-Tyr was synthesized as described in Chapter 2 [28]. For the Blank Particle, IGF-1 and TGF-β1 Release Rate and Combination Studies (Sections 4.3.3–4.3.6), a HA-Tyr concentration of 0.8 wt% was used, while a HA-Tyr concentration of 0.5 wt% was used for the Dosage Study (Sections 4.3.7). Microparticles and porcine chondrocytes (50×10^6 cells/mL) were suspended in a sterile-filtered HA-Tyr (dissolved in complete medium) and H_2O_2 (5 wt%, 5 μL per 25 mg of HA-Tyr) solution. 50 μL of the HA-Tyr/H_2O_2/chondrocyte/particle solution were combined with 5 μL of horseradish peroxidase (HRP) (0.125 mg/mL), and placed in a mold to create a cylindrical gel with a diameter of 8 mm and a thickness of ~ 1 mm. The gels (n = 6) were then implanted subcutaneously in the dorsum of SCID mice, which were sacrificed at weeks 2, 4 and 8. Chondrocytes used for implantation were encapsulated immediately post-harvest, and each experiment, i.e. each graph shown, was conducted with one set of chondrocytes harvested from an individual pig.

4.2.9 Injection Study

Liposomes were aseptically synthesized as described in Chapter 2 [28] with 60 mg/mL of lipid (DPPC:DMPC weight ratio = 2.3), 2 mg/mL of HRP, 30 min of sonication, -20°C freezing, and rehydration volume ratio = 0.1, and were washed with 0.1 M of $CaCl_2$. Liposomes were combined at 30 μL/mL (with a HRP activity of 90 Units/mL of liposome) with a solution of HA-Tyr (0.5 wt%), Type II collagen (0.05 wt%), H_2O_2 (5 wt%, 4 μL/mL), chondrocytes (50×10^6 cells/mL), 60 mg/mL of IGF-1-loaded 24 kDa PLGA-HAP nanocomposite microparticles and 20 mg/mL of TGF-β1-loaded 6 kDa PLGA-HAP nanocomposite microparticles. The precursor solution (100 μL, n = 6) was then injected subcutaneously in SCID mice with a 21-gauge needle, and harvested at weeks 2 and 4.

4.2.10 GAG Quantification

To evaluate GAG production (n = 4), constructs were sonicated with a probe-tip sonicator for 40–60 sec, and then digested in papain (0.125 mg/mL in 100 mM of PBS solution, 10 mM of ethylenediaminetetraacetic acid (EDTA) and 10 mM of cysteine) at 60°C for 15 h. Digested constructs were filtered through a 0.45-μm syringe filter, and the GAG concentration was calorimetrically determined by the Blyscan dimethylmethylene blue assay. GAG content was then calculated as a percentage of the wet weight of the harvested constructs. Papain was purchased from Worthington Biochemical, PBS was purchased from EMD Biosciences, EDTA and cysteine were purchased from Sigma-Aldrich, and the Blyscan kit was purchased from Biocolor.

In order to reflect the degree of improvement due to the growth factor-loaded microparticles in each experimental group, GAG content was normalized to the control group that did not contain any particles at the final time point. For the Blank Particle, IGF-1 and TGF-β1 Release Rate and Combination Studies (Sections 4.3.3–4.3.6), GAG production for control constructs was 0.7–0.9% of the wet weight at Week 8. For the Dosage Study, control constructs had a GAG content of 1.0% of the wet weight at Week 8. For the Injection Study, GAG content in the control constructs was 0.9% of the wet weight at Week 8.

4.2.11 Histology and Histomorphometry

Harvested constructs (n = 2) were fixed in neutral bufferd formalin for at least 24 h. The constructs were then paraffin-embedded and stained with Masson's Trichrome (Richard-Allan Scientific).

Histomorphometry was conducted on sections stained with Masson's Trichrome as a measure of collagen content. Digital images were acquired at the same brightness and exposure time on an Olympus DP71 camera mounted on an Olympus BX51 microscope, and on a Nikon DXM1200 camera mounted on an Olympus BX50 microscope. Images were then split into red, green and blue (RGB) planes on Image J software, and the data were loaded onto Matlab. To measure the blue intensity of the sections, a method similar to that developed by Martin *et al.* was employed [29]. For each pixel, the blue fraction, B_F, was defined as $B_F = B/(R+G+B)$. B_F was then normalized to $B_{F,N}$, where $B_{F,N}$ was set to 0 if $B_F < 0.38$ and if $R/G < 0.98$. This eliminated pixels that were not stained blue or were stained purple (the nuclei). All other pixels were proportionally scaled from 0 to 1, i.e. $B_{F,N} = \frac{1}{1-0.38}B_F - \frac{0.38}{1-0.38}$. The blue content for each pixel was then calculated as $B_C = B_F * B_{F,N}$, and the blue content of the image ($\overline{B_C}$) was calculated as the average of all pixels in the image. Results were reported as a percentage of the blue content of natural porcine articular cartilage stained at the same time, in order to account for variations in staining procedure and reagents. At least 3 sections of each sample were stained, and 4–5 pictures were taken of each section. Images shown represent the average.

4.2.12 Statistics

Graphs of particle size and GAG and collagen contents are depicted as mean ± standard deviation. One- or two-factor analysis of variance (ANOVA) was conducted to determine whether significance existed at $p < 0.05$. For GAG and collagen production, Tukey post hoc analysis was also conducted to determine whether there was significance at $p < 0.05$ between experimental groups. Calculations were performed on Matlab.

4.3 Results and Discussion

4.3.1 Adsorption of TGF-β1 and IGF-1 onto Apatite

The adsorption capacity of IGF-1 and TGF-β1 by HAP was evaluated by adding 2, 5 or 10 μg of each protein onto 5 mg of apatite in 1 mL of water, and measuring the protein

concentration remaining in the supernatant after 8 h of stirring. According to the R&D Systems product specifications, $ED_{50(IGF\text{-}1)}$ = 0.3–1.5 ng/mL, and $ED_{50(TGF\beta\text{-}1)}$ = 0.04–0.2 ng/mL, where ED_{50} is the effective dose observed to achieve a specific effect on 50% of the cell or animal population. Therefore, protein quantities above 10 μg were not tested. Figures 4.2–4.3 show that the majority of the growth factor added (~ 99% of IGF-1 and ~ 98% of TGF-β1) was adsorbed onto the apatite surface, demonstrating the high affinity between the proteins and HAP, and the efficiency of adsorption.

The IGF-1-loaded PLGA-HAP nanocomposite microparticles studied in the following sections were prepared with 1.6 μg of IGF-1 adsorbed/mg of HAP, while TGF-β1-loaded PLGA-HAP nanocomposite microparticles were prepared with 0.024 μg of TGF-β1 adsorbed/mg of HAP. Although previous studies have shown that nanocrystalline HAP has an adsorption capacity of 159 ± 0.8 μg of BSA/mg of HAP [24] and that the particles could potentially be loaded with higher concentrations of each growth factor, a higher loading was not examined as it might have dramatically decreased the working range of particle concentrations. Excessively low particle concentrations would have led to sparse particle distribution, and therefore less homogeneous growth factor distribution within the construct. In addition, a small number of microparticles might not have allowed for a representative sample within each scaffold.

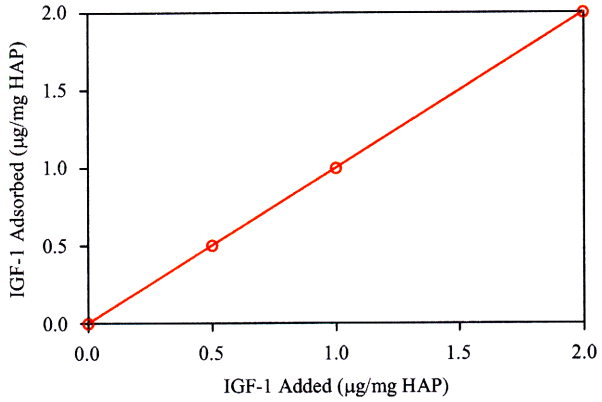

Figure 4.2. Adsorption of IGF-1 onto nanocrystalline HAP (y = 0.99x).

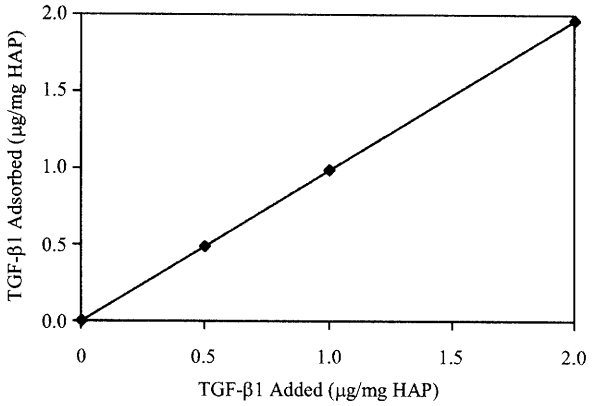

Figure 4.3. Adsorption of TGF-β1 onto nanocrystalline HAP (y = 0.98x).

4.3.2 Effect of Polymer Molecular Weight on Protein Release and Particle Size

The release of TGF-β1 and IGF-1 from the microparticles was studied as a function of the PLGA molecular weight (MW). As shown in previous studies by Yong *et al.*, as the MW decreased, the rate of polymer degradation and generation of lactic and glycolic acid increased, leading to an increase in protein release. This is demonstrated in Figure 4.4 for both IGF-1 and TGF-β1. Although the shapes of the release profiles differed between the two proteins, lower MW resulted in the more rapid release of each protein. Higher MW's, on the other hand, resulted in more prolonged, gradual and linear release.

It should be noted that a lower initial burst of TGF-β1 was measured with lower MW particles, counter to that seen at other time points and to that observed with IGF-1 or BMP-2 [24]. As MW decreased and degradation rate increased, the release rate and initial burst were expected to increase. Figure 4.5 shows the release of total protein, which includes the carrier protein BSA, from the particles. As MW decreased, the initial burst of total protein did increase. This was opposite to that measured by ELISA (Figure 4.4b), which was only a measure of the TGF-β1 concentration. Therefore, protein release did increase as MW decreased, but TGF-β1, itself, was released more slowly. Turbidity measurements in Figure 4.6 show that TGF-β1 precipitates out of solution at pH $\leq$ 2, and given that the pH within PLGA microspheres could fall below 1.5 [30], it was likely that at short times, TGF-β1 was desorbed from the apatite, but precipitated within the microparticles and was therefore not released from the microparticles. This might be particularly true for the low MW particles, which might have begun to degrade abruptly upon addition to solution and even during synthesis, generating large amounts of acid within the

microparticles. This trend was not observed with IGF-1 since IGF1 remained soluble at pH's as low as 1.

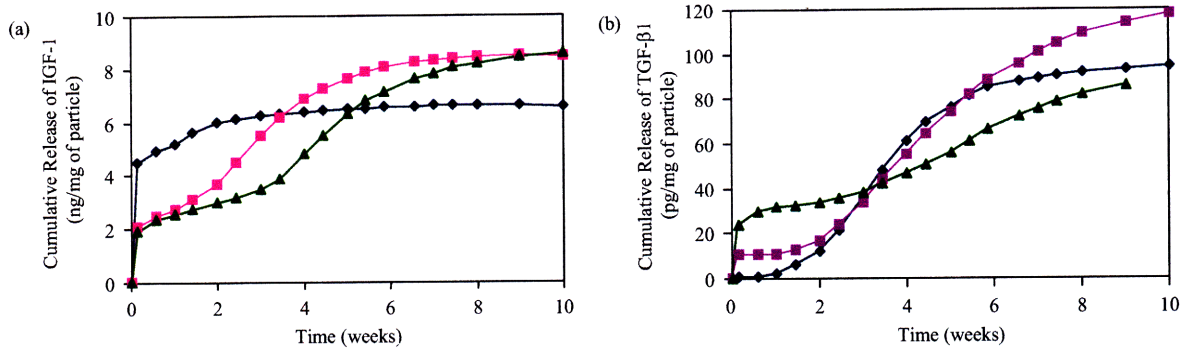

Figure 4.4. Release of (a) IGF-1 and (b) TGF-β1 from PLGA-HAP nanocomposite microparticles with PLGA MW's of (♦) 6 kDa, (■) 13 kDa, and (▲) 24 kDa.

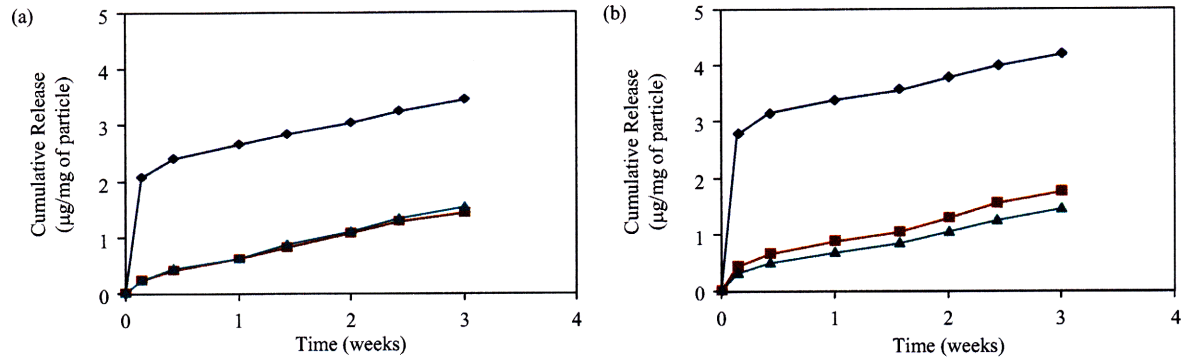

Figure 4.5. Total (a) BSA and IGF-1 and (b) BSA and TGF-β1 protein release from PLGA-HAP nanocomposite microparticles with PLGA MW's of (♦) 6 kDa, (■) 13 kDa, and (▲) 24 kDa.

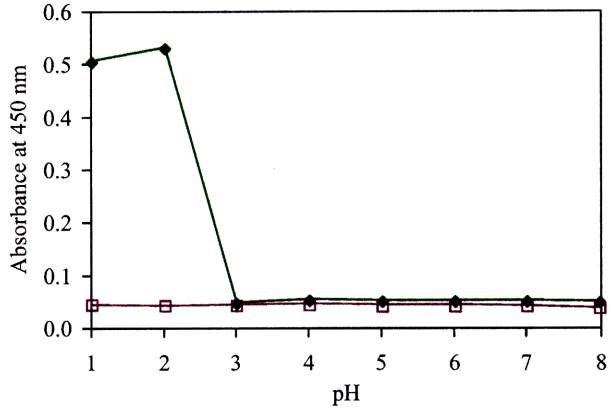

Figure 4.6. Turbidity of (□) IGF-1 and (♦) TGF-β1 solutions as a function of pH.

Figure 4.7 shows that as the PLGA MW increased, there was a statistically significant ($p < 0.05$) increase in the size of the microparticles. During synthesis, an increase in MW increased the viscosity of the PLGA/DCM solution, making the oil droplets more difficult to break up despite homogenization, and resulting in larger particles. Therefore, release from higher MW microparticles was slower likely due to a longer diffusion time, as well as the slower polymer degradation rate.

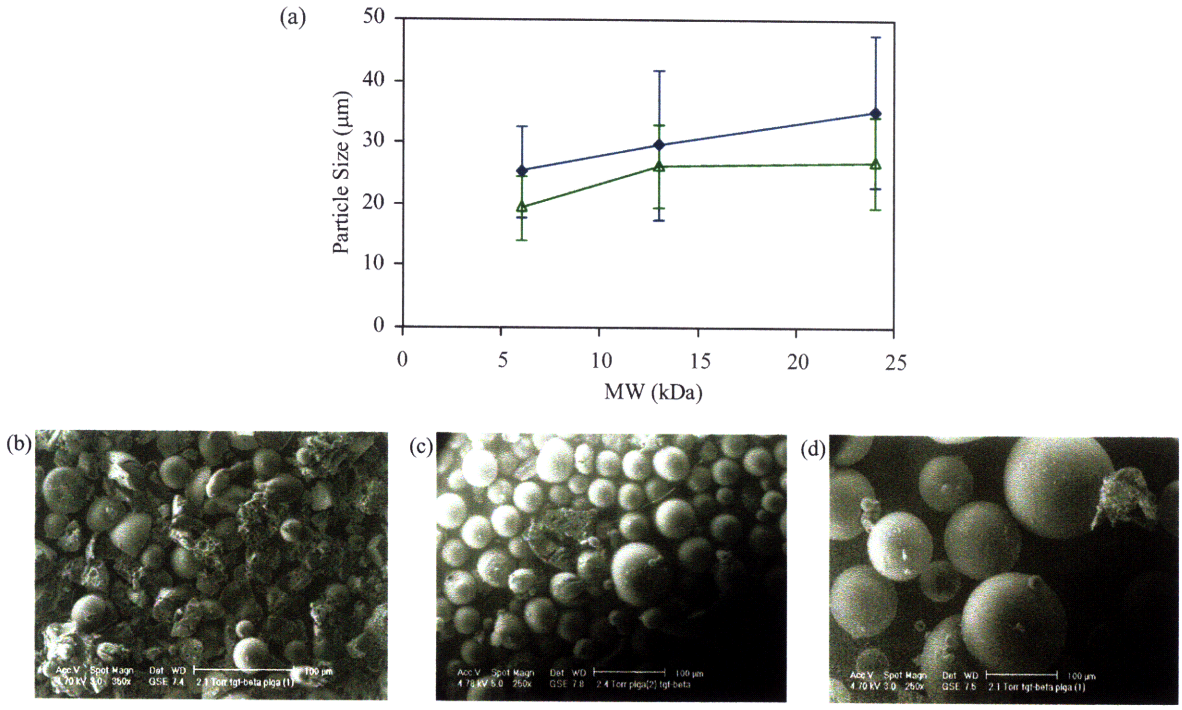

Figure 4.7. (a) Size (determined by ESEM) of PLGA-HAP nanocomposite microparticles containing (♦) IGF-1 and (Δ) TGF-β1, prepared with different PLGA MW's. (b–d) ESEM of PLGA-HAP nanocomposite microparticles with PLGA MW's of (a) 6 kDa, (b) 13 kDa, and (c) 59 kDa.

4.3.3 Effect of Blank Particles In Vivo

Blank microparticles were encapsulated in HA-Tyr/H_2O_2/HRP/chondrocyte hydrogels and implanted subcutaneously in mice to test for either positive or negative effects of the microparticles on chondrocyte matrix synthesis, measured by GAG production. Figure 4.8 shows the effect of PLGA MW and microparticle concentration on GAG production. At either 10 or 40 mg/mL, and at 6, 13 or 24 kDa, the microparticles did not have a negative effect on GAG production. By two-way ANOVA, at 10 mg/mL of microparticles, there was no significant

difference in treatments. However, there was a significant difference ($p < 0.05$) at 40 mg/mL; a slight positive effect was observed due to the presence of the microparticles. Nevertheless, from the post hoc test, only the 6 kDa microparticles showed a significant difference ($p < 0.05$) over the control over the 8-week period, increasing GAG production by 1.1-fold at Week 8. This positive effect might have been due to the generation of acids from microparticle degradation, which subsequently led to an increase in HA hydrolysis and thereby an increase in the degradation rate of the scaffold. In Chapter 3 [1], it was shown that increasing scaffold degradation rate improved chondrogenesis.

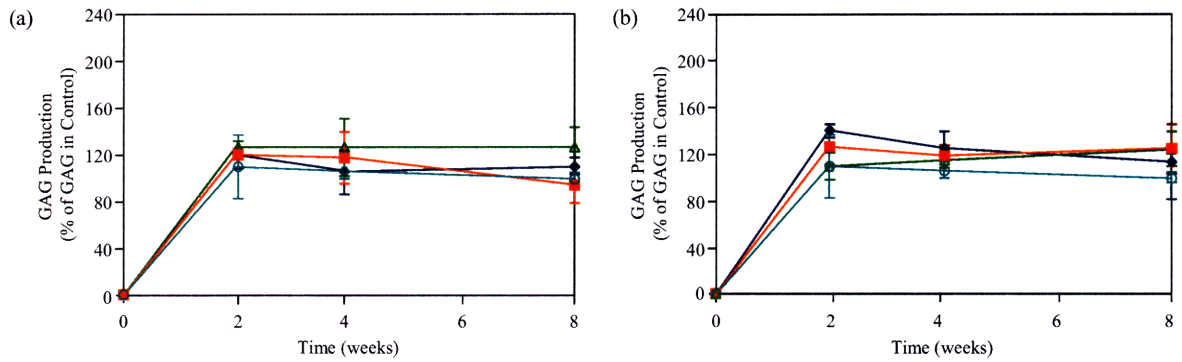

Figure 4.8. Increase in GAG production within HA-Tyr/H_2O_2/HRP/chondrocyte constructs with (a) 10 mg/mL and (b) 40 mg/mL of PLGA-HAP nanocomposite microparticles with PLGA MW's of (♦) 6 kDa, (Δ) 13 kDa, (■) 24 kDa, and (○) with no particles.

4.3.4 Effect of IGF-1 Release Rate on Cartilage Production

In order to study the effect of IGF-1 release rate *in vivo*, PLGA-HAP nanocomposite microparticles loaded with IGF-1 and composed of various PLGA MW's were encapsulated within HA-Tyr/H_2O_2/HRP/chondrocyte constructs, and implanted subcutaneously in mice. Figure 4.9 shows that only the 24 kDa microparticles caused a statistically significant increase in GAG production over the control, resulting in a 1.3-fold increase at Week 8. The blue content of the sections stained with Masson's Trichrome in Figures 4.10 were calculated as a measure of collagen production within the constructs. It was shown that all constructs containing IGF-1 particles resulted in greater collagen content than sections that only contained cells. At Week 8, the 13 kDa microparticles induced a 2.1-fold increase in collagen production over the control, while the 6 and 24 kDa microparticles induced 1.4-fold and 1.5-fold increases, respectively. Based on GAG and collagen production, the more gradual to medium release of IGF-1 was most beneficial in this system. Chondrocyte responsiveness to IGF-1 is dependent on the formation of

focal adhesion plaques to the ECM [6]. However, since HA is anionic, it was unlikely that cells were able to adhere to the scaffold until they, themselves, had deposited sufficient matrix to bind, a process that could take several days or even weeks. Therefore, the slower release of IGF-1 from the microparticles might have more effectively promoted matrix production.

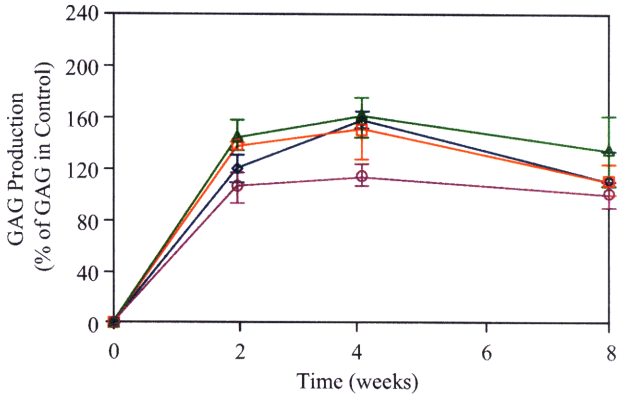

Figure 4.9. Increase in GAG production within HA-Tyr/H_2O_2/HRP/chondrocyte constructs with 40 mg/mL of IGF-1-loaded PLGA-HAP nanocomposite microparticles with PLGA MW's of (◊) 6 kDa, (□) 13 kDa and (Δ) 24 kDa, and (○) with no particles.

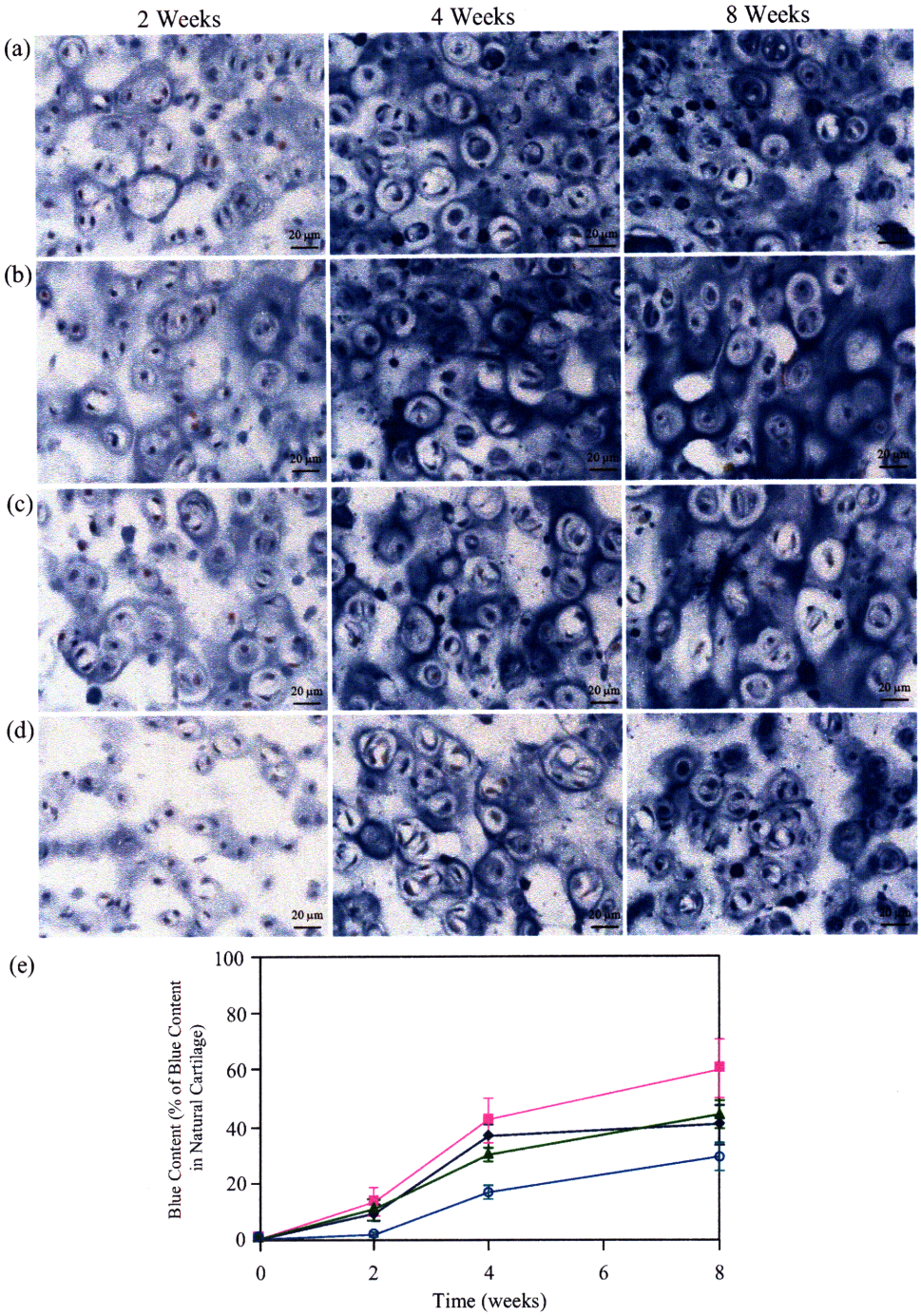

Figure 4.10. (a–d) Masson's Trichrome staining for collagen and (e) quantification of blue content within HA-Tyr/H_2O_2/HRP/chondrocyte constructs with 40 mg/mL of IGF-1-loaded PLGA-HAP nanocomposite microparticles with PLGA MW's of (a, ♦) 6 kDa, (b, ■) 13 kDa and (c, ▲) 24 kDa, and (d, ○) with no particles.

4.3.5 Effect of TGF-β1 Release Rate on Cartilage Production

TGF-β1-loaded PLGA-HAP nanocomposite microparticles were synthesized with 6, 13 or 24 kDa PLGA to achieve different release kinetics. They were co-encapsulated with chondrocytes in HA-Tyr constructs, which were then implanted subcutaneously in mice. Figure 4.11 shows that the incorporation of TGF-β1 microparticles increased GAG production ($p < 0.05$) within the constructs over that of the control constructs. The 6 kDa microparticles demonstrated more GAG production than the 13 and 24 kDa microparticles, and achieved a 1.5-fold increase over the control by Week 8. Figure 4.12 shows that at Week 8, a 1.6-fold increase in collagen production was found in the 6 kDa microparticles, while the collagen production associated with the 13 and 24 kDa microparticles was similar to the control. Thus, as shown by both ECM components, the earlier and higher gradient release of TGF-β1 from the 6 kDa microparticles increased chondrogenesis more than the prolonged, linear release of TGF-β1 from the higher MW microparticles.

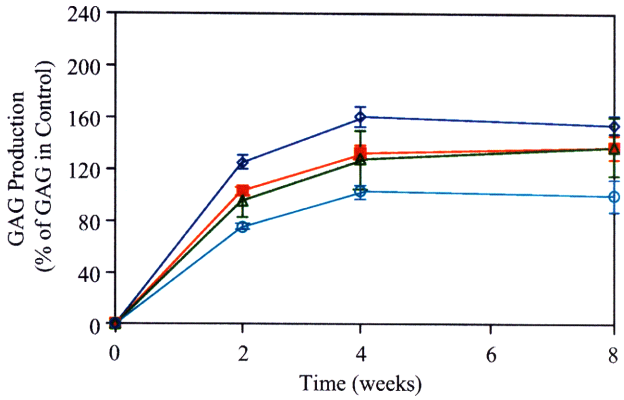

Figure 4.11. Increase in GAG production within HA-Tyr/H_2O_2/HRP/chondrocyte constructs with 10 mg/mL of TGF-β1-loaded PLGA-HAP nanocomposite microparticles with PLGA MW's of (◊) 6 kDa, (■) 13 kDa and (Δ) 24 kDa, and (○) with no particles.

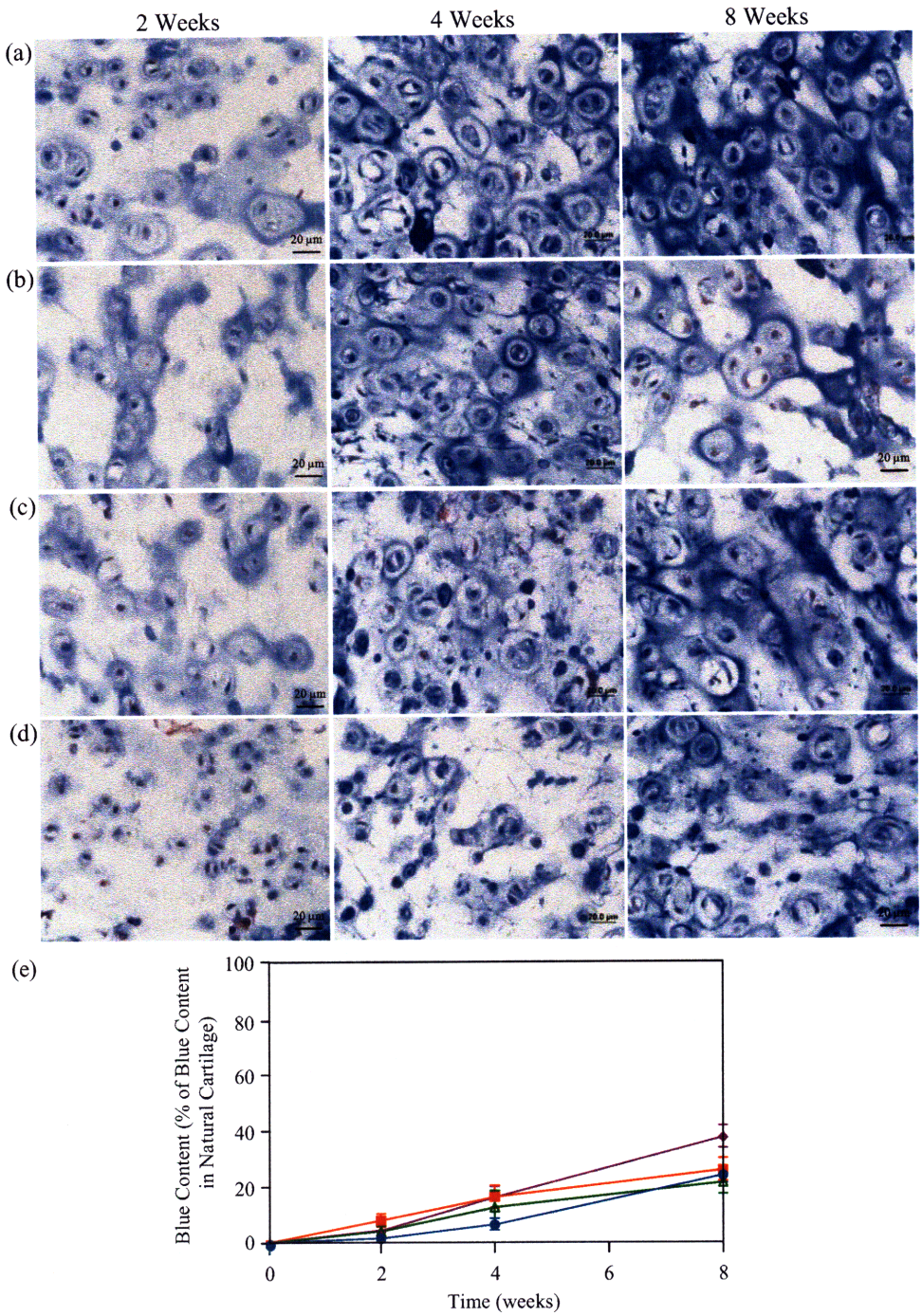

Figure 4.12. (a–d) Masson's Trichrome staining for collagen and (e) quantification of blue content within HA-Tyr/H_2O_2/HRP/chondrocyte constructs with 10 mg/mL of TGF-β1-loaded PLGA-HAP nanocomposite microparticles with PLGA MW's of (a, ♦) 6 kDa, (b, ■) 13 kDa and (c, Δ) 24 kDa, and (d, ●) with no particles.

4.3.6 Effect of Protein Combination on Cartilage Regeneration

IGF-1 and TGF-β1 are known to influence the action of one another, in many cases acting synergistically [2]. Tsukazaki *et al.* found that combining IGF-1 and TGF-β1 increased chondrocyte proliferation *in vitro* and increased DNA synthesis by up to ten-fold [31]. The sequential delivery of TGF-β1 (Days 3–10) and IGF-1 (Days 10–28) was also shown to be effective in promoting first chondrocyte proliferation, and then rapid chondrogenesis and tissue growth [32]. Therefore, in addition to controlling the release rates of growth factors, the combination and order of growth factor release are important considerations.

To study this effect, IGF-1-loaded PLGA-HAP nanocomposite microparticles and TGF-β1-loaded PLGA-HAP nanocomposite microparticles with different PLGA MW's (and therefore release profiles) were co-encapsulated with chondrocytes within HA-Tyr hydrogels, and implanted subcutaneously. A statistically significant increase in GAG production was observed with all combinations of IGF-1-loaded microparticles and TGF-β1-loaded microparticles over that of the control ($p < 0.05$) (Figure 4.13). According to post hoc analysis, the combination of IGF-1-loaded 24 kDa microparticles and TGF-β1-loaded 6 kDa microparticles showed higher GAG content than the other combinations, with a 2.1-fold increase over the control after 8 weeks. Collagen staining also showed that all combinations induced statistically greater collagen production ($p < 0.05$) over the control (Figure 4.14). The combination of IGF-1-loaded 24 kDa microparticles and TGF-β1-loaded 24 kDa microparticles and the combination of IGF-1-loaded 24 kDa microparticles and TGF-β1-loaded 6 kDa microparticles resulted in the highest increase over the control, with 3.8-fold and 3.5-fold increases, respectively. With regard to GAG production, the gradual, linear delivery of IGF-1 combined with the high-gradient release of TGF-β1 was most beneficial, reflecting the results in Sections 4.3.4 and 4.3.5. In terms of collagen production, this combination also resulted in a significant increase in collagen content, but slightly more collagen was synthesized with the simultaneous gradual release of both growth factors.

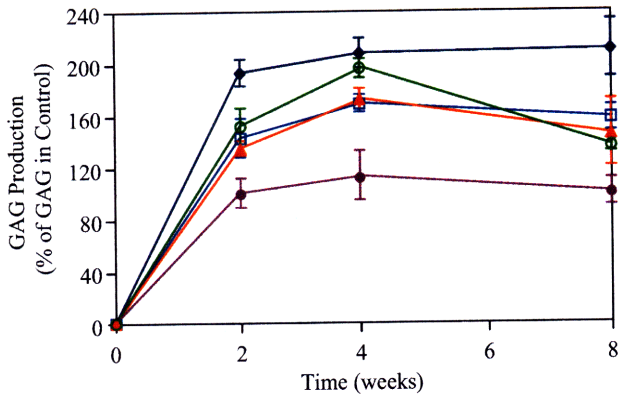

Figure 4.13. Increase in GAG production within HA-Tyr/H_2O_2/HRP/chondrocyte constructs with 40 mg/mL of IGF-1-loaded PLGA-HAP nanocomposite microparticles and 10 mg/mL of TGF-β1-loaded PLGA-HAP nanocomposite microparticles with PLGA MW's of (▲) 6 kDa and 6 kDa, (□) 6 kDa and 24 kDa, (♦) 24 kDa and 6 kDa, and (○) 24 kDa and 24 kDa, respectively, and (●) with no particles.

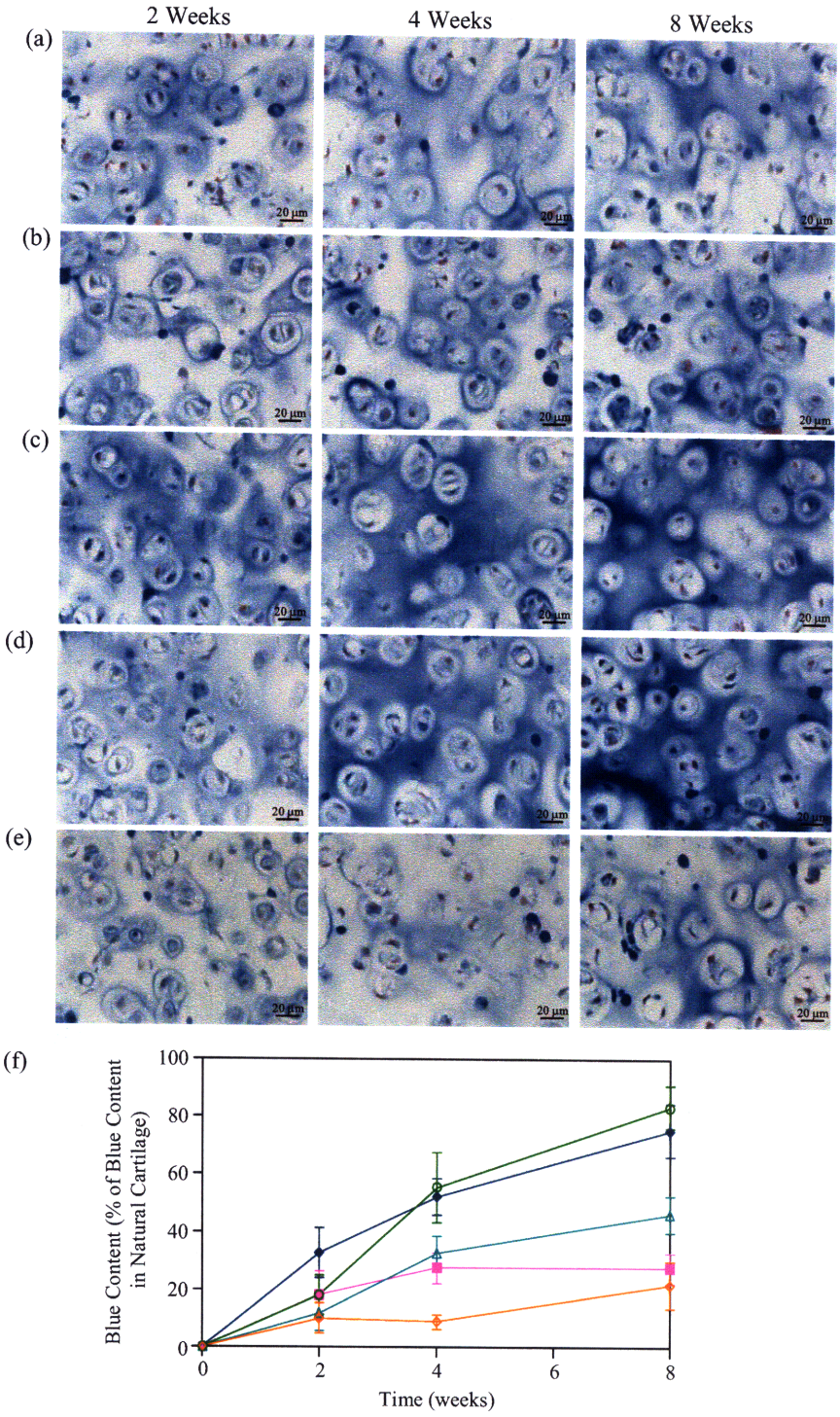

Figure 4.14. (a–e) Masson's Trichrome staining for collagen and (f) quantification of blue content within HA-Tyr/H_2O_2/HRP/chondrocyte constructs with 40 mg/mL of IGF-1-loaded PLGA-HAP nanocomposite microparticles and 10 mg/mL of TGF-β1-loaded PLGA-HAP nanocomposite microparticles with PLGA MW's of (a, Δ) 6 kDa and 6 kDa, (b, ■) 6 kDa and 24

kDa, (c, ♦) 24 kDa and 6 kDa, and (d, ○) 24 kDa and 24 kDa, respectively, and (e, ◊) with no particles.

4.3.7 Dosage Study

The dosage of growth factors is critical, as the effects of the growth factors can be dependent on their concentrations [3]. TGF-β1, for example, can either induce or inhibit cell proliferation, depending on its dosage [33]. Furthermore, low concentrations are often ineffective, while high concentrations can be toxic [2, 4]. To determine the effect of IGF-1 and TGF-β1 dosage, HA-Tyr/H_2O_2/HRP/chondrocyte constructs were implanted with various concentrations of either IGF-1-loaded 24 kDa PLGA-HAP nanocomposite microparticles or TGF-β1-loaded 6 kDa PLGA-HAP nanocomposite microparticles. Dosages of IGF-1-loaded microparticles and TGF-β1-loaded microparticles of 20–60 mg/mL and 5–40 mg/mL, respectively, were evaluated for GAG and collagen production. The concentrations were chosen such that, when combined, the total particle concentration would not exceed 100 mg/mL. At 100 mg/mL, the viscosity of the precursor solution was already high enough that passing it through a 21-gauge needle became difficult; a higher concentration would make the injection of this system problematic. In addition, by occupying substantial space within the construct, excessively high particle concentrations could hinder matrix production.

Figure 4.15 shows that all concentrations of IGF-1-loaded microparticles increased GAG production over the control ($p < 0.05$). The highest concentration (60 mg/mL) gave rise to the highest GAG production with a 1.7-fold increase over the control at Week 8. Figure 4.16 shows that the IGF-1-loaded microparticles also induced greater collagen content than the control. The higher concentrations of 50 and 60 mg/mL resulted in the most collagen synthesis, 2.5-fold and 2.7-fold greater than the control, respectively, at Week 8.

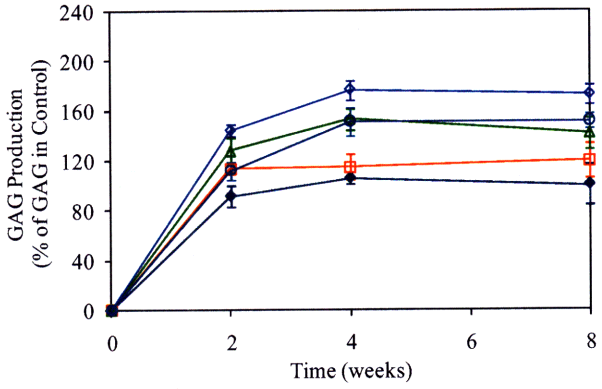

Figure 4.15. Increase in GAG production within HA-Tyr/H_2O_2/HRP/chondrocyte/collagen constructs with (□) 20 mg/mL, (Δ) 40 mg/mL, (○) 50 mg/mL and (◊) 60 mg/mL of IGF-1-loaded 24 kDa PLGA-HAP nanocomposite microparticles, and (♦) with no particles.

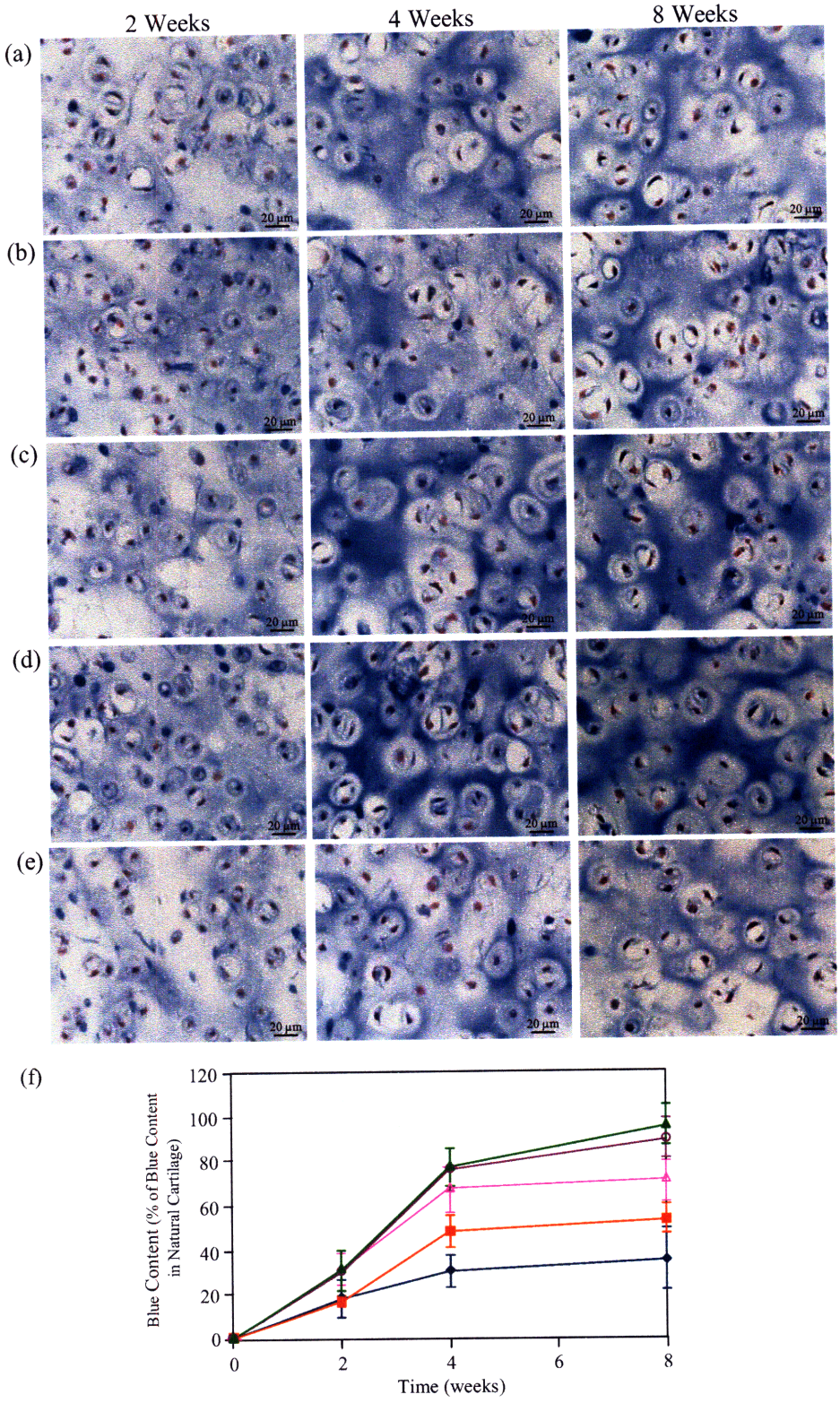

Figure 4.16. (a–e) Masson's Trichrome staining for collagen and (f) quantification of blue content within HA-Tyr/H_2O_2/HRP/chondrocyte/collagen constructs with (a, ■) 20 mg/mL, (b, Δ)

40 mg/mL, (c, ○) 50 mg/mL and (d, ▲) 60 mg/mL of IGF-1-loaded 24 kDa PLGA-HAP nanocomposite microparticles, and (e, ♦) with no particles.

Figure 4.17 shows that TGF-β1-loaded microparticles gave rise to increased GAG production over the control ($p < 0.05$). 20 and 40 mg/mL of TGF-β1-loaded microparticles induced the greatest GAG synthesis with 1.9-fold and 1.7-fold increases, respectively, at Week 8. Figure 4.18 also shows that TGF-β1-loaded microparticles induced greater collagen content than the control. The highest collagen content was associated with the highest particle concentration of 40 mg/mL, which resulted in a 2.7-fold increase over the control at Week 8.

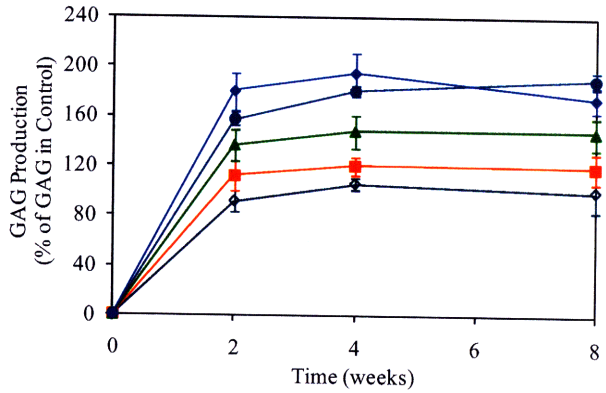

Figure 4.17. Increase in GAG production within HA-Tyr/H_2O_2/HRP/chondrocyte/collagen constructs with (■) 5 mg/mL, (▲) 10 mg/mL, (●) 20 mg/mL and (♦) 40 mg/mL of TGF-β1-loaded 6 kDa PLGA-HAP nanocomposite microparticles, and with (◊) no particles.

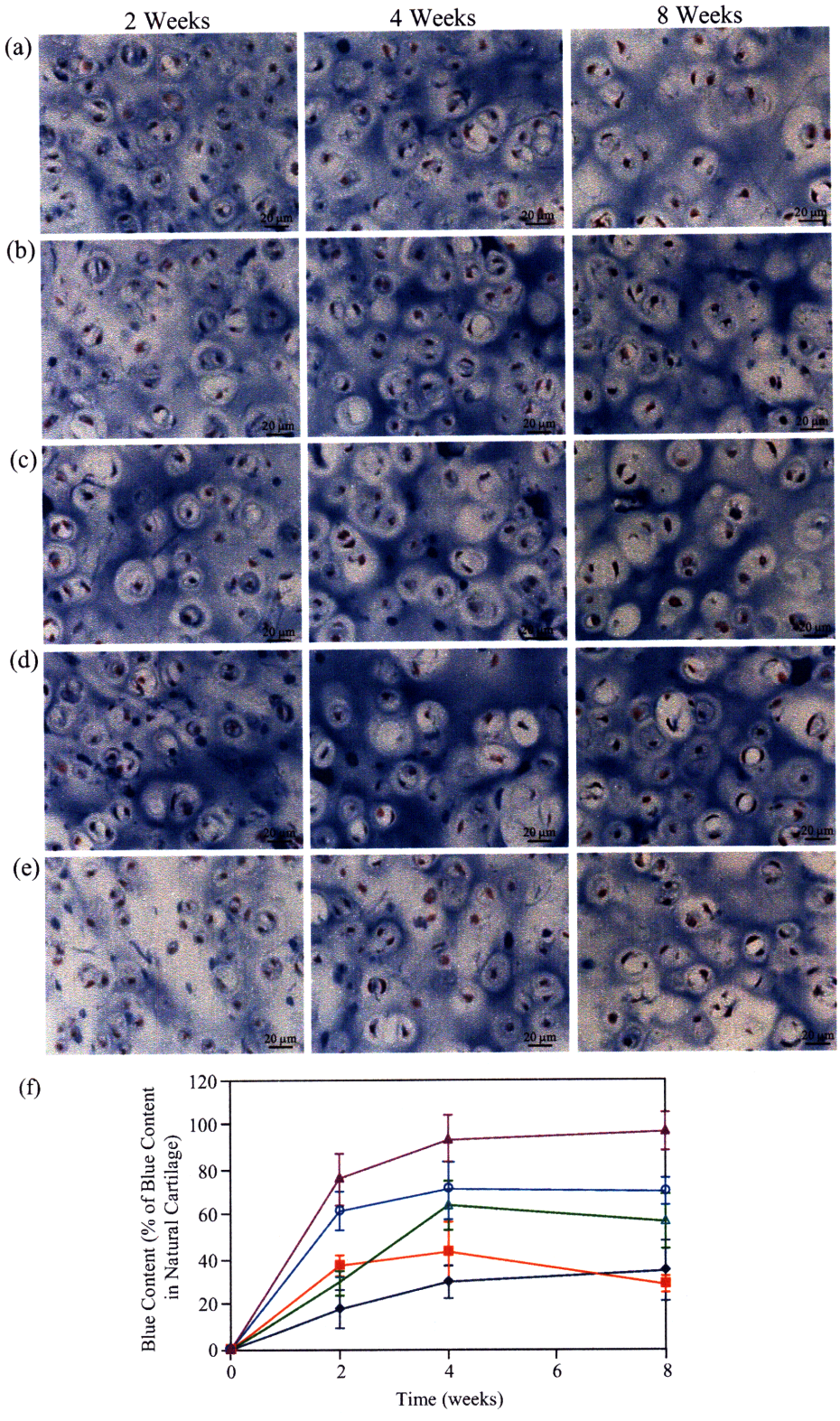
2 Weeks
4 Weeks
8 Weeks
(a)
(b)
(c)
(d)
(e)
(f)
20 μm
Blue Content (% of Blue Content in Natural Cartilage)
120
100
80
60
40
20
0
0
2
4
6
8
Time (weeks)

Figure 4.18. (a–e) Masson's Trichrome staining for collagen and (f) quantification of blue content within HA-Tyr/H_2O_2/HRP/chondrocyte/collagen constructs with (a, ■) 5 mg/mL, (b, Δ) 10 mg/mL, (c, ○) 20 mg/mL and (d, ▲) 40 mg/mL of TGF-β1-loaded 6 kDa PLGA-HAP nanocomposite microparticles, and (e, ♦) with no particles.

4.3.8 Injection Study

In order to test the effect of injecting the system, 60 mg/mL of IGF-1-loaded 24 kDa PLGA-HAP nanocomposite microparticles and 20 mg/mL of TGF-β1-loaded 6 kDa PLGA-HAP nanocomposite microparticles were combined with an HA-Tyr/H_2O_2/HRP liposome/chondrocyte/collagen precursor solution and injected subcutaneously in SCID mice. In response to the exposure to body temperature, HRP was released from the liposomes and successfully induced the formation of a hydrogel construct encapsulating the cells and particles. Particle concentrations were chosen based on the levels of increase in GAG production shown in Section 4.3.7, whereby 60 mg/mL of IGF-1-loaded 24 kDa microparticles and 20 mg/mL of TGF-β1-loaded 6 kDa microparticles (statistically equivalent to 40 mg/mL of TGF-β1-loaded 6 kDa microparticles) induced the highest GAG content. Precursor solutions containing 40 mg/mL of IGF-1-loaded 24 kDa microparticles and 10 mg/mL of TGF-β1-loaded 6 kDa microparticles were also injected, in order to compare the levels of improvement found in Section 4.3.6. As controls, a precursor solution containing no particles, a precursor solution containing 60 mg/mL of blank 24 kDa PLGA-HAP nanocomposite microparticles and 20 mg/mL of blank 6 kDa PLGA-HAP nanocomposite microparticles, and a precursor solution with 40 mg/mL of blank 24 kDa PLGA-HAP nanocomposite microparticles and 10 mg/mL of blank 6 kDa PLGA-HAP nanocomposite microparticles were also injected.

Harvested constructs showed that the combination of 60 mg/ml of IGF-1-loaded microparticles and 20 mg/mL of TGF-β1-loaded microparticles and of 40 mg/mL of IGF-1-loaded microparticles and 10 mg/mL of TGF-β1-loaded microparticles produced statistically equivalent increases in GAG production, 2.0-fold and 1.9-fold at Week 8, respectively (Figure 4.19). Both combinations also resulted in a 2.1-fold increase in collagen content over the control at Week 8 (Figure 4.20). These results show that when the particles were combined within these concentration ranges, improvements to GAG and collagen production were not generally dose-dependent. In addition, it was found that, at both sets of particle concentrations, the combinations of IGF-1-loaded microparticles and TGF-β1-loaded microparticles resulted in similar levels of

improvement in GAG and collagen production to that observed with 20 mg/mL of TGF-β1-loaded microparticles alone (Section 4.3.7). It should also be noted that although particle-induced increases to collagen production were not as high as that observed in Section 4.3.6 and for 60 mg/mL of IGF-1 particles alone (Section 4.3.7), constructs containing 60 mg/mL of IGF-1-loaded microparticles and 20 mg/mL of TGF-β1-loaded microparticles and those containing 40 mg/mL of IGF-1-loaded microparticles and 10 mg/mL of TGF-β1-loaded microparticles respectively achieved collagen contents of 95±12% and 92±7% that of natural articular cartilage. This study showed that growth factor-loaded microparticles could be injected with the precursor solution to form a construct *in vivo*, and that growth factors introduced by this method successfully increased matrix production within the constructs.

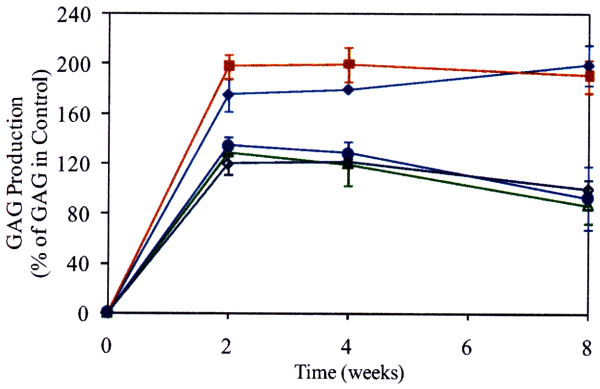

Figure 4.19. Increase in GAG production within HA-Tyr/H_2O_2/HRP liposome/chondrocyte/collagen constructs with (♦) 60 mg/mL of IGF-1-loaded 24 kDa PLGA-HAP nanocomposite microparticles and 20 mg/mL of TGF-β1-loaded 6 kDa PLGA-HAP nanocomposite particles, (■) 40 mg/mL of IGF-1-loaded 24 kDa PLGA-HAP nanocomposite microparticles and 10 mg/mL of TGF-β1-loaded 6 kDa PLGA-HAP nanocomposite particles, (Δ) 60 mg/mL of blank 24 kDa PLGA-HAP nanocomposite microparticles and 20 mg/mL of blank 6 kDa PLGA-HAP nanocomposite microparticles, (●) 40 mg/mL of blank 24 kDa PLGA-HAP nanocomposite microparticles and 10 mg/mL of blank 6 kDa PLGA-HAP nanocomposite microparticles, and (◊) no particles.

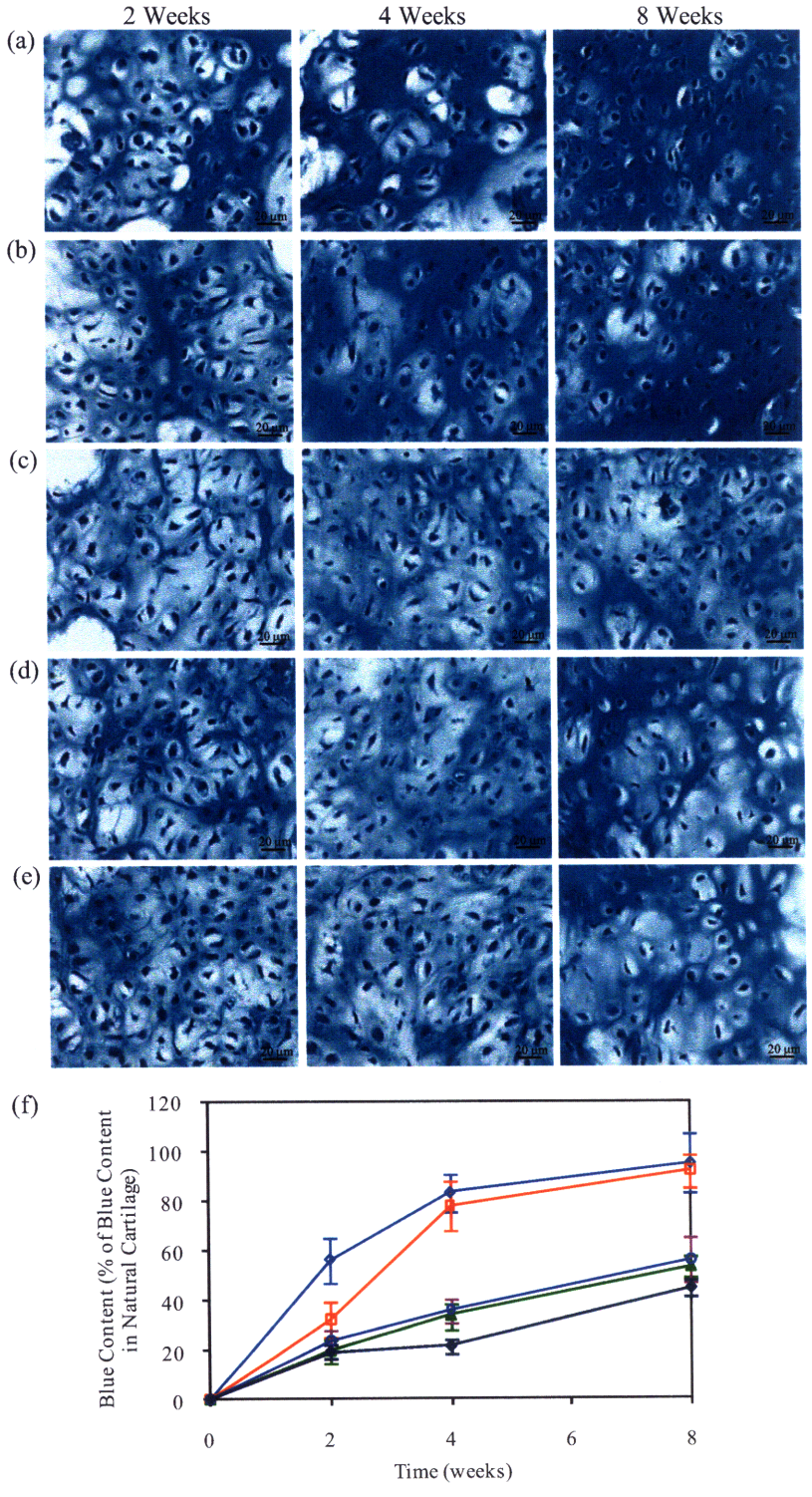

Figure 4.20. (a–e) Masson's Trichrome staining for collagen and (f) quantification of blue content within HA-Tyr/H_2O_2/HRP liposome/chondrocyte/collagen constructs with (a, ◊) 60 mg/mL of IGF-1-loaded 24 kDa PLGA-HAP nanocomposite microparticles and 20 mg/mL of

TGF-β1-loaded 6 kDa PLGA-HAP nanocomposite particles, (b, □) 40 mg/mL of IGF-1-loaded 24 kDa PLGA-HAP nanocomposite microparticles and 10 mg/mL of TGF-β1-loaded 6 kDa PLGA-HAP nanocomposite particles, (c, ▲) 60 mg/mL of blank 24 kDa PLGA-HAP nanocomposite microparticles and 20 mg/mL of blank 6 kDa PLGA-HAP nanocomposite microparticles, (d, ○) 40 mg/mL of blank 24 kDa PLGA-HAP nanocomposite microparticles and 10 mg/mL of blank 6 kDa PLGA-HAP nanocomposite microparticles, and (e, ♦) no particles.

4.4 Summary

IGF-1 and TGF-β1 were loaded into PLGA-HAP nanocomposite microparticles and incorporated into scaffolds to enhance cartilage regeneration. The particles were prepared by a S/O/W emulsion technique, and it was shown that the rate of growth factor release could be modulated by the PLGA MW. The release of growth factor from the particles was measured by suspending the particle in complete medium, and measuring the growth factor concentration in the supernatant over time. It was found that for both growth factors, increases in PLGA molecular weight decreased the rate of PLGA degradation, and therefore reduced the gradient and increased the period of release.

The effect of the microparticles themselves was verified by encapsulating chondrocytes and blank microparticles that did not contain growth factor within HA-Tyr hydrogels, which were then implanted subcutaneously in mice. The harvested constructs containing 10 mg/mL of microparticles showed equivalent GAG production to that of the control, while a slightly higher GAG content was observed in those containing 40 mg/mL of microparticles. This indicated that the microparticles did not hinder matrix synthesis, but enhanced chondrogenesis to a slight degree at higher concentrations. This might be attributed to the acidic by-products of particle degradation, which might have enhanced HA degradation and increased matrix production (as illustrated in Chapter 3 [1]).

Microparticles loaded with IGF-1 and composed of 6, 13 or 24 kDa PLGA were then encapsulated within the HA-Tyr hydrogels and implanted subcutaneously. It was found that the IGF-1-loaded 24 kDa microparticles increased GAG production over the control, while the lower MW microparticles did not exhibit a statistically significant increase. On the other hand, histomorphometry of the histological sections stained for collagen showed that all microparticles increased collagen production within the constructs relative to the control. The 13 kDa microparticles, with a medium release gradient, resulted in the greatest collagen synthesis. This

showed that within the HA-Tyr system, the gradual to medium release rates of IGF-1 were more effective in inducing GAG and collagen production by chondrocytes.

TGF-β1-loaded microparticles composed of 6, 13 or 24 kDa PLGA were also tested *in vivo*, and all showed a statistically significant increase in GAG production over the control. The higher gradient of TGF-β1 release from the 6 kDa microparticles resulted in the most GAG production and the most collagen production. In the HA-Tyr system, the early and rapid release of TGF-β1 was most beneficial in inducing greater tissue production.

The effect of multifactor release was then studied by creating HA-Tyr/H_2O_2/HRP/chondrocyte constructs with IGF-1-loaded microparticles and TGF-β1-loaded microparticles, and implanting them subcutaneously in mice. Various combinations of the microparticles composed of 6 or 24 kDa PLGA were investigated. It was found that all combinations resulted in greater GAG production and collagen production than the control. The combination of IGF-1-loaded 24 kDa microparticles and TGF-β1-loaded 6 kDa microparticles produced the most GAG. The combination of IGF-1-loaded 24 kDa microparticles and TGF-β1-loaded 24 kDa microparticles and the combination of IGF-1-loaded 24 kDa microparticles and TGF-β1-loaded 6 kDa microparticles showed the most collagen production.

The effect of IGF-1 particle dosage was studied by co-encapsulating 20–60 mg/mL of IGF-1-loaded 24 kDa microparticles with chondrocytes within HA-Tyr constructs, which were subsequently implanted *in vivo*. All particle concentrations resulted in a statistically significant increase in GAG production over the control, with 60 mg/mL giving the highest GAG content at Week 8. All concentrations were observed to increase collagen content over the control, but 50 and 60 mg/mL showed the greatest collagen synthesis.

TGF-β1 dosage was studied by encapsulating chondrocytes with 5–40 mg/mL of TGF-β1-loaded 6 kDa microparticles within the HA-Tyr hydrogels. All particle concentrations showed a statistically significant enhancement in both GAG and collagen production over the control. However, 20 and 40 mg/mL resulted in the highest GAG production, while 40 mg/mL induced the greatest collagen content.

The HA-Tyr/H_2O_2/HRP liposome/chondrocyte/collagen precursor solution was then injected subcutaneously with 60 mg/mL of IGF-1-loaded 24 kDa microparticles and 20 mg/mL of TGF-β1-loaded 6 kDa microparticles. It was shown that *in situ* scaffold formation could occur

in the presence of the microparticles. Delivery of the growth factors by this method significantly improved GAG and collagen production within the constructs by 2.0 and 2.1-fold, respectively, at Week 8.

This study shows that the delivery of IGF-1 and TGF-β1 via PLGA-HAP nanocomposite microparticles is promising for the enhancement of chondrogenesis in the HA-Tyr system. In optimizing matrix synthesis, the tunability of the polymer-apatite microparticle system allows for the incorporation of different growth factors, release kinetics, dosages as well as multifactor release. Furthermore, it has been shown that the microparticles can be effectively incorporated into an injectable system for minimally invasive administration.

4.5 References

[1] Ren, C. D., Gao, S., Ying, J. Y., to be submitted to Biomaterials.

[2] Babensee, J. E., McIntire, L. V., Mikos, A. G., *Pharm Res* **17**, 497–504 (2000).

[3] Trippel, S. B., Coutts, R. D., Einhorn, T. A., *et al.*, *J Bone Joint Surg* **78A**, 1272–1286 (1996).

[4] Elisseeff, J., McIntosh, W., Fu, K., *et al.*, *J Orthop Res* **19**, 1098–1104 (2001).

[5] Anseth, K., Metters, A. T., Bryant, S. J., *et al.*, *J Control Release* **78**, 199–209 (2002).

[6] Goessler, U. R., Hormann, K., Riedel, F., *Int J Mol Med* **13**, 505–513 (2004).

[7] Schoenle, E., Zapf, J., Humbel, R. E., *et al.*, *Nature* **296**, 252–253 (1982).

[8] Lo, M. Y., Kim, H. T., *J Orthop Res* **22**, 140–144 (2004).

[9] Darling, E., Athanasiou, K., *Cell Tissue Res* **322**, 463–473 (2005).

[10] Blunk, T., Sieminski, A. L., Gooch, K. J., *et al.*, *Tissue Eng* **8**, 73–84 (2002).

[11] Holland, T. A., Bodde, E. W. H., Cuijpers, V. M. J. I., *et al.*, *Osteoarthritis Cartilage* **15**, 187–197 (2007).

[12] Cancedda, R., Dozin, B., Giannoni, P., *et al.*, *Matrix Biol* **22**, 81–91 (2003).

[13] Sporn, M. B., Roberts, A. B., *Cell Regul* **1**, 875–882 (1990).

[14] Hu, J. C. Y., Athanasiou, K. A., in *Handbook of Histology Methods for Bone and Cartilage*, edited by Y. H. An and K. L. Martin (Humana Press, Totowa, 2003), p. 73–95.

[15] Glansbeek, H. L., van Beuningen, H. M., Vitters, E. L., *et al.*, *Lab Invest* **78**, 133–142 (1998).

[16] Tabata, Y., *Drug Discov Today* **10**, 1639–1646 (2005).

[17] Holland, T. A., Tessmar, J. K. V., Tabata, Y., *et al.*, *J Control Release* **94**, 101–114 (2004).

[18] Saltzman, W. M., Olbricht, W. L., *Nat Rev Drug Discov* **1**, 177–186 (2002).

[19] Jain, R. A., *Biomaterials* **21**, 2475–2490 (2000).

[20] Soppimath, K. S., Aminabhavi, T. M., *J Microencapsul* **19**, 281–292 (2002).

[21] Coombes, A. G. A., Yeh, M.-K., Lavelle, E. C., *et al.*, *J Control Release* **52**, 311–320 (1998).

[22] Ruan, G., Feng, S.-S., Li, Q.-T., *J Control Release* **84**, 151–160 (2002).

[23] Cleek, R. L., Ting, K. C., Eskin, S. G., *et al.*, *J Control Release* **48**, 259–268 (1997).

[24] Yong, T.-H., Ph. D. Thesis: *Apatite-Polymer Composites for the Controlled Delivery of Bone Morphogenetic Proteins* (Massachusetts Institute of Technology, Cambridge, Massachusetts, 2005).

[25] Combes, C., Rey, C., *Biomaterials* **23**, 2817–2823 (2002).

[26] Barralet, J. E., Aldred, S., Wright, A. J., *et al.*, *J Biomed Mater Res* **60**, 360–367 (2002).

[27] Ahn, E. S., Gleason, N. J., Nakahira, A., *et al.*, *Nano Lett.* **1**, 149–153 (2001).

[28] Ren, C. D., Kurisawa, M., Chung, J. E., *et al.*, to be submitted to Biomaterials.

[29] Martin, I., Obradovic, B., Freed, L. E., *et al.*, *Ann Biomed Eng* **27**, 656–662 (1999).

[30] Fu, K., Pack, D. W., Klibanov, A. M., *et al.*, *Pharm Res* **17**, 100–106 (2000).

[31] Tsukazaki, T., Usa, T., Matsumoto, T., *et al.*, *Exp Cell Res* **215**, 9–16 (1994).

[32] Pei, M., Seidel, J., Vunjak-Novakovic, G., *et al.*, *Biochem Biophys Res Commun* **294**, 149–154 (2002).

[33] Massagué, J., *Annu Rev Cell Biol* **6**, 597–641 (1990).

Chapter 5 – Recommendations for Future Work

5.1 Study of Scaffolds in Articular Defect Models

In this thesis, an injectable hyaluronic acid scaffold was developed for cartilage tissue engineering. While the subcutaneous results have been useful in quantifying the effects of various parameters on cartilage production *in vivo*, the HA-Tyr system as well as the growth factor-loaded nanocomposite microparticles should next be tested in an articular defect model. Although the load-bearing characteristics and cartilage repair rates of larger animal models, such as dogs, goats or horses, would more closely resemble that of humans, it would be more cost-effective to conduct initial studies on a smaller animal model, such as rabbits [1, 2]. Joint defects treated with HA-Tyr/H_2O_2/HRP/chondrocyte/microparticle constructs could be compared to those treated with HA-Tyr/H_2O_2/HRP/chrondrocyte, those treated with autologous chondrocyte implantation (ACI) and those left untreated. Evaluation of healing could be based on filling of the defect site, integration with the existing tissue, histology, quantification of GAG and collagen production, mechanical measurements, such as compression or indentation, and signs of inflammation. Constructs could be harvested and tested for initial healing at shorter time points, such as 4–8 weeks, and for durability at longer time points, such as 6–12 months.

In addition, while it was shown that the HA-Tyr/H_2O_2/HRP liposome/chondrocyte system was able to form a construct subcutaneously in response to the exposure to body temperature, the injectability within the joint should also be studied. The gelation time should be optimized to ensure retention of the precursor solution within the defect site, while preventing premature gelation *ex vivo*. Though joint fluid is present, it might be aspirated out temporarily and replaced after scaffold formation has occurred.

5.2 Exploration of Cell Source

While primary chondrocytes were chosen in this study, mesenchymal stem cells (MSCs), which have the capability of differentiating to chondrocytes, have also shown the ability to achieve chondrogenesis under proper culture conditions [3, 4, 5]. MSCs can be derived from the periosteum, perichondrium, muscles and bone marrow, and would therefore not require the sacrifice of cartilage from non-load-bearing sites in order to attain chondrocytes. Bone marrow stromal cells (BMSCs), in particular, are of great interest because they can be aspirated directly

from bone marrow [3]. MSCs could be cultured *in vitro* to induce differentiation with the aid of growth factors, such as TGF-β1, which could be delivered via the PLGA-HAP nanocomposite microparticles [4, 5, 6]. The cells could be subsequently seeded in scaffolds and introduced into the defect sites. Alternatively, MSCs might be directly implanted with the scaffold in the defect site in order to test the scaffold and joint environment's ability to induce differentiation. Differentiation can be measured by the expression of cartilage-specific markers, such as Type II collagen, aggrecan and Sox9 [7].

In addition, whether chondrocytes or MSCs, it would be best to test treatments on different cell sources. Each graph depicting GAG and collagen content in the thesis represented the results from constructs composed of chondrocytes isolated from one pig. Future experiments could be designed to test whether the same trends exist for different cells derived from animals of varying size, age, sex and health.

5.3 Study of Other Growth Factors and Chondrocyte Signaling Pathways

While IGF-1 and TGF-β1 were shown to effectively enhance chondrogenesis, several other growth factors are also known to regulate the growth and differentiation of cartilage, such as bone morphogenetic proteins, fibroblast growth factor, platelet-derived growth factor and cartilage-derived morphogenetic protein [8, 9]. The effects of the release rates, dosages and combinations, not only on matrix production, but also on the differentiation of MSCs, can be studied and compared to those of IGF-1 and TGF-β1.

The signaling pathways within chondrocytes and MSCs can also be further studied to understand the mechanisms behind growth factor upregulation of matrix synthesis and differentiation and the relationships between the growth factors. This knowledge would aid in designing the optimal rates and sequences of delivery within future constructs.

5.4 Application to Other Scaffolds

As scaffold composition determines cell-substrate interactions, which in turn affect tissue synthesis and the actions of growth factors, different types of scaffolds can also be studied. Liposomes are versatile encapsulating agents, and thermosensitivity may potentially be imparted to various polymer-crosslinking agent or monomer-catalyst systems, e.g. collagen-transglutaminase, elastin-lysyl oxidase, and fibrinogen-thrombin [10, 11, 12]. The abilities of

these scaffold systems to induce cartilage synthesis could be compared to that of the HA-Tyr system. In addition, the scaffolds could be explored for other applications, such as bone regeneration, wound healing, drug delivery, or cosmetic soft tissue filling.

5.5 References

[1] Reinholz, G. G., Lu, L., Saris, D. B. F., *et al.*, *Biomaterials* **25**, 1511–1521 (2004).

[2] Shortkroff, S., Barone, L., Hsu, H.-P., *et al.*, *Biomaterials* **17**, 147–154 (1996).

[3] Ochi, M., Adachi, N., Nobuto, H., *et al.*, *Artif Organs* **28**, 28–32 (2004).

[4] Redman, S. N., Oldfield, S. F., Archer, C. W., *Eur Cell Mater* **9**, 23–32 (2005).

[5] Bosnakovski, D., Mizuno, M., Kim, G., *et al.*, *Biotechnol Bioeng* **93**, 1152–1163 (2006).

[6] Goessler, U. R., Hormann, K., Riedel, F., *Int J Mol Med* **13**, 505–513 (2004).

[7] Nesic, D., Whiteside, R., Brittberg, M., *et al.*, *Adv Drug Deliv Rev* **58**, 300–322 (2006).

[8] Trippel, S. B., Coutts, R. D., Einhorn, T. A., *et al.*, *J Bone Joint Surg* **78A**, 1272–1286 (1996).

[9] Reddi, A. H., *Microsc Res Tech* **43**, 131–136 (1998).

[10] Chau, D. Y. S., Collighan, R. J., Verderio, E. A. M., *et al.*, *Biomaterials* **26**, 6518–6529 (2005).

[11] Elbjeirami, W. M., Yonter, E. O., Starcher, B. C., *et al.*, *J Biomed Mater Res* **66A**, 513–521 (2003).

[12] Kaminski, M., McDonagh, J., *J Biol Chem* **258**, 10530–10535 (1983).

Chapter 6 – Conclusions

A thermally triggered injectable scaffold was developed by utilizing thermoresponsive liposomes to segregate a crosslinking agent from a polymer. Liposomes were synthesized by a dehydration-rehydration vesicle method to encapsulate HRP. The HA-Tyr/H_2O_2/HRP liposome precursor solution remained a liquid for several hours at room temperature, and formed a hydrogel scaffold within minutes when exposed to body temperature. HRP encapsulation and gelation kinetics were modified by various material and processing parameters, such as lipid content, HRP loading and composition of wash solution.

In vivo studies showed the potential of the HA-Tyr system as a cartilage tissue engineering scaffold. Chondrocytes encapsulated within the constructs and implanted subcutaneously showed significant production of GAG and collagen, including Type II collagen, which is characteristic of articular cartilage. The effects of crosslink density, Type II collagen incorporation and cell seeding density on GAG and collagen synthesis were studied. Subcutaneous injection of the HA-Tyr/H_2O_2/HRP liposome/chondrocyte/collagen precursor solution demonstrated the feasibility of thermally triggered scaffold formation, and showed that injected scaffolds could induce matrix synthesis levels comparable to those that were implanted.

TGF-β1- and IGF-1-loaded PLGA-HAP nanocomposite microparticles were synthesized by a solid-in-oil-in-water emulsion process. The rate of growth factor release could be modulated by the molecular weight of PLGA. Nanocomposite microparticles co-encapsulated with chondrocytes within the HA-Tyr scaffolds illustrated the effects of growth factor release rate, combination and dosage on the enhancement of GAG and collagen synthesis. An HA-Tyr/H_2O_2/HRP liposome/chondrocyte/collagen/microparticle precursor solution was injected subcutaneously in a mouse model. It was demonstrated that the growth factor-loaded nanocomposite microparticles could be incorporated into the injectable system, and retained the ability to significantly increase matrix production.